

Modeling and Experimental Evaluation of the Effective Bulk Modulus for a Mixture of Hydraulic Oil and Air

A Thesis Submitted to the College of
Graduate Studies and Research
in Partial Fulfillment of the Requirements
for the Degree of Doctor of Philosophy
in the Department of Mechanical Engineering
University of Saskatchewan
Saskatoon

By

Hossein Gholizadeh

© Copyright Hossein Gholizadeh, September, 2013. All rights reserved.

PERMISSION TO USE

In presenting this thesis in partial fulfillment of the requirements for a Postgraduate degree from the University of Saskatchewan, I agree that the Libraries of this University may make it freely available for inspection. I further agree that permission for copying of this thesis in any manner, in whole or in part, for scholarly purposes may be granted by the professor or professors who supervised my thesis work or, in their absence, by the Head of the Department or the Dean of the College in which my thesis work was done. It is understood that any copying or publication or use of this thesis or parts thereof for financial gain shall not be allowed without my written permission. It is also understood that due recognition shall be given to me and to the University of Saskatchewan in any scholarly use which may be made of any material in my thesis.

Requests for permission to copy or to make other use of material in this thesis in whole or part should be addressed to:

Head of the Department of Mechanical Engineering
University of Saskatchewan
57 Campus Drive
Saskatoon, Saskatchewan, S7N 5A9
Canada

ABSTRACT

The bulk modulus of pure hydraulic oil and its dependency on pressure and temperature has been studied extensively over the past years. A comprehensive review of some of the more common definitions of fluid bulk modulus is conducted and comments on some of the confusion over definitions and different methods of measuring the fluid bulk modulus are presented in this thesis.

In practice, it is known that there is always some form of air present in hydraulic systems which substantially decreases the oil bulk modulus. The term effective bulk modulus is used to account for the effect of air and/or the compliance of transmission lines. A summary from the literature of the effective bulk modulus models for a mixture of hydraulic oil and air is presented. Based on the reviews, these models are divided into two groups: “compression only” models and “compression and dissolve” models.

A comparison of various “compression only” models, where only the volumetric compression of air is considered, shows that the models do not match each other at the same operating conditions. The reason for this difference is explained and after applying some modifications to the models, a theoretical model of the “compression only” model is suggested.

The “compression and dissolve” models, obtained from the literature review, include the effects of the volumetric compression of air and the volumetric reduction of air due to the dissolving of air into the oil. It is found that the existing “compression and dissolve” models have a discontinuity at some critical pressure and as a result do not match the experimental results very well. The reason for the discontinuity is discussed and a new “compression and dissolve” model is proposed by introducing some new parameters to the theoretical model.

A new critical pressure (P_C) definition is presented based on the saturation limit of oil. In the new definition, the air stops dissolving into the oil after this critical pressure is reached and any remaining air will be only compressed afterwards.

An experimental procedure is successfully designed and fabricated to verify the new proposed models and to reproduce the operating conditions that underlie the model assumptions. The pressure range is 0 to 6.9 MPa and the temperature is kept constant at 24 ± 1 °C. Air is added to the oil in different forms and the amount of air varies from about 1 to 5%. Experiments are conducted in three different phases: baseline (without adding air to the oil), lumped air (air added as a pocket of air to the top of the oil column) and distributed air (air is distributed in the

oil in the form of small air bubbles). The effect of different forms and amounts of air and various volume change rates are investigated experimentally and it is shown that the value of P_C is strongly affected by the volume change rate, the form, and the amount of air. It is also shown that the new model can represent the experimental data with great accuracy.

The new proposed “compression and dissolve” model can be considered as a general model of the effective bulk modulus of a mixture of oil and air where it is applicable to any form of a mixture of hydraulic oil and air. However, it is required to identify model parameters using experimental measurements. A method of identifying the model parameters is introduced and the modeling errors are evaluated. An attempt is also made to verify independently the value of some of the parameters.

The new proposed model can be used in analyzing pressure variations and improving the accuracy of the simulations in low pressure hydraulic systems. The new method of modeling the air dissolving into the oil can be also used to improve the modeling of cavitation phenomena in hydraulic systems.

ACKNOWLEDGMENTS

I would like to express my sincere gratitude to my supervisors, Professors Richard Burton and Greg Schoenau, for their thoughtful guidance, advice and encouragement throughout this research. They have always supported me with promptness and care, and have always been patient and encouraging. It would not have been possible to write this thesis without their help and support.

I would like to extend my sincere thanks to Mr. D. V. Bitner for his enthusiastic participation and essential technical assistance during all phases of the research and also writing of this thesis. I also greatly appreciate my thesis committee members: Professors David Sumner, David Torvi and Richard Evitts, for their encouragement, valuable comments and help.

Financial assistance provided by my supervisors in the form of a research assistantship and also from the University of Saskatchewan in the form of a teaching assistantship is greatly acknowledged.

Finally, I wish to express a lot of thanks to my friends and family, particularly my mother and my wife, Rabia, for their support and love during the preparation of this thesis.

TABLE OF CONTENTS

PERMISSION TO USE	i
ABSTRACT	ii
ACKNOWLEDGMENTS	iv
LIST OF TABLES	ix
LIST OF FIGURES	x
NOMENCLATURE	xv
CHAPTER 1: INTRODUCTION	1
1.1 Project background.....	1
1.2 Objectives.....	2
1.3 Outline of thesis.....	3
CHAPTER 2: BULK MODULUS DEFINITIONS AND MEASUREMENTS	4
2.1 Preamble.....	4
2.2 Introduction	4
2.3 Definitions of fluid bulk modulus	4
2.4 Properties of fluid bulk modulus	9
2.4.1 Effect of pressure on fluid bulk modulus.....	9
2.4.2 Effect of temperature on fluid bulk modulus	10
2.4.3 Effect of air on fluid bulk modulus.....	10
2.5 Measured values of fluid bulk modulus and their relationship to other variables.....	11
2.6 Experimental test systems for fluid bulk modulus testing.....	16
2.7 Effective bulk modulus measurement techniques	19
2.8 Summary	23
CHAPTER 3: EFFECTIVE BULK MODULUS MODELS IN THE PRESENCE OF AIR.....	24
3.1 Introduction	24
3.2 Volumetric fraction of air at atmospheric pressure	24

3.3	Models of the effective bulk modulus of an oil-air mixture.....	25
3.3.1	“Compression only” models	25
3.3.1.1	Merritt model	25
3.3.1.2	Nykanen-model.....	27
3.3.1.3	Cho model.....	30
3.3.1.4	Comparison of the compression only models	32
3.3.2	“Compression and dissolve” models	36
3.3.2.1	Determination of the volumetric variation of air content in oil	36
3.3.2.2	Yu model	40
3.3.2.3	LMS model	43
3.3.2.4	Ruan and Burton model	48
3.3.2.5	Comparison of the compression and dissolve models	50
3.4	Summary and Discussion	50
 CHAPTER 4: NEW EFFECTIVE BULK MODULUS MODEL FOR THE MIXTURE OF HYDRAULIC OIL AND AIR.....		 56
4.1	Introduction	56
4.2	Effective bulk modulus of a mixture of oil and air.....	57
4.2.1	Development of the initial new effective bulk modulus model	57
4.2.2	Experimental verification of the initial new isothermal effective bulk modulus model	66
4.2.3	Final new effective bulk modulus model.....	69
4.3	Summary and discussion	72
 CHAPTER 5: EXPERIMENTAL SETUP AND PROCEDURE.....		 74
5.1	Introduction	74
5.2	Experimental apparatus	74
5.3	Experimental uncertainty.....	78
5.4	Calculation of the effective bulk modulus.....	80
5.5	Experimental procedure.....	81
5.5.1	Baseline phase	83
5.5.2	Lumped air phase.....	86
5.5.3	Distributed air phase	90
5.6	Summary	92

CHAPTER 6: EXPERIMENTAL RESULTS	93
6.1 Introduction	93
6.2 Experimental results of the baseline phase.....	93
6.2.1 Isothermal tangent bulk modulus of the test oil	96
6.2.2 Adiabatic tangent bulk modulus of the test oil.....	97
6.2.3 Tangent bulk modulus of the test oil for other volume change rates	98
6.3 Experimental results of the effective bulk modulus of the lumped air phase.....	101
6.3.1 Experimental results with 1% of lumped air.....	103
6.3.2 Experimental results with 3% of lumped air.....	105
6.3.3 Experimental results with 5% of lumped air.....	107
6.4 Experimental results of the effective bulk modulus of the distributed air phase.....	109
6.4.1 Experimental results of the distributed air phase for a rapid volume change rate.....	111
6.4.2 Experimental results of the distributed air phase for a slow volume change rate	116
6.4.3 Experimental results of the distributed air phase at an intermediate volume change rate.....	121
6.5 Summary	123
CHAPTER 7: SUMMARY, CONCLUSIONS AND RECOMMENDATIONS	126
7.1 Summary	126
7.2 Main contributions.....	128
7.3 Conclusions	129
7.4 Recommendations for future work.....	132
LIST OF REFERENCES	134
APPENDIX A: TANGENT BULK MODULUS CALCULATION USING SECANT BULK MODULUS DATA.....	140
APPENDIX B: RELATION BETWEEN ADIABATIC AND ISOTHERMAL BULK MODULUS.....	142
APPENDIX C: PROPOGATION OF WAVE IN FLUID.....	143
APPENDIX D: ISOTHERMAL AND ADIABATIC BULK MODULUS ESTIMATION OF “ESSO NUTO H68” OIL.....	147
APPENDIX E: ESTIMATING THE DEFORMATION OF TESTING VOLUME	150

APPENDIX F: MEASUREMENT UNCERTAINTIES	152
F.1 Sensors	152
F.2 Uncertainty in measuring pressure	153
F.3 Uncertainty in measuring displacement	155
F.4 Uncertainty in measuring volume	155
APPENDIX G: COPYRIGHT INFORMATION.....	157

LIST OF TABLES

Table 2.1 Bulk modulus values for typical hydraulic oil (no entrained air) at 20°C and 50 MPa (Hayward, 1970)	8
Table 3.1 Summary of the investigated “compression only” models and their definitions for developing the models	33
Table 3.2 Summary of the investigated models and their definitions for developing the models	50
Table 6.1 $K_l(P_0, T)$ versus the oil compression time obtained from the baseline phase	101
Table D.1 Viscosity of test fluid (Esso Nuto H68) at 40°C and 100°C provided by the manufacturer	147
Table E.1 Specifications of each element of testing volume	150

LIST OF FIGURES

Figure 2.1 Comparison of different bulk modulus definitions	7
Figure 3.1 Comparison between the Nykanen and Merritt models	29
Figure 3.2 Comparison between the Nykanen and Cho models	32
Figure 3.3 Secant and tangent bulk modulus representation	33
Figure 3.4 Volumetric fraction of air (θ) versus pressure (Henry's law)	40
Figure 3.5 Plot of the Yu model based on the parameters obtained using the identification method.....	42
Figure 3.6 Plot of the LMS model based on the specified conditions. Note the discontinuity at the critical pressure.	46
Figure 3.7 Modified Henry's law used in the LMS model.....	47
Figure 3.8 Comparison of the LMS models at specified conditions.....	48
Figure 3.9 Comparison of compression only model for isothermal and adiabatic compression of air when $X_0 = 0.1$	52
Figure 3.10 Comparison of compression only model for isothermal and adiabatic compression of air at low pressure when $X_0 = 0.1$	53
Figure 3.11 Comparison of LMS Models with the compression only model.....	54
Figure 4.1 Modified Henry's law used in the LMS model.....	58
Figure 4.2 Comparison of the LMS models with the “compression only” model when $K_l = 1652 + 10.4(P - P_0)$, $P_C = 5.5$ MPa, $X_0 = 3\%$ and isothermal conditions ($n = 1$) is assumed	59
Figure 4.3 Graphical representation showing how to use “compression only” bulk modulus curves in order to find k_{ecd}	63
Figure 4.4 Theoretical comparison of LMS models and the initial new model with assumed conditions of $X_0 = 3\%$, $P_C = 5$ MPa and $K_l = 1652 + 10.4(P - P_0)$	66
Figure 4.5 Comparison of the experimental results with the initial new model and LMS models when $X_0 = 3.33\%$, $P_C = 5.5$ MPa and $K_l = 1652 + 10.4(P - P_0)$	67
Figure 4.7 A new critical pressure definition is introduced based on the saturation limit of oil..	69

Figure 4.8 Volumetric fraction of entrained air due to dissolving which is based on the new definition for the critical pressure	70
Figure 4.9 Theoretical comparison of the initial new model, final new model and compression only model when $X_0 = 3\%$, $P_C = 2$ MPa and $(X_0)_C = 1.5$ MPa for isothermal process	73
Figure 5.2 An experimentally measured pressure/volume curve is fitted with piecewise least square splines in order to facilitate the computation of dP/dV . The experimental data cannot be readily observed since the fitted curve when superimposed on the experimental data masks the data.....	81
Figure 5.3 The maximum slope of a pressure versus change in the volume curve is used to obtain the volumetric fraction of air at atmospheric pressure (X_0)	83
Figure 5.4 Pressure change as a result of applying different volume change rates in the baseline phase. The volume change rate is given in terms of percent of volume change per second $((\Delta V/V_0)/s)$	84
Figure 5.5 A typical example of bulk modulus measurement in the baseline phase (-0.0041 %/s)	85
Figure 5.6 Uncertainty of bulk modulus measurements in the baseline phase.....	85
Figure 5.7 Repeatability of the results in the baseline phase when the volume change rate is -0.0041 %/s	86
Figure 5.8 A change in the pressure when a lumped air content of 3.2% is added to the oil and the mixture is compressed with the volume change rate of -0.0123 %/s.....	87
Figure 5.9 A typical example of bulk modulus measurement when the lumped air content is 3.2% and the volume change rate is -0.0123 %/s.....	88
Figure 5.10 Uncertainty of bulk modulus measurements in the lumped air phase.....	89
Figure 5.11 Repeatability of the results in the lumped air phase when the amount of lumped air was 3.2 % with the volume change rate of -0.0123 %/s	89
Figure 5.12 A typical example of bulk modulus measurement when the distributed air content is 3.48% and the volume change rate is -0.0125 %/s	90
Figure 5.13 Uncertainty of bulk modulus measurements in the distributed air phase.....	91
Figure 5.14 Repeatability of the results in the distributed air phase.....	91
Figure 6.1 A typical example of a bulk modulus measurement in the baseline phase (-0.0044 %/s)	94

Figure 6.2 Nonlinear least squares curve fit of the experimental data in the baseline phase when the volume change rate was -0.0006 %/s.....	96
Figure 6.3 Nonlinear least squares curve fit of the experimental data in the baseline phase when the volume change rate was -0.216 %/s.....	97
Figure 6.4 Nonlinear least squares curve fit of the experimental data in the baseline phase	100
Figure 6.5.a $K_l(P_0, T) = 1972$ MPa, $n = 1.068$ and $E = 50$ MPa.....	104
Figure 6.5.b $K_l(P_0, T) = 1898$ MPa, $n = 1$ and $E = 27$ MPa.....	104
Figure 6.5.c $K_l(P_0, T) = 1838$ MPa, $n = 1$ and $E = 31$ MPa.....	105
Figure 6.5(a, b and c) Nonlinear least squares curve fit of the experimental data with 1% of lumped air and different volume change rates	105
Figure 6.6.a $K_l(P_0, T) = 1972$ MPa, $n = 1.206$ and $E = 34$ MPa.....	106
Figure 6.6.b $K_l(P_0, T) = 1920$ MPa, $n = 1.079$ and $E = 45$ MPa.....	106
Figure 6.6.c $K_l(P_0, T) = 1910$ MPa, $n = 1.085$ and $E = 42$ MPa.....	107
Figure 6.6 (a, b and c) Nonlinear least squares curve fit of the experimental data with 3% of lumped air and different volume change rates	107
Figure 6.7.a $K_l(P_0, T) = 1972$ MPa, $n = 1.331$ and $E = 30$ MPa.....	108
Figure 6.7.b $K_l(P_0, T) = 1930$ MPa, $n = 1.083$ and $E = 39$ MPa.....	108
Figure 6.7.c $K_l(P_0, T) = 1900$ MPa, $n = 1.059$ and $E = 45$ MPa	109
Figure 6.7 (a, b and c) Nonlinear least squares curve fit of the experimental data with 5% of lumped air and different volume change rates	109
Figure 6.8.a $K_l(P_0, T) = 1972$ MPa, $X_0 = 1.5\%$, $P_C = 6.5$ MPa, $(X_0)_C = 0.97\%$ and $E = 20$ MPa	112
Figure 6.8.b $K_l(P_0, T) = 1970$ MPa, $X_0 = 3.35\%$, $P_C = 6.5$ MPa, $(X_0)_C = 2.49\%$ and $E = 20$ MPa	112
Figure 6.8.c $K_l(P_0, T) = 1970$ MPa, $X_0 = 4.5\%$, $P_C = 6.5$ MPa, $(X_0)_C = 3\%$ and $E = 31$ MPa.	113
Figure 6.8 (a, b and c) Nonlinear least squares curve fit of the experimental data for different amounts of distributed air when the volume change rate was fast	113
Figure 6.9.a $K_l(P_0, T) = 1972$ MPa, $X_0 = 1.5\%$, $n = 1.16$ and $E = 162$ MPa	114

Figure 6.9.b $K_l(P_0, T) = 1970$ MPa, $X_0 = 3.35\%$, $n = 1.18$ and $E = 139$ MPa	115
Figure 6.9.c $K_l(P_0, T) = 1970$ MPa, $X_0 = 4.5\%$, $n = 1.17$ and $E = 129$ MPa	115
Figure 6.9 (a, b and c) Comparison of the “compression only” and “compression and dissolve” model for different amounts of distributed air when the volume change rate was rapid (Note that the given values represent the parameters of the “compression only” model)	115
Figure 6.10.a $K_l(P_0, T) = 1935$ MPa, $X_0 = 1.8\%$, $P_C = 6.5$ MPa, $(X_0)_C = 0.1\%$ and $E = 49$ MPa	116
Figure 6.10.b $K_l(P_0, T) = 1900$ MPa, $X_0 = 1.9\%$, $P_C = 6.1$ MPa, $(X_0)_C = 1.09\%$ and $E = 37$ MPa	117
Figure 6.10 (a and b) Nonlinear least squares curve fit of the experimental data for 1.8% and 1.9 % of distributed air when the volume change rate was slow	117
Figure 6.11.a $K_l(P_0, T) = 1925$ MPa, $X_0 = 3.48\%$, $P_C = 1.1$ MPa, $(X_0)_C = 1.91\%$ and $E = 15$ MPa	118
Figure 6.11.b $K_l(P_0, T) = 1890$ MPa, $X_0 = 3.42\%$, $P_C = 1$ MPa, $(X_0)_C = 2.22\%$ and $E = 18$ MPa	119
Figure 6.11 (a and b) Nonlinear least squares curve fit of the experimental data for 3.48% and 3.42 % of distributed air when the volume change rate was slow	119
Figure 6.12.a $K_l(P_0, T) = 1940$ MPa, $X_0 = 4.4\%$, $P_C = 0.9$ MPa, $(X_0)_C = 2.18\%$ and $E = 11$ MPa	120
Figure 6.12.b $K_l(P_0, T) = 1932$ MPa, $X_0 = 4.4\%$, $P_C = 0.8$ MPa, $(X_0)_C = 2.12\%$ and $E = 18$ MPa	120
Figure 6.12 (a and b) Nonlinear least squares curve fit of the experimental data for 4.4 % of distributed air when the volume change rate was slow	120
Figure 6.13.a $K_l(P_0, T) = 1972$ MPa, $X_0 = 1.9\%$, $P_C = 6.4$ MPa, $(X_0)_C = 0.1\%$ and $E = 36$ MPa	121
Figure 6.13.b $K_l(P_0, T) = 1970$ MPa, $X_0 = 3.45\%$, $P_C = 2.2$ MPa, $(X_0)_C = 2.14\%$ and $E = 16$ MPa	122

Figure 6.13.c $K_l(P_0, T) = 1972$ MPa, $X_0 = 4.4\%$, $P_C = 2.1$ MPa, $(X_0)_C = 2.24\%$ and $E = 9$ MPa	122
Figure 6.13 (a,b and c) Nonlinear least squares curve fit of the experimental data for 1.9%, 3.45% and 4.4 % of distributed air when the volume change rate was slow.....	122
Figure 6.14. Comparison of the experimental data for different amounts of distributed air and slow volume change rate.....	125
Figure D.1 Viscosity variation of Esso Nuto H68 with temperature.....	148
Figure D.2 Isothermal and adiabatic tangent bulk modulus variation of Esso Nuto H68 oil with pressure at a temperature of 24°C.....	149
Figure F.1 Calibration curve for the pressure transducer	154

NOMENCLATURE

A_T	Slope of pure oil bulk modulus versus pressure plot	[-]
b	Bias limit	[-]
C	Velocity of sound in fluid	[ms ⁻¹]
C_p	Specific heat at constant pressure	[JK ⁻¹ kg ⁻¹]
C_v	Specific heat at constant volume	[JK ⁻¹ kg ⁻¹]
c_1	Coefficient of air bubble volume variation due to the variation of the ratio of the entrained and dissolved air content in oil (has been used in Yu model)	[-]
E	Average error	[MPa]
H	Henry's constant	[MPa]
K	Tangent bulk modulus	[MPa]
K_0	Tangent bulk modulus at P_0	[MPa]
K_e	Tangent effective bulk modulus	[MPa]
K_{ec}	“Compression only” effective bulk modulus model	[MPa]
K_{ecd}	“Compression and dissolve” effective bulk modulus model	[MPa]
K_g	Tangent bulk modulus of air	[MPa]
K_l	Tangent bulk modulus of oil	[MPa]
K_S	Adiabatic tangent bulk modulus	[MPa]
K_T	Isothermal tangent bulk modulus	[MPa]
\bar{K}	Secant bulk modulus	[MPa]
\bar{K}_c	Secant bulk modulus of container	[MPa]
\bar{K}_e	Secant effective bulk modulus	[MPa]
\bar{K}_g	Secant bulk modulus of air	[MPa]
\bar{K}_l	Secant bulk modulus of oil	[MPa]
\bar{K}_S	Adiabatic secant bulk modulus	[MPa]
\bar{K}_T	Isothermal secant bulk modulus	[MPa]
\hat{K}_e	Experimental value of K_e	[MPa]
l_0	Initial height of fluid inside cylinder	[mm]
l'_0	True value of l_0	[mm]

l_{\max}	Maximum measurement range of instrument to measure l_0	[mm]
M	Total mass	[kg]
M_g	Mass of air	[kg]
M_l	Mass of oil	[kg]
m	Slope of the pure oil bulk modulus versus pressure curve	[-]
N_{dg}	Number of moles of dissolved air at pressure P	[mole]
N_g	Number of moles of entrained air	[mole]
N_l	Number of moles of oil	[mole]
n	Polytropic index of air	[-]
n_1	Polytropic index of air before critical pressure	[-]
n_2	Polytropic index of air after critical pressure point	[-]
P	Instantaneous absolute pressure	[MPa]
P_0	Atmospheric pressure	[MPa]
P_C	Critical pressure (absolute)	[MPa]
P_g	Instantaneous gauge pressure	[MPa]
P_{op}	Pressure at operating point	[MPa]
P_{sat}	Saturation pressure	[MPa]
P_{vap}^H	High saturated vapor pressure	[MPa]
P_{vap}^L	Low saturated vapor pressure	[MPa]
P'	True value of P	[MPa]
p	Precision limit	[-]
q	Volumetric flow rate	[m ³ /s]
R	Ideal gas constant	[m ³ PaK ⁻¹ mol ⁻¹]
T	Instantaneous temperature	[°C]
T_0	Initial temperature	[°C]
T_{op}	Temperature at operating point	[°C]
U	Total uncertainty	[-]
V	Total volume at P	[m ³]
V_0	Total volume at P_0	[m ³]

V_C	Volume of container at P	[m ³]
V_{C_0}	Volume of container at P_0	[m ³]
V_g	Volume of entrained air at P	[m ³]
V_{g_0}	Volume of entrained air at P_0	[m ³]
V_{gc}	Volume of entrained air when it is only compressed in accordance with the ideal gas law	[m ³]
V_{gcd}	Volume of entrained air as a result of the compression and loss of mass of entrained air due to dissolving	[m ³]
V_{gd_0}	Volume of dissolved air at P_0	[m ³]
$V_{(gt)_0}$	Total volume of air (including both entrained and dissolved) at P_0	[m ³]
V_l	Volume of oil at P	[m ³]
V_{l_0}	Volume of oil at P_0	[m ³]
V_{\max}	Maximum measurement range of instrument to measure V	[m ³]
V'	True value of V	[m ³]
X_0	Volumetric fraction of entrained air at atmospheric pressure (P_0) and temperature of interest (T)	[-]
$(X_0)_C$	Critical volumetric fraction of entrained air. It is defined as the volumetric fraction of entrained air at atmospheric pressure and temperature of interest which is related to the critical “compression only” bulk modulus curve	[-]
x	Displacement	[mm]
x_{\max}	Maximum measurement range of instrument to measure x	[mm]
x'	True value of x	[mm]
Z	Optimization matrix	[-]
Z_l	Z lower limit	[-]
Z_u	Z upper limit	[-]
α	Coefficient of dissolubility defined in Ruan and Burton model	[-]
α_p	Volumetric expansion coefficient at constant pressure	[°C ⁻¹]
β	Volume fraction of air present in baseline phase	[-]
ε_p	Dimensionless uncertainty of pressure measurements	[-]
ε_{V_0}	Dimensionless uncertainty of volume measurements	[-]
ε_x	Dimensionless uncertainty of the displacement measurements	[-]

	Volumetric fraction of entrained air due to dissolving. The exact definition in terms of the number of moles is: The ratio of the number of moles of entrained air at pressure P to the number of moles of entrained air at pressure P_0	
θ		[-]
$\mu_{0,T}$	Kinematic viscosity of fluid at P_0 and T	[cSt]
ρ	Total mass density at P	[kgm ⁻³]
ρ_0	Total mass density at P_0	[kgm ⁻³]
ρ_{g_0}	Mass density of entrained air at P_0	[kgm ⁻³]
ρ_{gd_0}	Mass density of dissolved air at P_0	[kgm ⁻³]
ρ_{l_0}	Mass density of oil at P_0	[kgm ⁻³]
ρ_{op}	Mass density at operating point	[kgm ⁻³]
σ_x	Standard deviation	[-]

CHAPTER 1: INTRODUCTION

1.1 Project background

Bulk modulus is one of the most important parameters in fluid power applications and is usually defined as the reciprocal of compressibility. Fluid bulk modulus reflects both the “stiffness” of the system and the speed of transmission of pressure waves. Therefore, stability of servo-hydraulic systems and efficiency of hydraulic systems are affected by the value of fluid bulk modulus (Hayward, 1963). Hence, it is very important to know the correct bulk modulus of hydraulic fluids and different factors which influence the numerical value of the fluid bulk modulus.

In a comprehensive review of the fundamental concepts, definitions and experimental techniques for the measurement of fluid bulk modulus (Gholizadeh et al., 2011, and Chapter 2 of this thesis) it was concluded that in addition to the molecular structure of the hydraulic oil, other parameters such as the oil pressure, oil temperature, pipe rigidity, air content of oil and interface conditions between the oil and the air will influence the numerical value of the fluid bulk modulus. The measured fluid bulk modulus which includes the effect of all of these parameters has been labeled the “effective” fluid bulk modulus (Merritt, 1967). The effect of pressure and temperature on the bulk modulus of hydraulic oil in the absence of air has been well studied and some semi-empirical equations have been provided which can predict the variation of the hydraulic oil bulk modulus with pressure and temperature with very good accuracy.

However, the presence of air in the hydraulic oil significantly reduces the fluid bulk modulus and these empirical equations are no longer valid. Assuming the oil is inside a rigid container, the theoretical models to find the effective fluid bulk modulus in the presence of the mixture of oil and air has been derived by various researchers. However, a comparison of these models in the low pressure region where the effect of air on the fluid bulk modulus is significant has indicated that several issues do need to be addressed (detailed in Chapter 3). A “compression only” model has been developed in some studies where only the volumetric compression of air was considered. Experimental verification of the “compression only” model was presented by Kajaste et al. (2005) and recently by Sunghun and Murrenhoff (2012). In Kajaste et al. (2005), the air was added as a free pocket (lumped air) at the top of the oil and the maximum amount of air added was 1%. In Sunghun and Murrenhoff (2012), the free air content was varied in a range up to 0.5%. The air was injected through a valve, but the air distribution

was unknown or at least not mentioned in the paper. In both studies, the applicability of the “compression only” model was verified successfully in the range of their experimental limitations. However, in none of the above mentioned studies, the exact conditions under which the “compression only” model would match the experimental results were mentioned. It is therefore very important to define the conditions in which the “compression only” model can be used and this became one of the motivations for this research.

There is also another condition that exists which has not been extensively studied and this is the situation where air both compresses and dissolves into solution. Several models have been developed and are detailed in Chapter 3. As mentioned, very limited literature exists in which the effect of air dissolving into solution has been incorporated into the model of the effective bulk modulus. A “compression and dissolve” model introduced by Yu et al. (1994) did not match well with the experimental results at the lower pressures (up to about 10 MPa). A “compression and dissolve” model which is developed by LMS IMAGINE (2008) and is used in AMESim simulation software, was investigated experimentally in Gholizadeh et al. (2012.a) and it was found that the model greatly underestimated the amount of air that was being dissolved in the oil, especially at higher amounts of air (more than 2%). Moreover, the “compression and dissolve” model introduced by LMS IMAGINE (2008) experienced a discontinuity at some critical pressure. Thus, the discontinuity issue and the fact that the previous “compression and dissolve” models failed to truly represent the experimental measurements were two additional motivations for the development of a new model based on sound physical principles.

1.2 Objectives

Based on some of the concerns expressed in Section 1.1 and detailed in Chapters 2 and 3, the objectives of this thesis are:

- To present a comprehensive review of the more recent literature on fluid bulk modulus that includes the common definitions used for fluid bulk modulus and a summary of methods of measurement to obtain it;
- To investigate and review different models of the effective bulk modulus of a mixture of hydraulic oil and air;
- To develop a new model based on sound physical concepts of the effective bulk modulus which arose from the review of the previous models and their limitations;

- To design and fabricate an experimental set up and procedure in order to verify the new proposed model under different conditions and volume change rates.

In this thesis, the reason for the discontinuity is addressed and a new model based on fundamental concepts is presented in which the discontinuity problem found in the LMS model no longer exists. An experimental apparatus was designed and built which was capable of compressing the test fluid at different volume change rates. The test fluid could be used in the form of pure oil, oil and lumped air or oil and distributed air. The fluid bulk modulus was calculated based on the experimental results and the proposed theoretical models verified with the calculated fluid bulk modulus.

1.3 Outline of thesis

This thesis is organized as follows:

In Chapter 2, the concept of fluid bulk modulus, the basic definitions, some of the important properties of the fluid bulk modulus and experimental techniques for the measurement of fluid bulk modulus are presented. In addition, a summary of some of the literature from which this information is based, is also presented.

Chapter 3 gives an extensive review of the effective bulk modulus models of a mixture of oil and air. Some modifications to the models are proposed and the models are categorized into two groups. A discontinuity problem associated with the second groups of the models (compression and dissolve) is also discussed.

In Chapter 4, the reason for the discontinuity is discussed and a new model based on sound physical concepts is proposed where the discontinuity problem no longer exists.

Chapter 5 describes the experimental apparatus and procedures used to measure the change in volume at various pressures and volume change rates.

In Chapter 6, a detailed description of the experimental results and the model verifications is presented.

Finally in Chapter 7, the contributions of the thesis and possible directions of future research are listed.

CHAPTER 2: BULK MODULUS DEFINITIONS AND MEASUREMENTS

2.1 Preamble

The majority of the text of Chapters 2 and 3 has been directly extracted from two comprehensive journal papers (Gholizadeh et al., 2011) and (Gholizadeh et al., 2012.a). Because of page limitations in these journals, much of the content had to be edited. Thus, Chapters 2 and 3 will expand where necessary the text from these papers to provide a more comprehensive summary of the literature and greater detail of the models which have been developed for bulk modulus.

2.2 Introduction

The Bulk modulus of a fluid represents the resistance of a fluid to compression and is the reciprocal of compressibility (Manring, 2005). Bulk modulus is a fundamental and inherent property of fluids which expresses the change in density of the fluid as external pressure is applied to the fluid. It shows both the “stiffness” of the system and the speed of transmission of pressure waves. Therefore, the stability of servo-hydraulic systems and efficiency of hydraulic systems are affected by the value of compressibility (Hayward, 1963).

There have been many studies and publications on the topic of fluid bulk modulus. It is clear that the numerical value of this property depends on the operating conditions, the amount of entrained air present, the way compression is applied and to some extent, the mathematical formulation. It is also evident that there is often confusion over which form of bulk modulus should be used for a particular situation. Thus it is an objective of this Chapter to present some general definitions of fluid bulk modulus, to present a comprehensive review of the more recent literature on fluid bulk modulus, and to summarize methods of measurement. The pressure and temperature range over which these bulk modulus measurements can be made are dependent on the design of the test apparatus. But generally the pressure range is from atmospheric pressure to 690 MPa and the temperature range is from -40 to 270°C .

2.3 Definitions of fluid bulk modulus

In order to understand the definition of fluid bulk modulus and how it was derived, the equation of state for fluids must be introduced first. The equation of state for fluids which

represents change in density as a function of change in pressure or temperature can be approximated by using the first three terms of a Taylor's series (Merritt, 1967). Therefore

$$\rho = \rho_{op} + \left(\frac{\partial\rho}{\partial P}\right)_T (P - P_{op}) + \left(\frac{\partial\rho}{\partial T}\right)_P (T - T_{op}). \quad (2.1)$$

This equation can be re-written in this form

$$\rho = \rho_{op} \left(1 + \frac{1}{K_T} (P - P_{op}) - \alpha_p (T - T_{op}) \right), \quad (2.2)$$

where $K_T = \rho_{op} \left(\frac{\partial P}{\partial \rho}\right)_T$ and is known as the *isothermal fluid bulk modulus*. (Note: In some of the literature, the letters B and K are used for bulk modulus; in this thesis K will be adopted), and $\alpha_p = -\frac{1}{\rho_{op}} \left(\frac{\partial P}{\partial T}\right)_P$ is known as the *cubical expansion coefficient* which is the fractional change in volume due to a change in temperature.

In these equations, ρ_{op} , T_{op} and P_{op} are the density, temperature and pressure of the fluid at an *operating point*. However, this has caused some confusion in the literature since instead of ρ_{op} , ρ_0 is often used in Eq. (2.1) which is sometimes mistakenly considered as the fluid density at atmospheric (zero gauge) pressure. To avoid this problem, the isothermal fluid bulk modulus should be defined as the “*isothermal tangent bulk modulus*” (to be formally defined in the following paragraph) which accounts for the “instantaneous” density of fluid at any operating point as in

$$K_T = \rho \left(\frac{\partial P}{\partial \rho}\right)_T. \quad (2.3)$$

Considering the relation between the density and volume of the fluid, the bulk modulus definition in terms of volume can be written as

$$K_T = -V \left(\frac{\partial P}{\partial V}\right)_T, \quad (2.4)$$

where V is the instantaneous volume of fluid during the compression.

Hayward (1965a) pointed out that misinterpretation of the published data for fluid bulk modulus can be a real problem because how the measurement is made can influence the actual

bulk modulus value. Knowledge of some basic facts about the compressibility of fluids and fully understanding the conditions under which a test is made can be very important in defining a bulk modulus value (Hayward, 1965a).

As reported by Hayward (1965a), it is important to understand that since fluids under compression do not follow Hooke's law, the relationship between pressure and volume change is not linear; consequently, at a given pressure P , the bulk modulus can be defined either based on the slope of the tangent to the curve at P (called *tangent or instantaneous bulk modulus*) or is based on the slope of a line connecting P to the origin which can be regarded as an average value of bulk modulus over the range from P_0 to P (called *secant bulk modulus*) (Hayward, 1965a). From a thermodynamic point of view, the tangent bulk modulus is more correct (see Eqs. (2.1) and (2.2)) since it is derived from the approximate equation of state for a fluid (liquid). Stecki and Davis, stated that “*tangent bulk modulus is always greater than the secant bulk modulus, except at atmospheric pressure where they are equal*” (Stecki and Davis, 1981). According to Klaus and O’Brien, “*tangent bulk modulus at pressure P is equal to the secant bulk modulus at $2P$ within ± 1 percent error*” (Klaus and O’Brien, 1964).

What makes the definition of bulk modulus more complex is that at any desired temperature and pressure, there are four different values of bulk modulus with considerable differences between them (Hayward, 1965a). With reference to Fig. 2.1, these four different bulk moduli (which relates to the thermodynamic condition as well as the mathematical condition) are (Hayward, 1965b):

- **Isothermal secant** bulk modulus

$$\bar{K}_T = -V_0 \left(\frac{P - P_0}{V - V_0} \right)_T, \quad (2.5)$$

- **Isothermal tangent** bulk modulus

$$K_T = -V \left(\frac{\partial P}{\partial V} \right)_T, \quad (2.6)$$

- **Isentropic (adiabatic) secant** bulk modulus

$$\bar{K}_S = -V_0 \left(\frac{P - P_0}{V - V_0} \right)_S, \quad (2.7)$$

- Isentropic (adiabatic) tangent bulk modulus

$$K_s = -V \left(\frac{\partial P}{\partial V} \right)_s. \quad (2.8)$$

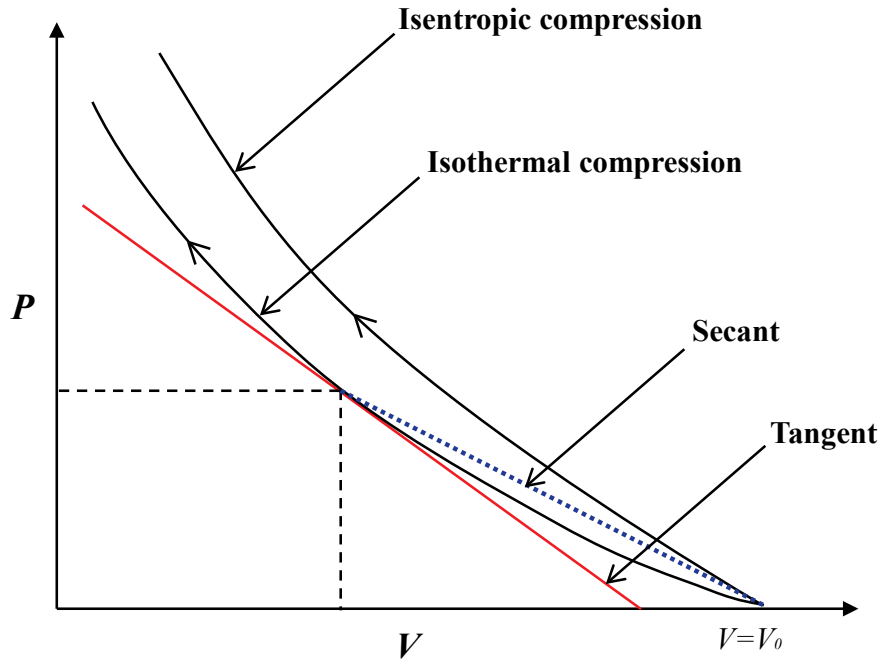


Figure 2.1 Comparison of different bulk modulus definitions

Subscripts S and T in Eqs. (2.5) to (2.8) denote the conditions of constant entropy and temperature respectively. In this thesis, the “bar” which occurs over K will refer to a secant (isothermal or adiabatic) bulk modulus. At conditions of constant entropy and absence of heat transfer, the bulk modulus is defined as the *isentropic bulk modulus*. As it can be seen from Fig. 2.1, for the same change in the volume of the oil, the isentropic compression requires more pressure than the isothermal one. Therefore, the value of isentropic bulk modulus is larger than isothermal bulk modulus (Hayward, 1965a).

In reality, it is only in reversible processes that constant entropy happens and as such, processes are always irreversible. This implies that the entropy is not constant in real applications. Because of this, many sources refer to the isentropic bulk modulus as the “*adiabatic bulk modulus*” which means that the entropy during the compression process is not necessarily

constant but no heat transfer occurs during the process (Stecki and Davis, 1981) and (Smith, 1965). For the remaining of this paper, the term adiabatic will be used rather than isentropic.

Another form of bulk modulus that is referred to in the literature is called “*sonic* bulk modulus” (Stecki and Davis, 1981). However, its value is the same as the adiabatic bulk modulus, and will not be considered as a separate form of bulk modulus. Rather it can be considered as a different method of measuring the adiabatic bulk modulus of the fluid.

It should be noted that in the definition of secant bulk modulus, the volume in the numerator refers to V_0 , while that in the tangent bulk modulus refers to V . Sometimes incorrect replacement of V_0 for V in the bulk modulus equation can affect the numerical value especially at high pressures or when calculating the bulk modulus of fluids containing air (Smith, 1965) and (Hayward, 1970). Therefore, it is very important in reporting the values for bulk modulus that the ***condition of the test*** and the ***exact definitions*** used should always be followed (Smith, 1965) and (Hayward, 1970). Unfortunately, this is often not done in much of the literature.

Table 2.1 shows different bulk modulus values for different definitions for a typical hydraulic mineral oil of viscosity 100 cSt at 20°C and 50 MPa in the absence of air bubbles (Hayward, 1970). Differences are observed and therefore it is very important to choose the appropriate bulk modulus definition according to the conditions of operation. Hayward (1970) has suggested using the adiabatic secant modulus for sudden changes of pressure, the isothermal secant modulus for slow changes of pressure, and the adiabatic tangent modulus for the pressure changes due to the propagation of a sound wave.

Table 2.1 Bulk modulus values for typical hydraulic oil (no entrained air) at 20°C and 50 MPa (Hayward, 1970)

Adiabatic secant bulk modulus	2.15 GPa
Adiabatic tangent bulk modulus	2.41 GPa
Isothermal secant bulk modulus	1.88 GPa
Isothermal tangent bulk modulus	2.15 GPa

As already mentioned, from a thermodynamic point of view, equations involving the tangent bulk modulus are those that should be used. However, these equations involve a

differential coefficient $\frac{\partial P}{\partial \rho}$ (slope at an operating condition) which may not be easily evaluated from experimental readings (Hayward, 1967). Therefore, usually secant (isothermal or adiabatic) bulk modulus is used in engineering applications which involve algebraic equations and can be easily evaluated (Hayward, 1967). In addition, secant bulk modulus \bar{K} can be used to derive tangent bulk modulus at any pressure. This relationship in which it is assumed that secant bulk modulus increases linearly with pressure is given by Hayward (1967) (details are provided in Appendix A) as

$$K = \frac{\bar{K}(\bar{K} - P_g)}{\bar{K} - P_g \frac{d\bar{K}}{dP}}. \quad (2.9)$$

Often it is easier to measure the adiabatic tangent bulk modulus than the isothermal one; for example using ultrasonic measurement techniques (Hayward, 1970). Using thermodynamic relationships, it is then possible to convert the measured adiabatic tangent bulk modulus values to the isothermal ones (Hayward, 1970). This relationship is given by (details are given in Appendix B)

$$\frac{C_P}{C_v} = \frac{K_S}{K_T}. \quad (2.10)$$

Bulk modulus is found to vary with pressure, temperature and the amount of entrained air in the fluid. In the following section, the effect of each of these variables on fluid bulk modulus will be discussed.

2.4 Properties of fluid bulk modulus

2.4.1 Effect of pressure on fluid bulk modulus

As pressure increases, bulk modulus of all fluids at first increases rapidly because of a decrease in the intermolecular gaps; as the pressure becomes higher, molecules become in contact with their neighbors and the rate of increase in bulk modulus value is reduced (Temperley and Trevena, 1978). From experimental results, it can be shown that over moderate pressure ranges (up to about 80 MPa with mineral oil), the secant bulk modulus (isothermal or adiabatic) can be expressed as a linear function of pressure (Hayward, 1971),

$$\bar{K} = K_0 + mP_g, \quad (2.11)$$

where K_0 is the bulk modulus at zero gauge pressure and m is a constant which for a particular fluid is temperature independent (Hayward, 1971).

2.4.2 Effect of temperature on fluid bulk modulus

With increase in temperature, the bulk modulus of most fluids is known to decrease. As temperature increases, molecules will move faster which results in the expansion of hydraulic fluid and a corresponding reduction in the density of the fluid. Reduction in the density means increase in the intermolecular gaps in the fluid which results in the reduction of the fluid bulk modulus (Temperley and Trevena, 1978).

2.4.3 Effect of air on fluid bulk modulus

Air is known to have a substantial effect on the compressibility of a fluid. Thus it would be expected that the bulk modulus value would vary as well. Air is known to exist in hydraulic systems in three forms (Magorien, 1978):

(1) Free air: air pockets trapped in part of the hydraulic system and can be removed from the hydraulic system by accurate venting of the system.

(2) Entrained air: air bubbles (typically 0.127 to 0.635 mm in diameter) which are distributed in the oil. Existence of free or entrained air in a hydraulic fluid significantly reduces the fluid bulk modulus. The term “bubbly oil” is used by Hayward (1961) for oil which contains separate air bubbles in which nearly thick films of oil have isolated these bubbles from each other.

(3) Dissolved air: invisible air bubbles stored in the empty space between the fluid molecules and uniformly spread throughout the fluid (Magorien, 1978). Test data indicate that as long as the air is in solution, it does not affect the fluid bulk modulus (Magorien, 1968).

The process of air dissolving into the fluid is usually described by Henry’s law, which states that at a constant temperature, the weight of a given gas dissolved in a given type and volume of fluid, will increase as the pressure of the gas increases. The amount of gas that can be dissolved in fluid is referred to its solubility (Totten, 2000).

Magorien (1967) suggested that the term *adsorption* instead of *absorption* can be used to better explain the process of dissolving air bubbles into the fluid. Adsorption is defined as a process in which an extremely thin film of air is accumulated on the surface of the fluid in contact with the air (Magorien, 1967). Absorption indicates a process in which the air diffuses into the body of the fluid. The adsorption rate is increased with pressure and decreased as the diameter of the air bubble increases (Magorien, 1967). Hayward (1961) showed that when a column of bubbly oil is compressed, at first the rate of dissolving is very fast, and then slows down because of saturation of the skin of oil around each bubble with dissolved air (adsorption). Thereafter, the rate of dissolving will depend upon the air diffusion rate from this surface layer into the body of the oil (absorption). He also studied the compressibility of bubbly oil under sudden compression and showed that the polytropic index (n) that air bubbles follow is much closer to isothermal ($n = 1$) than adiabatic ($n = 1.4$). In hydraulic applications, the rate of dissolving of air when the bubbly oil is suddenly compressed (for example, from the inlet to the outlet of a pump) is of interest. Experiments show that using higher operating point pressure or a less viscous oil will increase the rate of dissolving (Hayward, 1961).

By increasing the temperature or lowering the external pressure, air will leave the free intermolecular spaces and will come out of solution (Magorien, 1978). Therefore, depending on the operating conditions in which the fluid is subjected, it is possible for the dissolved air to become entrained (and vice versa). Magorien (1978) explains that by increasing the pressure, the entrained air can be re-dissolved into the fluid, but it is possible that not all of the released air re-dissolves again even by increasing the pressure. The reason for this behavior is explained by the fact that some air bubbles are not always close to an empty intermolecular space; as a result they cannot dissolve and consequently stay in entrained form (Magorien, 1978).

2.5 Measured values of fluid bulk modulus and their relationship to other variables

Carrying out experiments to measure fluid bulk modulus is expensive and difficult (Wright, 1967). Therefore, attempts have been made to estimate bulk modulus value of fluids at desired pressure and temperature utilizing easy to measure variables.

Klaus and O'Brien (1964) conducted a fundamental study on fluids and lubricants bulk modulus. They introduced some experimental relationships for the "prediction" of isothermal tangent, adiabatic tangent and isothermal secant bulk modulus values of some studied fluids. The

fluids studied in this research were paraffinic and naphthenic mineral oils, a dibasic acid ester, a polymer-thickened mineral oil, two types of silicones, two polyphenyl ethers and water. The isothermal secant bulk moduli of these fluids were measured in their bulk modulus apparatus over the pressure range of 0 to 69 MPa and temperature range of 0 to 177 °C. To check the validity of these relationships, the data were then compared to measurements taken at higher pressures and different types of bulk modulus apparatus. Their prediction method required at least one measured value of bulk modulus at one operating point.

They found that the plot of isothermal secant bulk modulus versus pressure was linear and except for water, all the other fluids studied had the same slope of 5.30. The predicted equation (which was found to be accurate within $\pm 2\%$ for the fluids studied over the 177°C temperature range) showed that at a constant temperature, the fluid bulk modulus changed linearly with pressure; that is

$$\bar{K}_T(P, T) = \bar{K}_T(0, T) + 5.30P_g. \quad (2.12)$$

They also found that increasing temperature causes the secant bulk modulus to decrease logarithmically; that is over the temperature range of 0 to 218°C,

$$\log \left[\frac{\bar{K}_T(P, T_1)}{\bar{K}_T(P, T_2)} \right] = \beta(T_2 - T_1), \quad (2.13)$$

where β is a function of pressure and its value can be found from the graph provided in their paper. Since the effect of temperature on the bulk modulus is logarithmic, its effect on fluid bulk modulus is greater than the effect of pressure. This is a factor that is seldom considered in the literature.

Wright (1967) provided some graphs for predicting the isothermal secant and tangent bulk modulus values over the temperature range of 0 to 260°C and pressure range of 0 to 690 MPa with an average error of less than 1%. For prediction, it was only required to know the density of fluid at atmospheric pressure and temperature of interest. Wright's technique was limited to petroleum oils and pure hydrocarbons only and no equations were provided.

Hayward (1970) also provided some experimental equations which can be used to estimate fluid bulk modulus. Hayward found that the bulk modulus of any normal mineral hydraulic oil can be estimated knowing either its density or viscosity at atmospheric pressure and 20 °C. This was found to be true to an accuracy of 5% for all oils with a viscosity range from 30

to 1500 cSt at 20°C, a pressure range of 0 to 80 MPa and a temperature range of 5 to 100°C. For oils with very low viscosity and viscosity-index-improved oils, he suggested using the density based relationships.

Isdale et al. (1975) found that Hayward's test device (Hayward, 1965a) gave accurate results at medium pressures and was not accurate at low or high pressures. At low pressures the volumetric change of the oil is very small and any movement of rubber seals used in Hayward's device or presence of small amounts of air will produce large errors in determining the volumetric change of the oil (Isdale et al., 1975). An error of 1% in measuring the volumetric change at 69 MPa would cause an error of more than 25% in the secant bulk modulus (Wright, 1967). At higher pressures, the seal friction will be very high (Isdale et al., 1975). Therefore, Isdale et al. used the sound velocity method to measure the fluid bulk modulus at low pressures and the bellows compression method (change in the length of the sealed bellows containing the fluid was used to measure the fluid bulk modulus) at high pressures. According to Isdale et al.'s results, Hayward's prediction method gives accurate results at pressures up to 200 MPa. At higher pressures, Wright's prediction method gives more accurate results.

Song et al. (1991) developed equations for the predictions of the isothermal secant bulk moduli of mineral oils, polymer solutions with hydrocarbon bases and non-hydrocarbon based oils. The chemical structure of the fluid, the fluid density and viscosity at atmospheric pressure and temperature of interest were required for any prediction. The theory behind their work was developed by Chu and Cameron (1966) in which the bulk modulus was related to the viscosity and free volume of a fluid. Free volume is the volume of empty space between the molecules. Calculations of free volume for different oils showed that all hydrocarbons had essentially the same free volume and the difference in bulk modulus value of hydrocarbons versus non-hydrocarbons related to the difference in their free volumes (Song et al., 1991).

The relationship to find the isothermal secant bulk modulus of mineral oils and nonpolymeric pure hydrocarbons at any required temperature and pressure was represented by (Song et al., 1991) as

$$\bar{K}_T(P, T) = \bar{K}_T(0, T) + A_T P_g, \quad (2.14)$$

where

$\bar{K}_T(P, T)$ = Isothermal secant bulk modulus at pressure P and temperature T , GPa,

$\bar{K}_T(0,T)$ = Isothermal secant bulk modulus at atmospheric pressure and temperature T , GPa, and
 A_T = Slope of bulk modulus versus pressure plot, GPa/GPa.

This relationship is similar to Klause's findings in that the isothermal bulk modulus is linearly related to the pressure. In this equation, Song et al. found a relationship between $\bar{K}_T(0,T)$ and viscosity, and between A_T and temperature. These relationships were found to be

$$\log (\bar{K}_T(0,T))=0.3766 \left\{ \log (\mu_{0,T}) \right\}^{0.3307} -0.2766, \quad (2.15)$$

where $\mu_{0,T}$ is the kinematic viscosity of fluid at 1 atm (centistokes). A_T was found to have a linear relationship with temperature and is given by

$$A_T = -0.01382 T (^{\circ}C) + 5.851. \quad (2.16)$$

The accuracy for the prediction of $\bar{K}_T(0,T)$ was found to be within $\pm 3.7\%$ over the pressure range of 0 to 140 MPa.

In standard ANSI/B93.63M (1984), some charts and equations have been provided in order to predict the isothermal secant, isothermal tangent and adiabatic tangent bulk modulus of petroleum or hydrocarbon oils over the temperature range of 0 to 270°C with a pressure range from atmospheric to 700 MPa. The density of oil at atmospheric pressure and temperature of interest is needed in order to estimate the isothermal secant and isothermal tangent bulk modulus. For the calculation of adiabatic tangent bulk modulus, specific heats of the oil are required to be known.

Borghi et al. (2003) presented some equations for the prediction of physical and thermodynamic properties of hydraulic fluids based on utilizing both the analytical and experimental approaches. These empirical-analytical equations can be used to predict the variation of isothermal secant, isentropic secant, isothermal tangent and isentropic tangent bulk modulus with pressure 0 to 60 MPa and temperature 0 to 160°C. The knowledge of fluid viscosity at 40 and 100°C (at atmospheric pressure) and fluid density at 15°C (at atmospheric pressure) is required in these equations.

Karjalainen et al. (2005) measured the bulk modulus, density and velocity of sound for some commercial hydraulic fluids at different temperatures and high pressures up to over 60 MPa. They measured the velocity of sound in the fluid by measuring the wave propagation time between two pressure transducers.

The fluid bulk modulus was calculated by removing the estimated value of the compressibility of other components from the measured values. Experimental values were compared with semi-empirical equations provided by Borghi et al. (2003) available for density and bulk modulus (isothermal secant, isothermal tangent, adiabatic secant, and adiabatic tangent) as a function of changes in pressure and temperature. In comparing the densities, measured densities were found to be the same as the density values calculated using the semi-empirical equations. But depending on the type of the fluid, the results of measured bulk modulus values were different from the bulk modulus values calculated using the semi-empirical equations. They found that for mineral oil based fluids, the measured value of isothermal tangent bulk modulus was exactly the same as the isothermal tangent bulk modulus value calculated using the semi-empirical equations. But for pine oil, the measured value of isothermal tangent bulk modulus was close to the adiabatic tangent bulk modulus calculated using the semi-empirical equations. Therefore, they concluded that the commonly held idea that adiabatic tangent bulk modulus should be considered in many hydraulic systems could be questionable and further research needed.

In another paper by Karjalainen et al. (2007), the authors suggested that generalizing the definition of adiabatic bulk modulus only based on rapid change of state, might not be valid and further information regarding the dynamics of the system might be necessary. They used two different methods which are commonly considered equivalent, but gave different results. The first method used a continuous pumping approach and measured the velocity of sound by measuring the wave propagation time between two pressure transducers. This method was used for pressures up to 60 MPa. For pressures higher than this value, another method called a single pressure peak system was used. In this method, static pressure was produced by using an intensifier and then by subjecting a hydraulic cylinder to an external perturbation, a dynamic pressure peak was produced in the measuring pipe. Pressures over 100 MPa were obtained using this method.

The results of density, velocity of sound and bulk modulus values for both methods were presented and compared for ISO VG 46 mineral oil and ISO VG 46 HF-E synthetic ester fluid. The measured densities for both fluids were found to be the same for both systems. For the velocity of sound, no difference between two fluids was observed in the same system; however, variations in the measured values were found when two different systems were used. For

example, at 40°C and 20 MPa (200 bar), the velocity of sound for the mineral oil at continuous pumping method was measured as 1400 m/s; however for the same fluid, the single pressure pick system measured approximately 1480 m/s. Therefore, they concluded that based on their experimental results the fluid behavior was different in the two systems.

They compared the measured values with the semi-empirical equations available for bulk modulus and it was concluded that the continuous pumping system compared well with isothermal values, while the single peak method agreed with adiabatic values. For confirmation of results, the authors suggested comparing the measured values with the results of ISO standardized method which is similar to the continuous pumping method.

The results by Karjalainen et al. (2005), however, are inconsistent with the results of Johnston and Edge (1991). These researchers used the three transducer method in a continuous pumping technique for the measurement of the velocity of sound and their calculated bulk modulus for the oil was close to the adiabatic bulk modulus values reported by the fluid manufacturer's data.

It is very important to note that all the mentioned relations for the prediction of fluid bulk modulus can only be used for the oils with no presence of free or entrained air in it.

2.6 Experimental test systems for fluid bulk modulus testing

The basic concept of fluid bulk modulus and methods of measurements has been known for many years. A summary of earlier studies is presented in (O'Brien, 1963) and (Burton, 1971).

O'Brien (1963) designed a system which was capable of determining the isothermal secant bulk modulus in the pressure range of 0 to 69 MPa. He used calibrated pycnometers in which the test liquids were put inside tubes and externally pressurized using nitrogen gas. A volumetric change of the liquid was measured visually by a change in the length of the liquid. A precision of $\pm 0.5\%$ was claimed for bulk modulus values obtained using this device.

Hayward (1965b), expressed concern that in reporting the bulk modulus values, conditions of the test were not defined and the use of different definitions of fluid bulk modulus resulted in confusion. Therefore, he proposed "adequate" definitions of bulk modulus and methods of reporting data. He proposed the following method to report bulk modulus values: *"Isentropic (adiabatic) and isothermal curves of pressure against relative volume decrease (*

$-\frac{\delta V}{V_0}$) from zero to 10000 psi should be quoted, at temperatures of 25°C, 50°C and 75°C”

(Hayward, 1965b). He also suggested that in situations in which the liquid has been designed to work at very high pressures, or at very high or very low temperatures, extra information can be added.

In another publication in the same year, Hayward (1965a), introduced an easily operated bulk modulus tester which was a modified compression machine in which a metal rod was inserted through an O-ring into a closed container full of fluid. By knowing the load and displacement of the rod, the liquid pressure and volume changes were calculated. An accuracy of $\pm 2\%$ was claimed for this apparatus.

Hayward (1971) also tried to determine the sources of error in traditional methods of measuring the fluid bulk modulus. He pointed out five main sources of error: “*Anisotropic distortion of pressure vessels, low pressure scatter, air entrainment, unsatisfactory joints and seals and poor temperature control*”. He mentioned studies which showed that the elastic modulus of many metals was not the same in all the directions and the general methods of calculating the bulk modulus of apparatus from elastic theory were not trustworthy enough. To avoid or reduce this source of error, he recommended calibration of the compressibility apparatus by carrying out a test on pure mercury and subtracting the measured value from the known compressibility values of the mercury. He also suggested that in order to prevent low pressure scatter, “*the pressure differential ($P_2 - P_1$) should never be less than 20% of the full pressure range of the apparatus, or less than 10 MPa*” (Hayward, 1971). In order to avoid problems associated with the presence of air or badly designed joints, he recommended that “*the initial pressure P_1 should never be less than 2% of P_2 , nor less than 1 MPa*” (Hayward, 1971). Finally he claimed that by following some rules that are mentioned in his paper, the isothermal compressibility of liquids can be directly measured with an accuracy of at least $\pm 0.4\%$.

Two other methods of measuring the fluid bulk modulus which are also commercially available (see for example Anton Paar (2011)) are the metal bellows piezometer and vibrating tube densitometer. In the metal bellows method (Tropea et al., 2007), the test fluid was sealed inside a metallic bellows. By applying external pressure to the bellows, the fluid volume was decreased and resulted in the reduction of the length of the bellows. The change in length was measured and used for the calculation of the volume change. Since volume reduction

measurement was made accurately, precise values of bulk modulus were obtained using this method (Tropea et al., 2007).

In a vibrating tube densitometer (Tropea et al., 2007), the fluid whose density needs to be measured is filled inside the tubular oscillator and subjected into harmonic oscillation. The vibration period of oscillation is dependent on the density of the sample in the tube. Therefore, by measuring the period of oscillation, the density or density-related values can be calculated to a high level of accuracy (Tropea et al., 2007). This density value can then be converted to a bulk modulus value.

In addition to the methods of measuring the isothermal secant bulk modulus, methods of measuring the adiabatic bulk modulus have also been developed under rapid compression and corrected for small heat flows which may occur. Ehlers (1960) introduced a method of measuring the adiabatic fluid bulk modulus using a Helmholtz resonator. The test fluid was placed inside a resonant chamber and vibrated using a diaphragm in the cavity. Adiabatic fluid bulk modulus was determined by finding resonant frequencies of the device.

Another common method of measuring adiabatic bulk modulus is to measure the velocity of sound in a fluid. The form of the bulk modulus obtained using velocity of sound measurements is limited to the adiabatic tangent form. Deriving the expression for the velocity of sound in any medium in terms of thermodynamic quantities can be found in almost every fluid mechanics text book, for example (Fox et al., 2009). By applying the conservation of mass and momentum to a differential control volume, the expression for the velocity of sound in a medium is found to be (Fox et al., 2009)

$$K_s = \rho C^2. \quad (2.17)$$

This relationship is valid for a lossless unbounded fluid at rest (Blackstock, 2000).

One common way of measuring the velocity of sound in fluids is through ultrasonic velocity measurements. Smith et al. (1960) mentioned three main methods of ultrasonic velocity measurements:

(a) Ultrasonic interferometer: Using a micrometer movement and interference of incident and reflected waves, the wave length can be directly measured. Knowing the wave length and frequency of the oscillator, the ultrasonic velocity can be calculated within 0.1% of accuracy.

(b) Pulse measurement: The delay time between the source and receiver can be measured. Knowing the time and the distance between the source and receiver, the velocity of sound in a fluid can be calculated within 0.1% or better.

(c) Optical measurement: In this method, a light ray that travels perpendicular to the sound wave is refracted. By measuring the refraction of the light, the wavelength of the sound wave can be calculated. The accuracy of bulk modulus calculations using this method is reported as approximately 1%.

2.7 Effective bulk modulus measurement techniques

In all of the previously mentioned methods, the fluid bulk modulus was determined by collecting a sample of the system fluid and making sure that there was no free or entrained air in the fluid. Those methods suffer a major drawback in which the actual operating conditions of the system were not considered.

The presence of air in hydraulic systems (which always changes with the pressure and temperature variations) and the elasticity of the container will affect the value of bulk modulus in hydraulic systems. The term “*effective bulk modulus (K_e)*” will be used from this point forward to show that these variables have been taken to account.

Different methods of measuring the effective bulk modulus have been presented by different researchers. Burton (1971) introduced a technique of estimating the fluid bulk modulus under actual operating conditions (which he defined as operational or effective bulk modulus) for a complex hydraulic system such as a pulsating flow system. The method used by Burton was based on the simulation of a hydraulic transmission line and comparing the simulated output with its experimental counterpart. The effective bulk modulus was estimated by finding the minimum difference between the simulated and actual outputs. However, the estimated value was not correlated to the amount of air in the hydraulic system.

Watton and Xue (1994) developed a method of measuring the effective bulk modulus by employing the theory of conservation of mass and using the formulation

$$K_e = \frac{V}{\left(\sum q_{in} - \sum q_{out} - \frac{dV}{dt} \right)} \frac{dP}{dt}, \quad (2.18)$$

to calculate the effective bulk modulus. $\frac{dV}{dt}$ represents piston or cylinder motion. Wall distortion as a result of pressure increase is assumed to be enclosed in the definition of effective bulk modulus.

Two flow meters and one pressure transducer which were capable of measuring the *transient* flow rate and *transient* pressure were needed. A rigid steel accumulator-type container and a long flexible hose were tested and the effective bulk moduli for the two components calculated. The repeatability of the measurements was reported to be within $\pm 5\%$.

Manring (1997) proposed a method for measuring the effective bulk modulus within a hydrostatic transmission system based on the conservation of mass within the system. He used *steady state measurements* of flow rate and pressure at the constant temperature of 50°C. Manring used the definition of tangent bulk modulus and derived an equation for instantaneous mass density of the fluid in each passage, by assuming a constant effective bulk modulus for the input, output and leakage passages. He showed that using the following equation

$$q_{in} = q_{out} \exp\left(\frac{P_{out} - P_{in}}{K_e}\right) + q_{leak} \exp\left(\frac{P_{leak} - P_{in}}{K_e}\right), \quad (2.19)$$

the unknown value of effective bulk modulus could be estimated knowing the volumetric flow rates (q_{in} , q_{out} and q_{leak}) and pressures (P_{in} , P_{out} and P_{leak}). The accuracy assessment by the author showed that the bulk modulus value obtained was acceptable within a range of ± 337 MPa. It should be noted that the assumption of constant effective bulk modulus in some instances may not be correct, since it is possible for the air to come out of solution in the inlet port of the motor which is the low pressure region, and which might change the effective bulk modulus.

Gholizadeh et al. (2010) established an experimental protocol in order to obtain reliable and repeatable measurements of oil filled pipes and hoses. Two methods of measuring the bulk modulus of oil filled pipes and hoses under static and isothermal conditions were chosen to show the importance of experimental set up in obtaining a reliable measurement of bulk modulus. It was concluded that the reliability of the results greatly depends on the testing procedure and uncertainty of the measurements.

One of the indirect ways to find the fluid bulk modulus which has also been part of the ISO standard is using the velocity of sound in the fluid (ISO/15086-2, 2000). Utilizing the velocity of sound to find the fluid bulk modulus has the advantage of avoiding errors of

measuring small volume changes in low working pressures. To facilitate the discussion of existing methods of measuring the velocity of sound in the fluid, the basics of propagation of sound in the fluid and the relationship between the bulk modulus and the velocity of sound are expanded upon in detail in Appendix C.

Yu and Kojima (2000) presented a summary of existing methods of measuring the velocity of sound in the fluid in a rigid pipe and then proposed a new method of measuring the velocity of sound in the fluid contained in a flexible tube. They categorized these methods as:

1. Cross correlation method: In this method, the cross correlation function of two dynamic pressure signals is calculated. This will give the wave propagation time from transducer 1 to 2 and by knowing the distance between the two pressure transducers, the velocity of sound can be calculated. This method has been used by Yu et al. (1994) to measure the effective bulk modulus of oil under different hydraulic system pressures. Using this method, the need to accurately calibrate the pressure transducer can be avoided. However, this method is not suitable for a piping system comprised of pipes with different materials. The change in the velocity of sound as a function of frequency cannot be also obtained using this method.
2. Three transducer method: Johnston and Edge (1991) used this method to measure the velocity of sound in high pressure transmission lines and from which the fluid bulk modulus could be calculated. This method is now a standard ISO method (ISO 15086-2, 2000) for measuring the velocity of sound. Unlike the cross correlation method which there is no need to understand the theory of pressure wave propagation, in the three transducer method, the theoretical understanding of the pressure wave propagation is vital. The appropriate value of the velocity of sound is found by measuring the pressure ripple at three positions throughout the pipeline. This method is very sensitive to the calibration of pressure transducers. An accuracy of $\pm 0.5\%$ over a broad frequency range has been claimed if the proper calibration of pressure transducers and suitable lengths between the transducers are chosen.
3. Anti resonance method: This method is also included in the ISO 15086-2 standard. A test pipe used in this method is a rigid pipe which is blocked at one end and two pressure transducers are used to measure the pressure ripple. On-line measurements of the velocity

of sound cannot be implemented using this method; however, it can be used to determine the velocity of sound under different off-line test conditions.

4. Transfer matrix method: Using this method, the velocity of sound can be measured in a fluid inside a soft tube. Although the velocity of sound can be measured in a soft tube, only the effective bulk modulus can be determined from this, and not the fluid bulk modulus. A test pipe (which can be a soft tube like a hose) is located between two uniform rigid pipes and then based on the measured and theoretically calculated dynamic transfer matrix parameters of the test pipe or pipe system, the unknown velocity of sound is determined.

Niezrecki et al. (2004) introduced a piezoelectric-based effective bulk modulus sensor. The displacement of piezoelectric stack transducers was used to estimate the effective bulk modulus. The authors used the secant bulk modulus definition to derive an equation relating the effective bulk modulus to parameters like the displacement of the actuator, cross sectional area and length of the actuator, modulus of elasticity of the piezoelectric material, area of the fluid column, length of the fluid, dielectric coefficient of the piezoelectric, applied voltage and the thickness of the actuator. The authors did not account for the effects of temperature or dynamic pressure in their study. Niezrecki et al. suggested that in order to enhance the response of the sensor in relation to the changes in bulk modulus, it was necessary to make the stiffness of piezoelectric actuator equal to the stiffness of the fluid. They concluded that more experimental work was needed to determine the applicability of this sensor.

In another similar work, Kim and Wang (2009) utilized measurements of the impedance of a piezoelectric transducer to estimate on-line effective bulk modulus. This idea was based on the fact that any change in the effective bulk modulus would affect the system resonant frequencies. The sensor composed of a piezoelectric stack transducer with a diaphragm joined to it and a fluid container. Simulation data were used to calibrate the sensor and to obtain curves that show the relationship between the change in bulk modulus and the impedance resonant frequency shift. The authors noted that, as an alternative of simulation data, offline measurement data can be also used for the calibration purpose of the device. Those calibration curves were then used to calculate the effective bulk modulus of a hydraulic system by on-line measuring of the impedance frequency response.

2.8 Summary

This Chapter has introduced the concept of fluid bulk modulus, the basic definitions and some of the important properties of this function. In addition, a summary of some of the literature from which this information was based, was also presented. In the next Chapter, some of the models which reflect the presence of air are considered.

CHAPTER 3: EFFECTIVE BULK MODULUS MODELS IN THE PRESENCE OF AIR

3.1 Introduction

As discussed in Chapter 2, fluid bulk modulus is a fluid property that has been studied extensively in the past. The numerical value of this property depends on the operating conditions, the amount of air, the way compression is applied and to some extent, the mathematical form it is defined. In the previous Chapter, an extensive review of fluid bulk modulus was presented. From this review, it was established that many models for fluid bulk modulus in the low pressure range (below critical pressure) have been forwarded. However, many of these models are based on assumptions that have not been explicitly defined. This Chapter considers these models and attempts to quantify the underlying assumptions. In addition some modifications to these models are proposed in order to compare their prediction in the case where air is entrained, for example. The Chapter concludes by categorizing the models into two groups and recommends the best model that can be used for each group. Finally some problems which observed in the models are discussed.

3.2 Volumetric fraction of air at atmospheric pressure

In a review of the literature in which the presence of air in oil has been considered, it was generally observed that different authors used different definitions for the volumetric fraction of the air at atmospheric pressure, which sometimes causes confusion and makes the comparison of the models difficult. Therefore, adopting one of these definitions as the “standard” definition was deemed necessary. In the next section the volumetric fraction of the air at atmospheric pressure used in various models where appropriate, will be changed to this standard definition. Thus, the following standard definition for the volumetric fraction of air at atmospheric pressure P_0 and temperature T is adopted,

$$X_0 = \frac{V_{g_0}}{V_{g_0} + V_{l_0}}, \quad (3.1)$$

where subscripts g and l represent gas and liquid, respectively. Assume that a unit volume of fluid is taken; therefore

$$\begin{aligned}
V_{g_0} + V_{l_0} &= 1 \\
X_0 &= V_{g_0} \\
1 - X_0 &= V_{l_0}
\end{aligned}
\tag{3.2}$$

For each of the models introduced, the definition of this parameter used by the various authors will be highlighted, and then where appropriate all of the models will be modified to follow this standard definition.

3.3 Models of the effective bulk modulus of an oil-air mixture

In practical hydraulic systems, fluid is a mixture of the basic fluid, dissolved air, air bubbles and sometimes vapor (Kajaste et al., 2005). In addition to the composition of the fluid, operating pressure and temperature as well as the mechanical compliance of hydraulic components would affect the fluid bulk modulus. To account for the effects of these variables on the fluid bulk modulus, different models have been proposed by different authors. In this section, some theoretical models that have been developed for the effective fluid bulk modulus are investigated. In terms of dealing with the air in the fluid, these models are categorized in two groups:

(a) “Compression only” models: Models which only consider the volumetric compression of the air; and

(b) “Compression and dissolve” models: Models which consider both the volumetric compression of the air and the volumetric reduction of the air due to air dissolving into solution.

The following sections will consider these groups. In this Chapter, the assumptions used for the development of each model and some modifications to the models will be introduced.

3.3.1 “Compression only” models

3.3.1.1 Merritt model

Merritt (1967) defined the effective bulk modulus model for an oil-air mixture in a flexible container. In his analysis, the following assumptions were made: secant bulk modulus was used to develop the model; air bubbles were assumed to be uniformly distributed throughout the oil; solubility of the air in the oil was not considered; air was treated as a perfect gas; surface

tension effects were neglected; and the oil and air were assumed to be at the same pressure and temperature.

The initial total volume is the sum of the initial volume of the oil and the air

$$V_0 = V_{g_0} + V_{l_0}. \quad (3.3)$$

By increasing pressure from P_0 to P , air and oil compress, but the container expands. The change in the total volume would be

$$\Delta V = -\Delta V_g - \Delta V_l - \Delta V_c. \quad (3.4)$$

The change in pressure is defined as ΔP which is $\Delta P = P - P_0$. By defining the secant effective bulk modulus as

$$\bar{K}_e = \frac{\Delta P V_0}{\Delta V}, \quad (3.5)$$

equation (3.5) can be written as

$$\bar{K}_e = \frac{\Delta P (V_{g_0} + V_{l_0})}{-\Delta V_g - \Delta V_l - \Delta V_c}, \quad (3.6)$$

and taking the inverse, yields

$$\frac{1}{\bar{K}_e} = \frac{-\Delta V_g - \Delta V_l - \Delta V_c}{\Delta P (V_{g_0} + V_{l_0})}, \quad (3.7)$$

then

$$\frac{1}{\bar{K}_e} = \frac{V_{g_0}}{V_0} \left(\frac{-\Delta V_g}{V_{g_0} \Delta P} \right) + \frac{V_{l_0}}{V_0} \left(\frac{-\Delta V_l}{V_{l_0} \Delta P} \right) + \left(\frac{-\Delta V_c}{V_{c_0} \Delta P} \right), \quad (3.8)$$

which results in

$$\frac{1}{\bar{K}_e} = \frac{1}{\bar{K}_c} + \frac{1}{\bar{K}_l} + \frac{V_{g_0}}{V_0} \left(\frac{1}{\bar{K}_g} - \frac{1}{\bar{K}_l} \right). \quad (3.9)$$

Using these assumptions the effective bulk modulus as presented by Merritt was defined as

$$\frac{1}{\bar{K}_e} = \frac{1}{\bar{K}_c} + \frac{1}{\bar{K}_l} + \frac{V_{g_0}}{V_0} \left(\frac{1}{\bar{K}_g} - \frac{1}{\bar{K}_l} \right). \quad (3.10)$$

In Eq. (3.10), \bar{K}_g represents the secant bulk modulus of the air; however, instead of replacing the secant bulk modulus formula in Eq. (3.10), Merritt has replaced it with the tangent bulk modulus formula for the air, which is

$$K_g = nP. \quad (3.11)$$

Assuming a rigid container; this model can be written as

$$\bar{K}_{Merritt} = \frac{\bar{K}_l}{1 + X_0 \left(\frac{\bar{K}_l}{nP} - 1 \right)}. \quad (3.12)$$

It should be noted that this model is the same as the model proposed by Wylie and Streeter (1983). An examination of Merritt model shows that in this model, the volumetric fraction of the air in the oil is always considered to be equal to the volumetric fraction of the air at atmospheric pressure and the effect of increasing pressure on the volumetric fraction of the air has not been considered. Since this has not been taken into account in this model, the effective bulk modulus value predicted in the Merritt model will be lower than the actual effective bulk modulus. This also shows that using the secant bulk modulus definition to find the effective bulk modulus leads to the lower effective bulk modulus values.

3.3.1.2 Nykanen-model

Nykanen et al. (2000) derived a two-phase model for an oil-air mixture. In this model, the effect of dissolving the air has not been considered. The bulk modulus definition used to develop his model was

$$K_{Nykanen} = \rho_0 \left(\frac{\partial P}{\partial \rho} \right). \quad (3.13)$$

This definition is not consistent with the standard definition of tangent bulk modulus in which ρ should be considered instead of considering ρ_0 which was defined as the initial density of the oil-air mixture. Volumetric fraction of the air at atmospheric pressure has been defined the same as the standard definition presented earlier in this Chapter. The initial density of the mixture was written as

$$\rho_0 = X_0 \rho_{g_0} + \rho_{l_0} (1 - X_0). \quad (3.14)$$

The final density of oil-air mixture was derived by

$$\rho = \frac{M_g + M_l}{V_g + V_l} = \frac{X_0 \rho_{g_0} + \rho_{l_0} (1 - X_0)}{\left(\frac{P_0}{P}\right)^{\frac{1}{n}} X_0 + \frac{1 - X_0}{\left(1 + \frac{1}{\bar{K}_l} (P - P_0)\right)}}. \quad (3.15)$$

Moreover, in order to find V_l based on the oil bulk modulus, Nykanen et al. used the secant bulk modulus form, that is

$$\bar{K}_l = -V_l \frac{P - P_0}{V_l - V_{l_0}}. \quad (3.16)$$

This definition is again in contrast with the standard secant bulk modulus definition which uses initial volume of fluid in the numerator. The derived equation for density is differentiated with respect to pressure and then multiplied by ρ_0 to determine the effective bulk modulus as follows

$$K_{Nykanen} = \frac{\left(\left(\frac{P_0}{P}\right)^{\frac{1}{n}} X_0 + \frac{1 - X_0}{1 + \frac{P - P_0}{\bar{K}_l}}\right)^2}{\frac{\left(\frac{P_0}{P}\right)^{\frac{1}{n}} X_0}{nP} + \frac{1 - X_0}{\left(1 + \frac{P - P_0}{\bar{K}_l}\right)^2 \bar{K}_l}}. \quad (3.17)$$

Assuming that $K_l \gg P$, the model is simplified as

$$K_{Nykanen} = \frac{\left(\left(\frac{P_0}{P}\right)^{\frac{1}{n}} X_0 + 1 - X_0\right)^2}{\frac{X_0}{nP} \left(\frac{P_0}{P}\right)^{\frac{1}{n}} + \frac{1 - X_0}{\bar{K}_l}}. \quad (3.18)$$

Figure 3.1 shows the difference between the Nykanen and Merritt models plotted for the specified conditions. Before comparing the models, it is important to mention that from this point

forward, all of the models will be compared based on the same assumed conditions of: $P_0 = 0.1$ MPa, $K_l = 1500$ MPa, $n = 1$ (isothermal condition) and $X_0 = 0.1$.

These conditions were arbitrary chosen just for comparison purposes. But for practical conditions, the real value of these parameters needs to be determined. Since for very small values of X_0 , the difference between the models was small, therefore, a larger value was chosen for X_0 in order to clearly show the differences between the models. It should be noted that none of the following models consider the effect of temperature on the oil bulk modulus (which is critical). Since the models were compared in the low pressure range (0 to 5 MPa), the effect of pressure on the oil bulk modulus was neglected and the constant value for the oil bulk modulus was assumed.

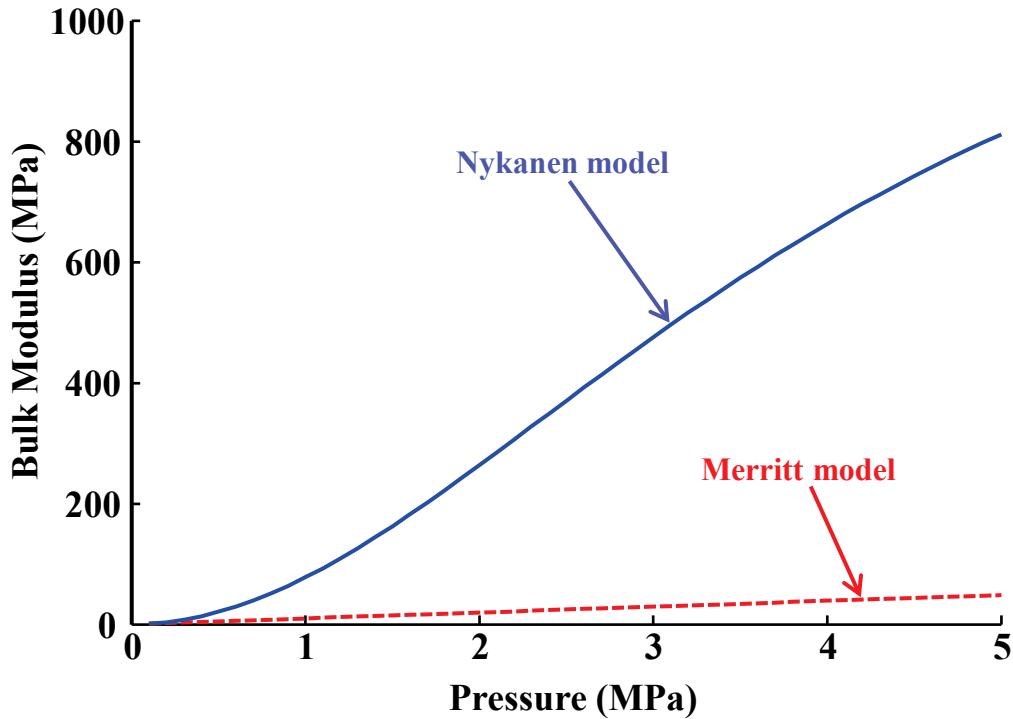


Figure 3.1 Comparison between the Nykanen and Merritt models

The Merritt model is based on the standard definition of secant bulk modulus, but the Nykanen model is based on the wrong definition of tangent bulk modulus. The problems related to the Merritt model were already discussed. For the Nykanen model, it can be observed that the effective bulk modulus does not converge to the specified oil bulk modulus ($K_l = 1500$ MPa) (see

Figure 3.2) because of the wrong definition used in deriving this model. Indeed, at very high pressures $K_{Nykänen} = (1 - X_0)K_l$.

3.3.1.3 Cho model

Cho et al. (2000) defined the effective bulk modulus model for an oil-air mixture in a rigid container. The assumptions are the same as Merritt model except that in this model, the definition of tangent bulk modulus has been used. The instantaneous total volume has been defined as the sum of the instantaneous volume of air and oil as

$$V = V_{gc} + V_l, \quad (3.19)$$

where V_{gc} is the instantaneous volume of air when it is only compressed in accordance with the ideal gas law. From the ideal gas law,

$$V_{gc} = \left(\frac{P_0}{P}\right)^{\frac{1}{n}} V_{g_0}, \quad (3.20)$$

and assuming a constant bulk modulus for oil, the instantaneous volume of oil is given by

$$V_l = V_{l_0} e^{-\frac{P-P_0}{K_l}}. \quad (3.21)$$

Therefore V becomes

$$V = \left(\frac{P_0}{P}\right)^{\frac{1}{n}} V_{g_0} + V_{l_0} e^{-\frac{P-P_0}{K_l}}. \quad (3.22)$$

Taking the derivative of this equation and inserting in the tangent bulk modulus formula, gives

$$K_{cho} = K_l \left[\frac{X_{cho} + \left(\frac{P}{P_0}\right)^{\frac{1}{n}} e^{-\frac{P-P_0}{K_l}}}{\frac{X_{cho}}{n} \frac{K_l}{P} + \left(\frac{P}{P_0}\right)^{\frac{1}{n}} e^{-\frac{P-P_0}{K_l}}} \right]. \quad (3.23)$$

Assuming that the oil bulk modulus is much larger than the pressure, the term $e^{-\frac{P-P_0}{K_l}}$ can be replaced by unity and the bulk modulus equation would be

$$K_{cho} = K_l \left[\frac{X_{Cho} + \left(\frac{P}{P_0} \right)^{\frac{1}{n}}}{\left(\frac{P}{P_0} \right)^{\frac{1}{n}} + \frac{X_{Cho} K_l}{n P}} \right]. \quad (3.24)$$

Cho et al. have defined the volumetric fraction of the air at atmospheric pressure as

$$X_{Cho} = \frac{V_{g0}}{V_{l0}}. \quad (3.25)$$

This can be compared with the X_0 as

$$X_{Cho} = \frac{X_0}{1 - X_0}. \quad (3.26)$$

If X_{Cho} is replaced in Eq. (3.24), the Cho model would be

$$K_{Cho} = \frac{\left((1 - X_0) + \left(\frac{P_0}{P} \right)^{\frac{1}{n}} X_0 \right)}{\frac{X_0}{nP} \left(\frac{P_0}{P} \right)^{\frac{1}{n}} + \frac{(1 - X_0)}{K_l}}. \quad (3.27)$$

Unlike the Nykanen model, the Cho model assumes the true definition of tangent bulk modulus. Thus, as it can be seen from Fig. 3.2 (which for comparison purposes, has been plotted to higher pressure values (0 to 30 MPa)), the Cho model converges to the specified oil bulk modulus (1500 MPa in this example) at higher pressure values and as such is more consistent with what would be expected at higher pressures than with the Nykanen model.

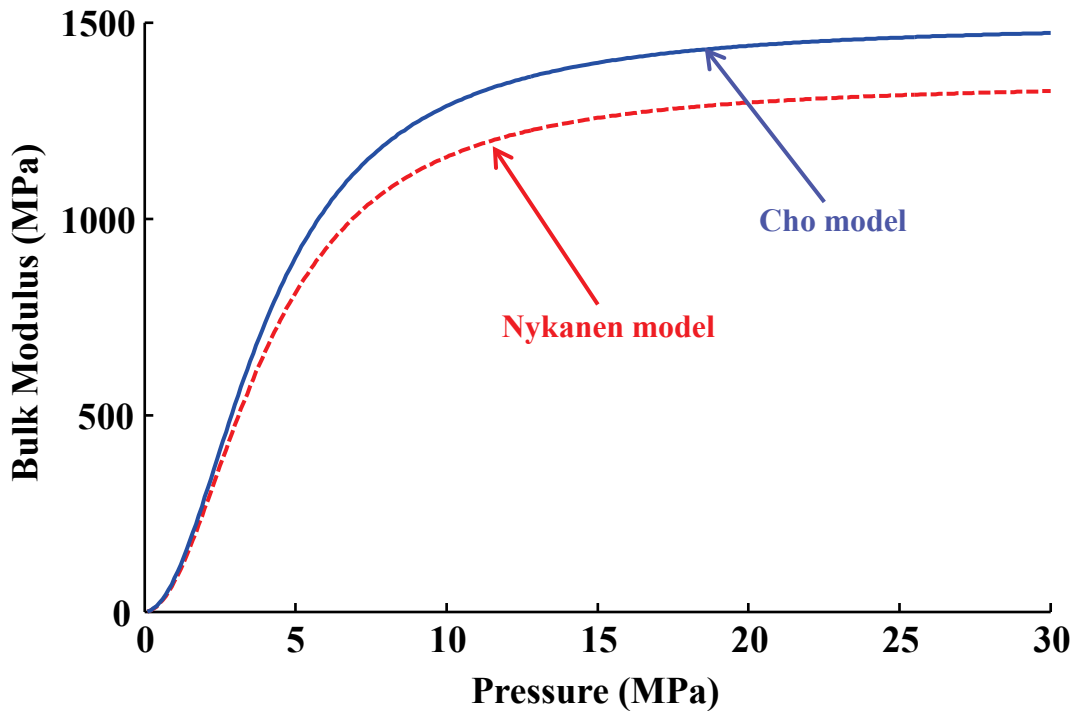


Figure 3.2 Comparison between the Nykanen and Cho models

3.3.1.4 Comparison of the compression only models

In the previous sections, it was observed that different authors used different definitions for the volumetric fraction of air at atmospheric pressure; therefore one of these definitions was adopted as the “standard” definition to provide a common base for comparison. For each of the models introduced, the definition of this parameter used by the authors was highlighted, and then where appropriate all of the models modified to follow this standard definition. It was also shown that using the secant bulk modulus definition to find the effective bulk modulus leads to lower effective bulk modulus values. Figure 3.3 clearly shows graphically that the secant bulk modulus of the mixture is different than its tangent bulk modulus (which is the true bulk modulus) in the lower pressure regions. For this reason, using the tangent bulk modulus definition is preferred.

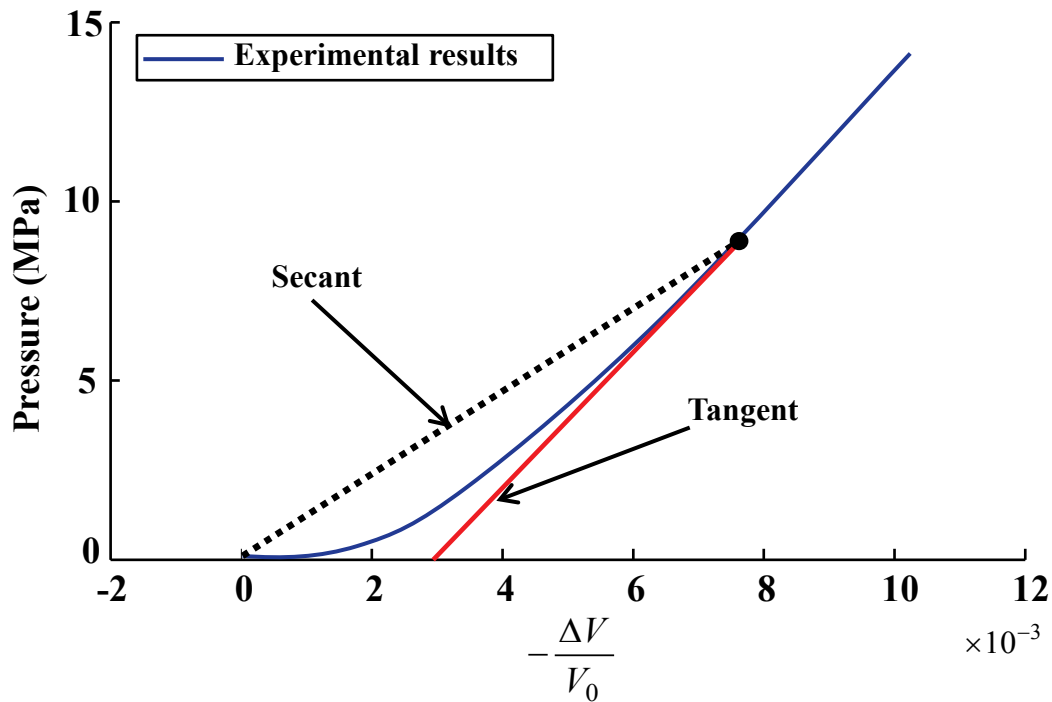


Figure 3.3 Secant and tangent bulk modulus representation

A summary of the investigated “compression only” models and their definitions used to develop the models is presented in Table 3.1.

Table 3.1 Summary of the investigated “compression only” models and their definitions for developing the models

Model	Definition of bulk modulus	Volumetric variation of air	Volumetric fraction of air definition
Merritt	Secant	Compression	$\frac{V_{g_0}}{V_{g_0} + V_{l_0}}$
Nykanen	Non-standard Tangent	Compression	$\frac{V_{g_0}}{V_{g_0} + V_{l_0}}$
Cho	Tangent	Compression	$\frac{V_{g_0}}{V_{l_0}}$

In developing Merritt and Nykanen models, the true definition of bulk modulus (tangent bulk modulus) has not been followed. This needs to be observed and corrected. In the Merritt

model, the volume of the mixture has been considered in developing the effective bulk modulus model. This is similar to the way that the Cho model has been developed. Since in the Cho model, the tangent bulk modulus definition has been followed to derive the effective bulk modulus model, it can be easily realized that modifying the Merritt model to follow the true bulk modulus definition, will result in the same model as the Cho model. It is also of interest to modify the Nykanen model to be consistent with the true definition of bulk modulus in which the final density is used, that is

$$K_e = \rho \left(\frac{\partial P}{\partial \rho} \right). \quad (3.28)$$

Using Nykanen's assumptions and equations, it can be shown that

$$\rho = \frac{M_g + M_l}{V_g + V_l} = \frac{X_0 \rho_{g_0} + \rho_{l_0} (1 - X_0)}{\left(\frac{P_0}{P} \right)^{\frac{1}{n}} X_0 + (1 - X_0) e^{-\frac{P - P_0}{K_l}}}, \quad (3.29)$$

where V_l is found using the tangent bulk modulus definition for the oil as

$$V_l = V_{l_0} e^{-\frac{P - P_0}{K_l}} = (1 - X_0) e^{-\frac{P - P_0}{K_l}}. \quad (3.30)$$

Replacing Eq. (3.29) into Eq. (3.28), the modified Nykanen model becomes

$$K_{\text{modified Nykanen}} = \frac{\left(\left(\frac{P_0}{P} \right)^{\frac{1}{n}} X_0 + (1 - X_0) e^{-\frac{P - P_0}{K_l}} \right)}{\frac{X_0}{nP} \left(\frac{P_0}{P} \right)^{\frac{1}{n}} + \frac{(1 - X_0) e^{-\frac{P - P_0}{K_l}}}{K_l}}. \quad (3.31)$$

In essence the modified Nykanen model is the same as the Cho model (Eq. (3.27)). This was expected, since the main differences between these two models were in the definition of the volumetric fraction of the air (which was adjusted to the standard definition) and in the way that the models were derived. In the modified Nykanen model, the density of the mixture of the air and oil was used to derive the effective bulk modulus, while in the Cho model the volume of the mixture has been considered. Since the total mass of the air and oil is always constant, it is expected that these two models should give the same results.

It can be concluded that the difference in the Merritt, Nykanen and Cho models is related to the definition of the volumetric fraction of air at atmospheric pressure and the way the effective bulk modulus is defined. By considering the true definition of bulk modulus (tangent bulk modulus) and the volumetric fraction of air at atmospheric pressure, it was found that all of these models are essentially representing the same model represented by Eq. (3.32) as

$$K_{ec} = \frac{\left(\left(\frac{P_0}{P} \right)^{\frac{1}{n}} X_0 + (1 - X_0) \right)}{\frac{X_0}{nP} \left(\frac{P_0}{P} \right)^{\frac{1}{n}} + \frac{(1 - X_0)}{K_l}}. \quad (3.32)$$

Equation (3.32) can be extended to include the pressure and temperature dependency of the oil bulk modulus (Kajaste et al., 2005). As it was discussed in Chapter 2, a linear function between the oil bulk modulus and pressure can be written as

$$K_l(P, T) = K_l(P_0, T) + m(P - P_0). \quad (3.33)$$

Combining the tangent bulk modulus definition of the oil and Eq. (3.33), an expression of the change in the volume of oil with pressure and temperature can be written as (Sunghun, 2012)

$$V_l(P, T) = V_l(P_0, T) \left(1 + \frac{m}{K_l(P_0, T)} (P - P_0) \right)^{-\frac{1}{m}}. \quad (3.34)$$

The extended form of Eq. (3.32) which relates the effective bulk modulus of an oil-air mixture to the volumetric variations of air due to only compression of air, and also due to the change in volume and bulk modulus of the pure oil as a function of pressure and temperature is given by

$$K_{ec} = \frac{V_l(P, T) + V_{gc}(P, T)}{\frac{V_l(P, T)}{K_l(P, T)} + \frac{1}{K_g} V_{gc}(P, T)}, \quad (3.35)$$

where

$$K_g = nP,$$

$$V_{gc}(P, T) = \left(\frac{P_0}{P} \right)^{\frac{1}{n}} \frac{T}{T_0} (X_0),$$

$K_l(P, T) = K_l(P_0, T) + m(P - P_0)$, and

$$V_l(P, T) = V_l(P_0, T) \left(1 + \frac{m}{K_l(P_0, T)} (P - P_0) \right)^{\frac{1}{m}}.$$

3.3.2 “Compression and dissolve” models

3.3.2.1 Determination of the volumetric variation of air content in oil

A review of the literature regarding the effective bulk modulus of the mixture of oil and air showed that there were inconsistencies in how the volumetric variation of air at different pressures and temperatures is determined when both compression and the dissolving of air into oil are considered. Therefore, before discussing this group of models, an analytical description of the change in volume of air as a function of pressure and temperature is given by applying the principle of mass conservation to a mixture of oil and air. In this analytical method, it is assumed that as pressure increases, the amount of air in oil decreases due to the fact that air is compressed via the ideal gas law and at the same time, starts to be dissolved into solution as dictated by Henry’s law.

Henry’s law for a mixture of air and oil can be written as (Manz and Cheng, 2007)

$$P = H \frac{N_{dg}}{N_{dg} + N_l}. \quad (3.36)$$

In Eq. (3.36), H represents Henry’s constant and N_{dg} and N_l represent the number of moles of dissolved air at pressure P and number of moles of oil, respectively. In Henry’s law it is assumed that the oil is in a thermodynamic equilibrium with air at absolute pressure P . Since usually $N_l \gg N_{dg}$, this equation simplifies to

$$P = H \frac{N_{dg}}{N_l}. \quad (3.37)$$

It is important to realize that this law refers to the thermodynamic equilibrium state; therefore, it is assumed that enough time is allowed for the mixture to reach an equilibrium state. As pressure increases, more of the entrained air is compressed and dissolved into the oil until the system pressure reaches a “critical pressure”. At this point it is assumed that all of the air is dissolved in the oil. Since it is well known that dissolved air has no effect on the bulk modulus of

oil, the fluid effective bulk modulus approaches that of pure oil once the critical pressure has been reached.

If it is assumed that the process is isothermal and under equilibrium conditions, according to the conservation of mass, the total moles of entrained and dissolved air are conserved. Therefore the sum of entrained and dissolved air at pressure P and temperature T is equal to the sum of entrained and dissolved air at pressure $P+dP$ and temperature T . That is

$$N_g(P, T) + N_{dg}(P, T) = N_g(P + dP, T) + N_{dg}(P + dP, T). \quad (3.38)$$

Therefore using the ideal gas law and Henry's law, Eq. (3.38) can be written as

$$\frac{PV_g}{RT} + \frac{PN_L}{H} = \frac{(P + dP)(V_g + dV_g)}{RT} + \frac{(P + dP)N_L}{H}. \quad (3.39)$$

Equation (3.39) can be simplified as

$$PV_g - \frac{N_L RT}{H} dP = (P + dP)(V_g + dV_g). \quad (3.40)$$

If the effect of air dissolving into oil is neglected, Eq. (3.40) will reduce to the well-known ideal gas law as

$$PV_g = (P + dP)(V_g + dV_g). \quad (3.41)$$

However, Eq. (3.40) shows that in order to include the effect of air dissolving into oil, the term $(\frac{N_L RT}{H} dP)$, which is due to air dissolving into oil, must be subtracted from the left side of the ideal gas law equation as a separate term. This model will be compared to other models found in the literature in later sections.

If Eq. (3.40) is rearranged and the following assumptions are made, V_g can be determined as follows. Assuming that Henry's law constant (H) does not change with temperature, it can be shown that $\frac{N_L R}{H}$ will always be a constant value λ . Assuming higher order differential products are negligible, Eq. (3.40) can be re-written as

$$\frac{-dV_g}{V_g + \lambda T} = \frac{dP}{P}. \quad (3.42)$$

It should be noted that the initial volume of entrained air is assumed to be measured at pressure P_0 and temperature T_0 . However, before starting compression it is possible for the

working temperature to be set at any temperature T . Therefore in defining the initial conditions for Eq. (3.42), the effect of temperature T on the volume of entrained air needs to be considered according to the ideal gas law. It means that when $P = P_0$, the volume of entrained air at temperature T is

$$V_g(P_0, T) = V_{g_0} \frac{T}{T_0}. \quad (3.43)$$

By solving the differential equation and applying the above initial conditions (P_0 , $V_g(P_0, T)$) the relationship between the volume of entrained air as a function of absolute pressure and temperature is obtained as Eq. (3.44). Note that the instantaneous volume of air which results from solving the differential equation (3.42) represents the instantaneous volume of entrained air as a result of the compression and loss of mass of entrained air due to dissolving; hence, from this point forward, this volume is represented by V_{gcd} ,

$$V_{gcd}(P, T) = \frac{P_0 V_{g_0}}{P} \frac{T}{T_0} + \left(\frac{P_0 - P}{P} \right) \lambda T. \quad (3.44)$$

From Eq. (3.44), it can be observed that the volume of entrained air changes with the isothermal pressure compression according to the expression $\frac{P_0 V_{g_0}}{P} \frac{T}{T_0}$. However, since the air is also being dissolved into solution, an additional volume reduction of $\left(\frac{P_0 - P}{P} \right) \lambda T$ will occur. In this later term, λ depends on the number of moles of oil, ideal gas constant (R) and Henry's law constant. As pressure increases, more air is dissolved into the oil, until the pressure reaches a critical pressure $P = P_C$, in which all the air becomes completely dissolved; at this point, the volume of entrained air is equal to zero. Therefore, the critical pressure can be described as

$$P_C = P_0 + \frac{P_0 V_{g_0}}{T_0} \frac{1}{\lambda}. \quad (3.45)$$

The value of λ can now be expressed in terms of P_C , that is

$$\lambda = \frac{N_L R}{H} = \frac{P_0 V_{g_0}}{(P_C - P_0) T_0}. \quad (3.46)$$

Substituting Eq. (3.46) into Eq. (3.44), the volumetric change of entrained air mixed in oil when pressure is less than the critical pressure ($P < P_C$) is found to be

$$V_{\text{gcd}}(P, T) = \frac{P_0 V_{g_0}}{P} \frac{T}{T_0} \left(\frac{P_C - P}{P_C - P_0} \right) \quad P < P_C . \quad (3.47)$$

For pressures equal to or higher than the critical pressure, all the air will be dissolved in the oil and the volume of entrained air will be zero. That is

$$V_{\text{gcd}}(P, T) = 0 \quad P \geq P_C . \quad (3.48)$$

In Eq. (3.47), the term $\frac{P_0 V_{g_0}}{P} \frac{T}{T_0}$ is due to the compression of air at pressure P and temperature T and the term $\left(\frac{P_C - P}{P_C - P_0} \right)$ is due to the effect of air dissolving into oil which is now defined as θ . Therefore

$$V_{\text{gcd}}(P, T) = \frac{P_0 V_{g_0}}{P} \frac{T}{T_0} \theta , \quad (3.49)$$

where

$$\theta = \left(\frac{P_C - P}{P_C - P_0} \right) . \quad (3.50)$$

Equations (3.49) and (3.50) represent the volumetric variation of air in the oil when both compression and the dissolving effect of air under isothermal conditions are considered. Equation (3.50) can be also shown graphically in Fig. 3.4 where θ , which is the volumetric fraction of entrained air, is equal to 1 at atmospheric pressure. As pressure increases, the value of θ decreases linearly until it reaches zero at the critical pressure. Equations (3.49) and (3.50) will be used later to derive the effective bulk modulus of a mixture of oil and air.

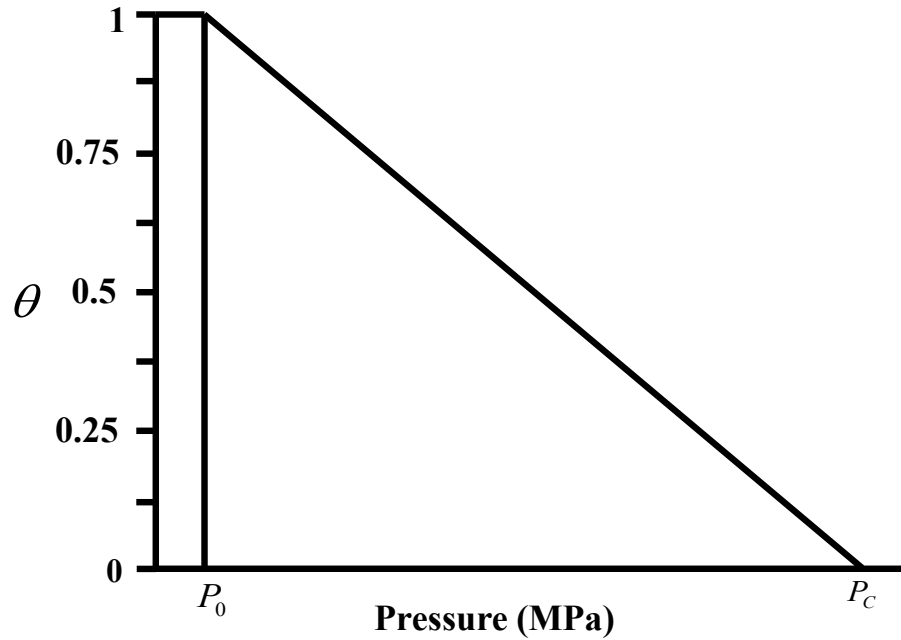


Figure 3.4 Volumetric fraction of air (θ) versus pressure (Henry's law)

3.3.2.2 Yu model

Yu et al. (1994) developed a theoretical model which was based on the definition of tangent bulk modulus. The measurements taken in their experimental work was based on the measurement of the velocity of sound because it was believed that the approach gave the isentropic (adiabatic) tangent bulk modulus values.

The method used by Yu et al. to derive the effective bulk modulus of an oil-air mixture is similar to the Merritt method. In the Yu model, in order to include the dissolving effect of air, a new constant named c_l was introduced. c_l was defined as the coefficient of air bubble volume variation due to the variation of the ratio of the entrained and dissolved air content in oil. Since the mass of the entrained air is changing by considering the dissolving effect, the following polytropic equation was used,

$$\left(V_{g_0} - c_l V_{g_0} (P - P_0) \right)^n P_0 = P V_{g_{cd}}^n. \quad (3.51)$$

Using the tangent bulk modulus definition, the effective bulk modulus derived by Yu et al. becomes

$$\frac{1}{K_{Yu}} = \frac{V_{gcd}}{V} \left(\frac{1}{K_g} \right) + \frac{V_l}{V} \left(\frac{1}{K_l} \right). \quad (3.52)$$

V_{gcd} found in Eq. (3.51) is used in Eq. (3.52). Considering the above discussion, the Yu model becomes

$$K_{Yu} = \frac{K_l \left(1 + \frac{P_g}{P_0} \right)^{1+\frac{1}{n}}}{\left(1 + \frac{P_g}{P_0} \right)^{1+\frac{1}{n}} + \frac{X_{Yu}}{P_0} (1 - c_1 P_g) \left(\frac{K_l}{n} - P_0 - P_g \right)}. \quad (3.53)$$

In this model, pressures have been expressed in gauge pressure and in order to be comparable with the other models, the pressures in this equation are changed to be with respect to absolute pressure. Thus every P_g in this equation is changed to $P - P_0$. Eq. (3.54) shows the Yu model where the pressures are expressed in absolute pressure,

$$K_{Yu} = \frac{K_l}{1 + X_{Yu} \left(\frac{P_0}{P} \right)^{\frac{1}{n}} (1 - c_1 (P - P_0)) \left(\frac{K_l}{nP} - 1 \right)}. \quad (3.54)$$

In the Yu model, despite the fact that the pressure range that they considers in their paper is high (up to 30 MPa), the pressure dependence of oil bulk modulus was not included. The values of X_{Yu} , c_1 and K_l were initially unknown and had to be determined using the identification method explained in their paper and were found to be $n = 1.4$, $c_1 = -9.307 \times 10^{-6}$, $K_l = 1701$ MPa and $X_{Yu} = 4 \times 10^{-5}$ (Yu et al., 1994).

The effective bulk modulus model proposed by Yu et al. is plotted as a function of pressure in Fig. 3.5 and is based on parameter values obtained using their identification method. This plot is different than that given in Yu et al.'s paper and the reason for this discrepancy is not known.

The identification method used by Yu is valid when the identified parameters are constant. For constant temperature and pump operating conditions, Yu et al. has assumed that these parameters are fixed. However, X_{Yu} has been defined in a way that is a function of pressure and X_{Yu} is defined (in their paper shown by R) as the entrained air content by volume in oil at atmospheric pressure, but mathematically it is shown as

$$X_{Yu} = \frac{V_{g0}}{V_{gcd} + V_l} \quad (3.55)$$

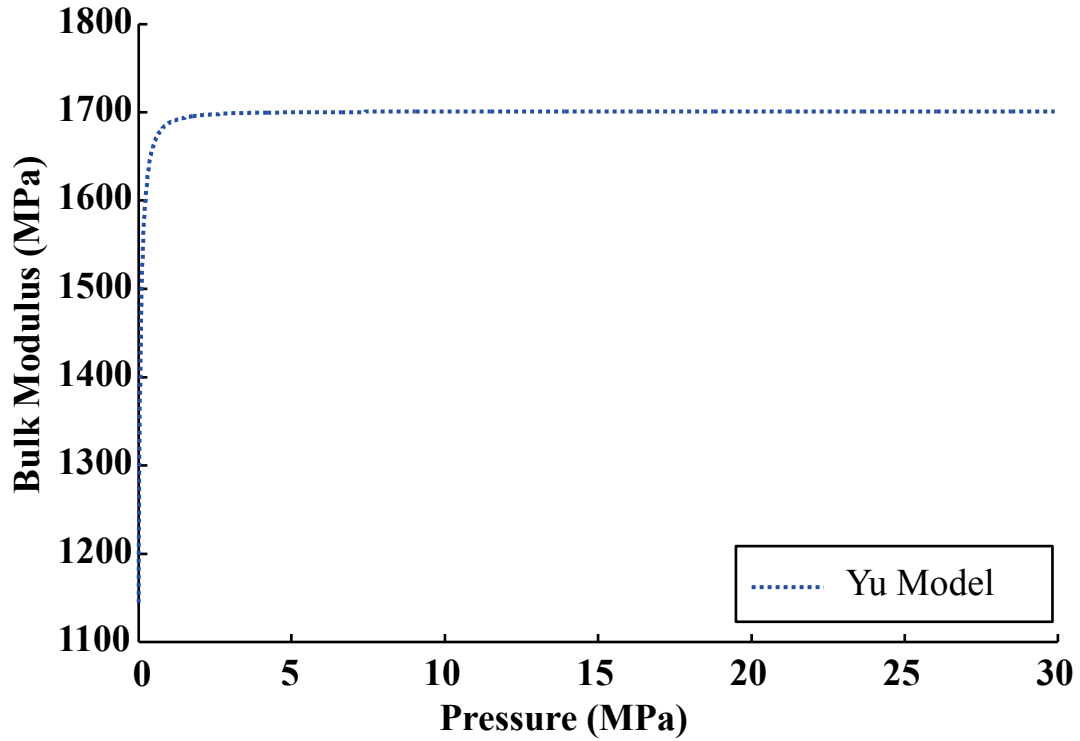


Figure 3.5 Plot of the Yu model based on the parameters obtained using the identification method

In Eq. (3.55), the variations of the oil volume can be neglected for the low pressure range but the final volume of air (V_g) will change dramatically by increasing pressure even in the low pressure range. Therefore, X_{Yu} will be a function of pressure. It should be also noted that after a critical pressure in which all of the air will dissolve in the oil, the value of c_l will be zero. Therefore c_l is also a function of pressure. Since these two parameters are not constant and are a function of pressure, the validity of the identification method may be suspect.

Yu et al. have also provided the simplified form of their model by assuming $c_l = 0$ which means the air dissolving effect is neglected. Considering this assumption, the Yu model will be reduced to

$$K_{Yu_reduced} = \frac{K_1}{1 + X_{Yu} \left(\frac{P_0}{P} \right)^{\frac{1}{n}} \left(\frac{K_1}{nP} - 1 \right)} \quad (3.56)$$

Eq. (3.56) is the same as the modified Wylie model proposed by Kajaste et al. (2005). However, it should be noticed that the X_{Yu} in Eq. (3.56) must be replaced by

$$X_{Yu} = \frac{V_{g_0}}{V_{g_0} \left(\frac{P_0}{P} \right)^{\frac{1}{n}} + V_{l_0}} = \frac{X_0}{V_{g_0} \left(\frac{P_0}{P} \right)^{\frac{1}{n}} + (1 - X_0)}. \quad (3.57)$$

Therefore Eq. (3.56) becomes

$$K_{Yu_reduced} = \frac{\left((1 - X_0) + \left(\frac{P_0}{P} \right)^{\frac{1}{n}} X_0 \right)}{\frac{X_0}{nP} \left(\frac{P_0}{P} \right)^{\frac{1}{n}} + \frac{(1 - X_0)}{K_l}}. \quad (3.58)$$

This is the same as the Cho and modified Nykanen models. It is therefore concluded that the Cho, modified Nykanen and Yu reduced models are the same model when the effect of air dissolving in the oil is not included and when the same definition for the volumetric fraction of air at atmospheric pressure is used.

3.3.2.3 LMS model

A comprehensive fluid bulk modulus model (LMS Model) is used in a commercial software AMESim developed by LMS IMAGINE S.A., (2008). Four cases have been considered in AMESim:

- 1) $P > P_{sat}$: There is no vapor and all air is dissolved.
- 2) $P_{vap}^H < P < P_{sat}$: There is no vapor and part of the air is dissolved and part entrained.
- 3) $P_{vap}^L < P < P_{vap}^H$: There is some vapor and all the air is entrained.
- 4) $P < P_{vap}^L$: There is vapor and air but no oil.

It is of interest to examine the second region, where the pressure is between the high vapor pressure and the saturation (or critical) pressure. It can be shown that P_{sat} is the same as P_C . In the following analysis, another modification to the LMS model is that P_{vap}^H has been replaced with P_0 . This change is due to the fact that the reference condition to measure the

amount of entrained air was considered to be at atmospheric pressure. This will also make the model comparable to the other models.

A different method of defining the volumetric fraction of air at atmospheric pressure and at 273K has been used by LMS. In this model, it was assumed that all the air, including the dissolved air, is separated from the fluid and stored at atmospheric pressure and at 273K. Another difference with respect to the standard definition of the proposed volumetric fraction of entrained air (Eq. (3.1)) is that a unit volume of oil at atmospheric pressure and 273K is considered. Therefore, the volumetric fraction of air for LMS model would be

$$X_{LMS} = \frac{V_{(gt)_0}}{V_{l_0} + V_{(gt)_0}} = \frac{V_{(gt)_0}}{1 + V_{(gt)_0}}. \quad (3.59)$$

Since X_{LMS} has been defined in a totally different manner than the proposed standard definition (Eq. (3.1)), it was decided not to change the formula of X_{LMS} to be consistent with the proposed standard definition X_0 . Instead, the derivation of the LMS effective bulk modulus will be explained and the results will be interpreted with respect to the proposed standard method (Eq. (3.1)).

In the LMS model, the following assumptions are made by LMS: air bubbles are uniformly distributed within the system, dissolved air molecules do not influence the bulk modulus of pure oil and the mass of oil with dissolved air is more than the mass of pure oil, but the volume of pure oil does not change because of the dissolved air molecules.

For the case that $P > P_C$ (recall, P_C is the same as P_{sat}) it is assumed that there is no entrained air and all of the air is dissolved in the hydraulic oil. In this case, the fluid bulk modulus is equal to the oil bulk modulus.

For the case that $P_{vap}^H < P < P_C$, the assumption is made that just a volume fraction of air (θ) is entrained and the remainder of air which is dissolved in the oil causes an increase in the mass of pure oil (Note: small air molecules hide themselves between the bigger oil molecules, therefore it is assumed that they become part of the oil, with no change in the volume of pure oil, but an increase in the mass of pure oil). The volumetric change of entrained air mixed in oil when pressure is less than the critical pressure ($P < P_C$) is expressed in the LMS model as

$$V_{\text{gcd}} = \left(\frac{P_0}{P}\right)^{\frac{1}{n}} V_{g_0} \left(\frac{P_C - P}{P_C - P_0}\right). \quad (3.60)$$

The LMS effective bulk modulus model was derived considering the change in the density of the fluid as pressure increases. The total mass of fluid (mass of entrained and dissolved air plus the mass of pure oil) at pressure P and temperature T was found to be

$$M = V_{l_0} \rho_{l_0} + V_{g_0} \rho_{g_0} + V_{gd_0} \rho_{gd_0}. \quad (3.61)$$

Eq. (3.61) shows that dissolved air increases the mass of pure oil, but does not affect the effective bulk modulus of the fluid. Since Eq. (3.61) shows that the total mass is always constant, it is evident in Eq. (3.62) that the effective bulk modulus can be obtained using either the density or volume of the fluid and the result will be the same.

$$K_e = \rho \frac{dP}{d\rho} = -V \frac{dP}{dV}. \quad (3.62)$$

The LMS effective fluid bulk modulus formula at pressure P and temperature T can then be expressed as

$$K_{LMS} = \frac{V_{l_0} + V_{g_0} \theta \frac{T}{273} \left(\frac{P_0}{P}\right)^{\frac{1}{n}}}{\frac{V_{l_0}}{K_l} + \frac{T}{273} \left(\frac{P_0}{P}\right)^{\frac{1}{n}} \left(\frac{\theta V_{g_0}}{nP} - V_{g_0} \frac{d\theta}{dP}\right)}. \quad (3.63)$$

In deriving Eq. (3.63), the LMS assumed a constant oil bulk modulus and that $K_l \gg P$. Simplifying Eq. (3.63) and writing it in terms of the nomenclature used in this manuscript, yields

$$K_{LMS} = \frac{1 + \left(\frac{T}{273}\right) \left(\frac{P_0}{P}\right)^{\frac{1}{n}} \left(\frac{X_0}{1 - X_0}\right) \left(\frac{P_C - P}{P_C - P_0}\right)}{\frac{1}{K_l} + \left(\left(\frac{P_0}{P}\right)^{\frac{1}{n}} \frac{T}{273} \frac{X_0}{1 - X_0} \frac{1}{P_C - P_0}\right) \left(\frac{P_C - P}{nP} + 1\right)}. \quad (3.64)$$

Figure 3.6 shows the plot of the LMS model with respect to pressure. Note that the critical pressure value was chosen to be 2 MPa for comparison purposes. The actual value of the critical pressure needs to be determined experimentally.

Figure 3.6 reveals that the LMS model has a discontinuity at the critical pressure where the gas phase disappears. This discontinuity is related to the derivative of the θ function which is not continuous at the critical pressure. Since this discontinuity can be a source of difficulties when applying numerical integration, another approach was used by LMS which mathematically, smoothed out the discontinuities at $P = P_C$ and $P = P_0$. In this thesis, this new approach is labeled as the “modified Henry’s law”. This is shown in Fig. 3.7.

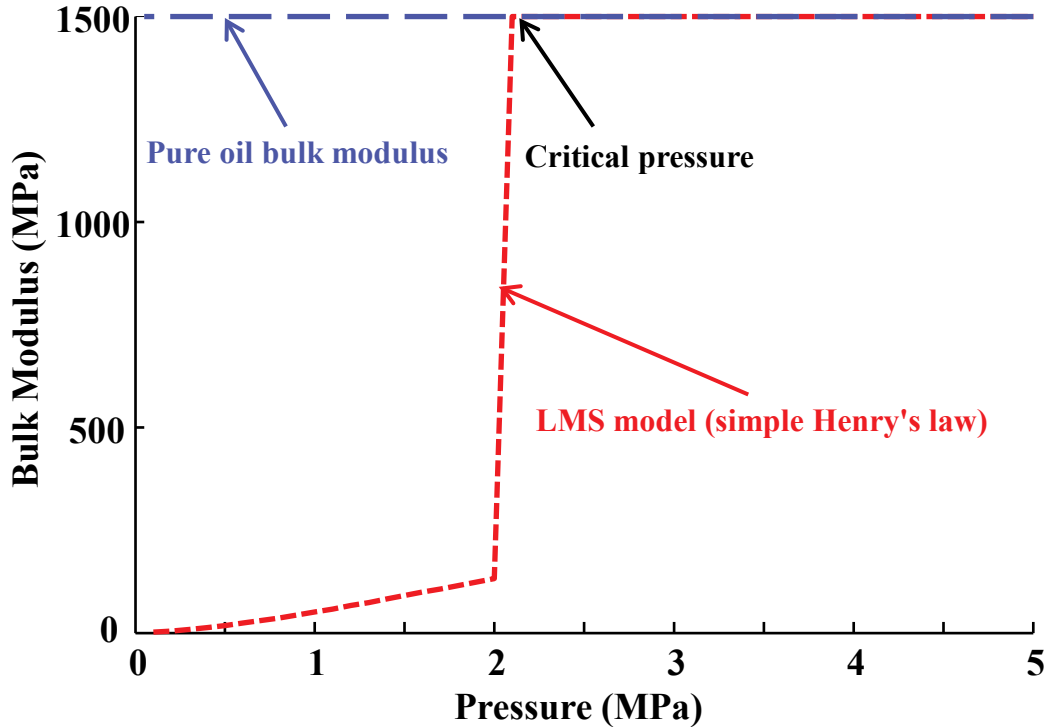


Figure 3.6 Plot of the LMS model based on the specified conditions. Note the discontinuity at the critical pressure.

In the LMS model, a new θ was proposed based on a modified Henry’s law, and was expressed as

$$\theta = (1 - y)^5 (1 + 5y + 15y^2 + 35y^3 + 70y^4)$$

$$y = \frac{P - P_0}{P_C - P_0} \quad (3.65)$$

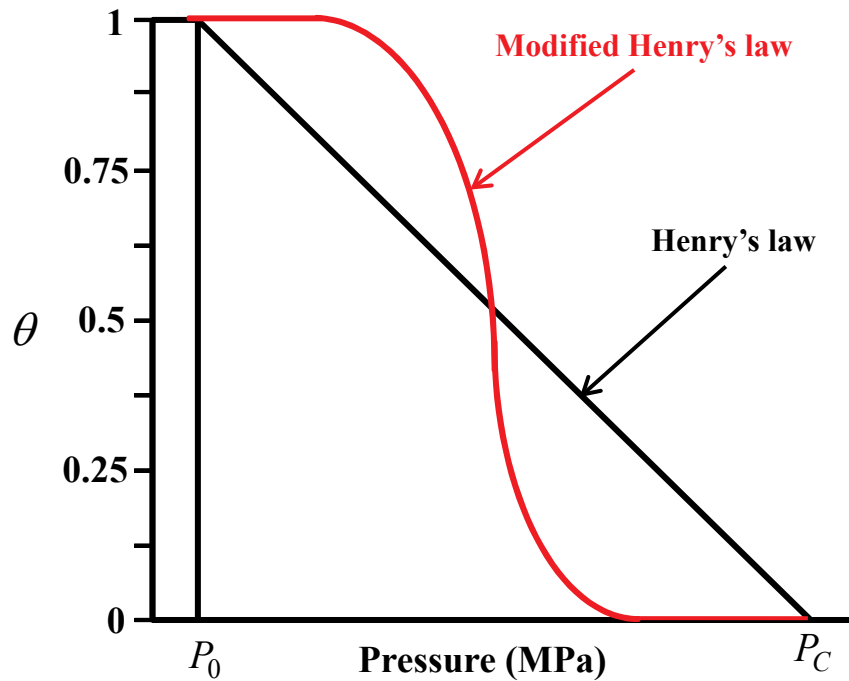


Figure 3.7 Modified Henry's law used in the LMS model

Figure 3.8 compares the LMS model (simple Henry's law) with the LMS model (modified Henry's law). As mentioned above, in the LMS model (simple Henry's law), there is a jump (discontinuity) in the bulk modulus value at the critical pressure point. In addition, the derivative of the bulk modulus at this point is also discontinuous. To compensate for these two problems, a smoothing function was used (Eq. (3.65)) which is shown in Fig. 3.7 as the modified Henry's law. This technique is not based on the true "physics" of what is really happening (when the air is both compressed and dissolved), but is only a mathematical smoothing approach. This will be investigated more in the next Chapter.

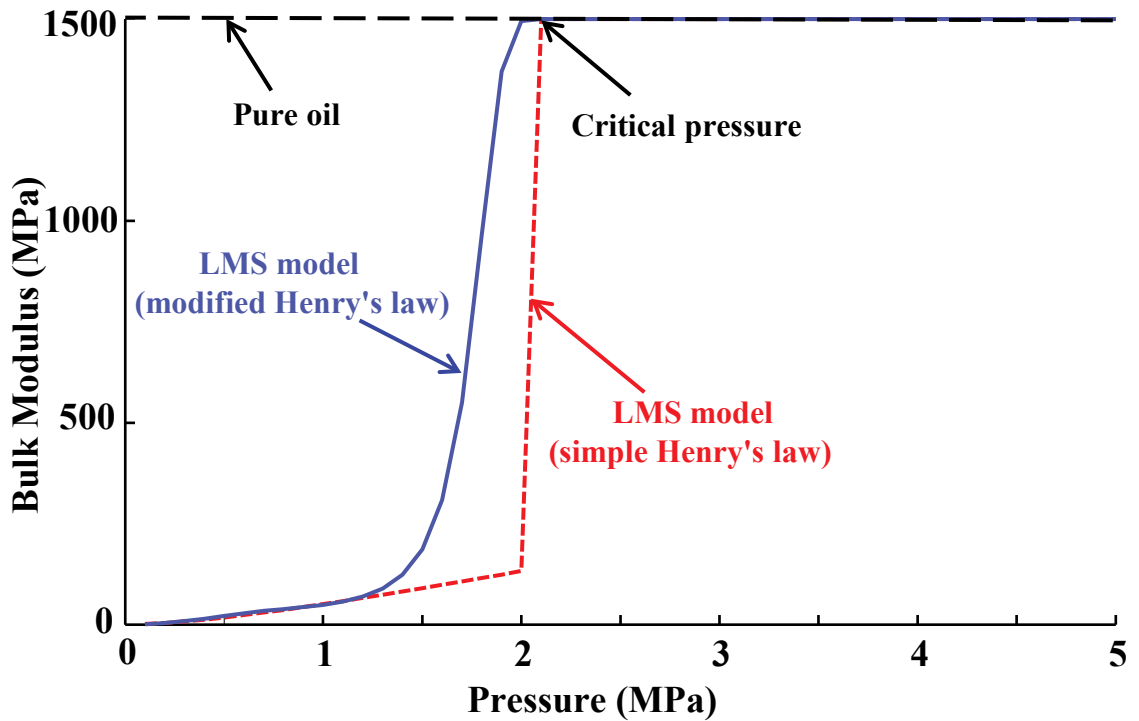


Figure 3.8 Comparison of the LMS models at specified conditions

3.3.2.4 Ruan and Burton model

Ruan and Burton (2006) developed a model of fluid effective bulk modulus which considers both the volumetric compression and volumetric reduction of the air due to the air dissolving in the oil. In their model, after some critical pressure, all the air completely dissolves in the oil and the effective bulk modulus becomes equal to the oil bulk modulus. They studied the fluid effective bulk modulus below this critical pressure and found that the critical pressure is proportional to the square root of the volume of the entrained air and the polytropic constant. They assumed an isothermal compression and used the polytropic equation of ideal gas in order to find the volumetric variation of the entrained air bubbles. They included the effect of volumetric reduction of air due to air dissolving in the oil and derived a differential equation to describe its behavior. Solving this differential equation, the volumetric change of the entrained air below the critical pressure for isothermal compression ($n = 1$) of the entrained air was found to be

$$V_{\text{gcd}} = \frac{P_0}{P} V_{g_0} \left(\frac{P_C^2 - P^2}{P_C^2 - P_0^2} \right). \quad (3.66)$$

It is of interest to notice that Eq. (3.66) is different from Eq. (3.47) where the volumetric variation of air was determined using the principle of mass conservation. The reason for this difference is that in Ruan and Burton's work, the volumetric variation of entrained air for isothermal conditions was determined using the differential equation

$$PV_g = (P + dP)(V_g + dV_g + \alpha dP), \quad (3.67)$$

where α is defined as the coefficient of dissolubility.

In Eq. (3.67), the initial state of the entrained air was specified as P and V_g . By increasing pressure to $(P+dP)$, the total change in volume of the entrained air was considered to be the change in volume of the air due to compression plus the change in volume due to dissolving. However, the extra term αdP inserted in Eq. (3.67) is not the same as Eq. (3.40) where $(PV_g - \alpha dP) = (P + dP)(V_g + dV_g)$ which was derived based on the principle of mass conservation (explained in section 3.3.2.1). According to Eq. (3.40), the term αdP which shows the volume of air dissolving into the oil, should instead be subtracted from the left side of the ideal gas law equation as a separate term $(PV_g - \alpha dP)$ to make it consistent with the principle of mass conservation.

If the volumetric variation of the air found by Ruan and Burton is modified to be the same as in Eq. (3.47), the modified Ruan and Burton model for the range of $(P < P_C)$ will essentially be the same as the LMS model.

$$K_{\text{modified Ruan \& Burton}} = \frac{1 + \left(\frac{P_0}{P} \right)^{\frac{1}{n}} \left(\frac{X_0}{1 - X_0} \right) \left(\frac{P_C - P}{P_C - P_0} \right)}{\frac{1}{K_l} + \left(\left(\frac{P_0}{P} \right)^{\frac{1}{n}} \left(\frac{X_0}{1 - X_0} \right) \frac{1}{P_C - P_0} \right) \left(\frac{P_C - P}{nP} + 1 \right)}. \quad (3.68)$$

3.3.2.5 Comparison of the compression and dissolve models

A summary of the investigated models and their definitions used to develop the models is presented in Table 3.2.

Table 3.2 Summary of the investigated models and their definitions for developing the models

Model	Definition of bulk modulus	Volumetric variation of air	Volumetric fraction of air definition
Yu	Tangent	Compression and dissolving	$\frac{V_{g_0}}{V_g + V_l}$
Ruan & Burton	Tangent	Compression and dissolving	$\frac{V_{g_0}}{V_g + V_l}$
LMS	Tangent	Compression and dissolving	$\frac{V_{(gt)_0}}{V_{(gt)_0} + V_{l_0}}$

In developing all the above mentioned models, the true definition of bulk modulus (tangent bulk modulus) was followed. The identification method used in the Yu model to find the unknown parameters was questioned. Modifying the Ruan and Burton model, resulted in the same model as the LMS model. In developing these two models it was assumed that after reaching the critical pressure (P_C), the air would be completely dissolved in the oil and the effective bulk modulus would be equal to the pure oil bulk modulus. This effect can be seen in Fig. 3.8 where the curve LMS model (simple Henry's law) reaches the pure oil bulk modulus very quickly at the critical pressure. The actual value of the critical pressure needs to be determined experimentally. Since the pressure range is low, it was assumed that the pure oil bulk modulus is constant and does not increase with increasing pressure.

3.4 Summary and Discussion

Bulk modulus is one of the most important parameters in fluid power applications because it reflects a system's stiffness. It is known that the presence of air in fluid has a substantial effect on the fluid bulk modulus. Since beyond the critical pressure, all the entrained air is dissolved, the density and fluid bulk modulus can be assumed to be the same as the oil and as a result, the measuring and modeling methods for these high pressure systems are quite

straightforward. But in the low pressure regions (below the critical pressure) where the effect of entrained air is substantial, it is important to be able to measure or predict the effective bulk modulus. The main purpose of this Chapter was to consider and compare different theoretical models for this low pressure region and make suggestions for improvement.

It was observed that different authors used different definitions for the volumetric fraction of air at atmospheric pressure; therefore one of these definitions was adopted as the “standard” definition to provide a common base for comparison. For each of the models introduced, the definition of this parameter used by the authors was highlighted, and then where appropriate, all of the models were modified to follow this standard definition. It was also shown that using the secant bulk modulus definition to find the effective bulk modulus leads to lower effective bulk modulus values (Merritt’s model) and using the tangent bulk modulus definition is preferred. Some authors have used definitions of tangent bulk modulus which deviate from the basic definition of tangent bulk modulus.

In terms of dealing with the air in the oil, the models can be categorized into two groups:

a) “Compression only” models: models with volumetric compression of air.

The models by Merritt, Nykanen, and Cho were introduced. After comparing and modifying these models, it was found that the difference in some models related to the definition of the volumetric fraction of air at atmospheric pressure and the way the effective bulk modulus is defined. By considering the same definition of bulk modulus and the volumetric fraction of air at atmospheric pressure, it was found that the modified Merritt, modified Nykanen and Cho models essentially represent the same model. Therefore, the model represented in Eq. (3.32) or Eq. (3.35) is recommended for this group of the models.

Figure 3.9 represents the plot of Eq. (3.32) for both the isothermal and adiabatic compression of air and it is evident that there is a big difference in the fluid bulk modulus value for two extreme cases of polytropic constants. The plot shows that depending on the actual polytropic constant (which can be any value between isothermal ($n = 1$) and adiabatic ($n = 1.4$)), the fluid bulk modulus can be any curve between these two curves. Consequently, it is essential to experimentally find the actual value of these polytropic constants.

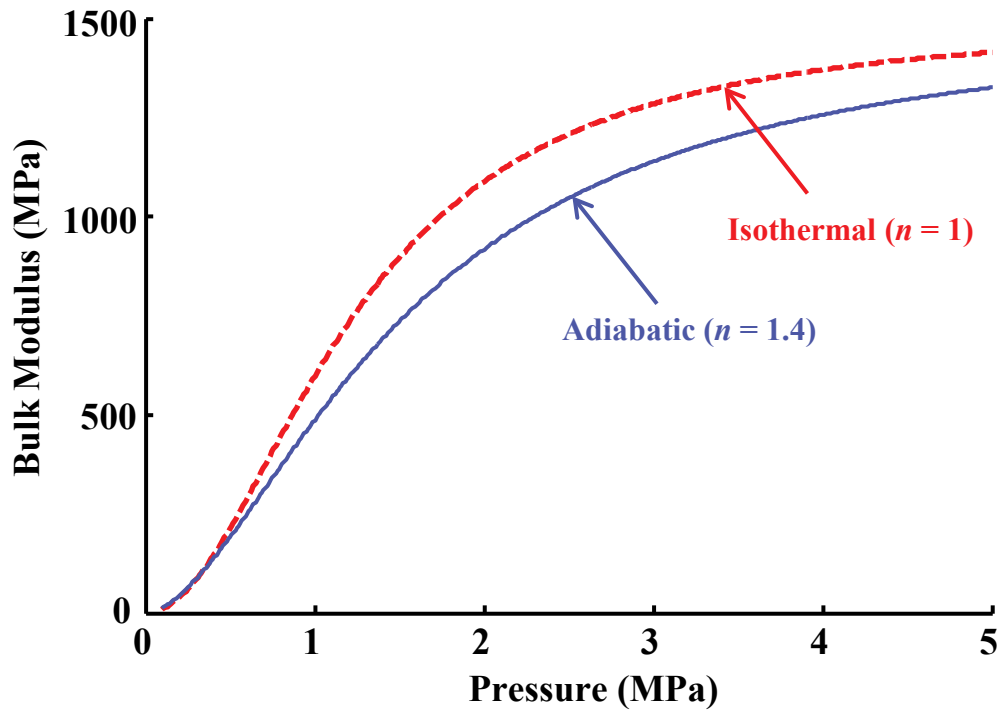


Figure 3.9 Comparison of compression only model for isothermal and adiabatic compression of air when $X_0 = 0.1$

Figures 3.9 and 3.10 also show that except at very low pressure values, the effective bulk modulus resulting from the isothermal compression of air is always higher than the adiabatic one. A detailed view of the low pressure region is shown in Fig. 3.10 where from 0 to 0.35 MPa, the effective bulk modulus resulting from adiabatic compression of air is higher than the isothermal one. This behavior can be explained by the fact that at lower pressures, the effect of adiabatic bulk modulus of air on the effective bulk modulus has more influence than the effect of the change in volume of the air. Since air has a higher adiabatic bulk modulus value, the change in volume of the air will be very slow until it reaches the equilibrium point. After this point, the change in the air volume will be dominant on the effective bulk modulus and as a result, the adiabatic process will give lower effective bulk modulus values (Sunghun, 2012).

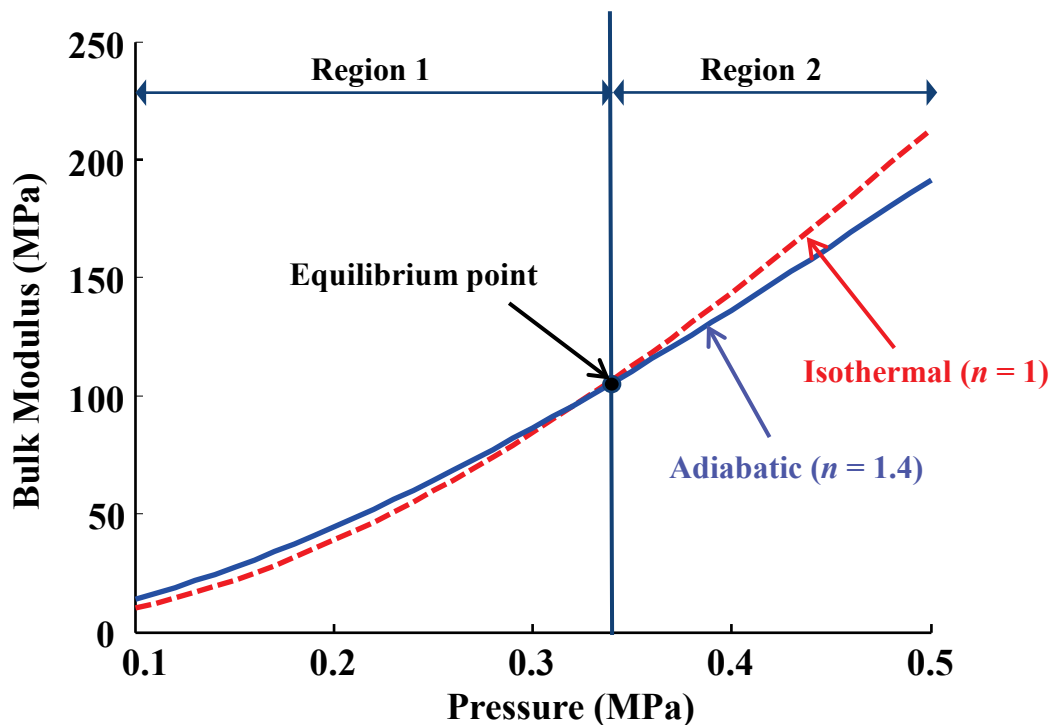


Figure 3.10 Comparison of compression only model for isothermal and adiabatic compression of air at low pressure when $X_0 = 0.1$

- b) “Compression and dissolve” models: models with both the volumetric compression and volumetric reduction of air due to air dissolving into solution.

The Yu, modified Ruan and Burton and LMS models were investigated. In the Yu model, there was a problem identifying some of the parameters. Comparing the modified Ruan and Burton and LMS models, it was found that these models are essentially the same. A common problem was found in both where the effective bulk modulus curve versus pressure experienced a big jump at the critical pressure. This concern needs to be addressed based on the physics of what is really happening.

Figure 3.11 shows a comparison between the LMS (with simple and modified Henry’s law) and the compression only models. The LMS model with the simple Henry’s law is approximately the same as the compression only model up to the critical pressure. This behavior is inconsistent with the physical behavior of bulk modulus in that by increasing density, the bulk modulus should also increase. As pressure increases, more of the air is dissolved in the oil and therefore it is expected that the LMS model would be above the “compression only” model at low pressures, not below it.

Another problem which is observed in the LMS model using the simple Henry's law is related to the jump (discontinuity) in the bulk modulus value at the critical pressure. At this pressure, the derivative of the bulk modulus is discontinuous. To compensate for these two problems, the modified LMS defined a smoothing function which was called the modified Henry's law and was given by Eq. (3.65). At the critical pressure point, all of the air suddenly disappears and a transition from the two phase flow (mixture of oil and air) to single phase oil (consisting of oil and dissolved air) occurs. Physically, a discontinuity in the bulk modulus when crossing the critical pressure point would be expected. However, the appearance of a big jump at the critical pressure is not physically expected.

As Fig. 3.11 shows, the LMS model with the modified Henry's law appears to be less than compression only models in the lower pressure regions (up to 1.5 MPa). This is a consequence of the particular smoothing equation that the model uses and does not reflect an error in the overall model derivation.

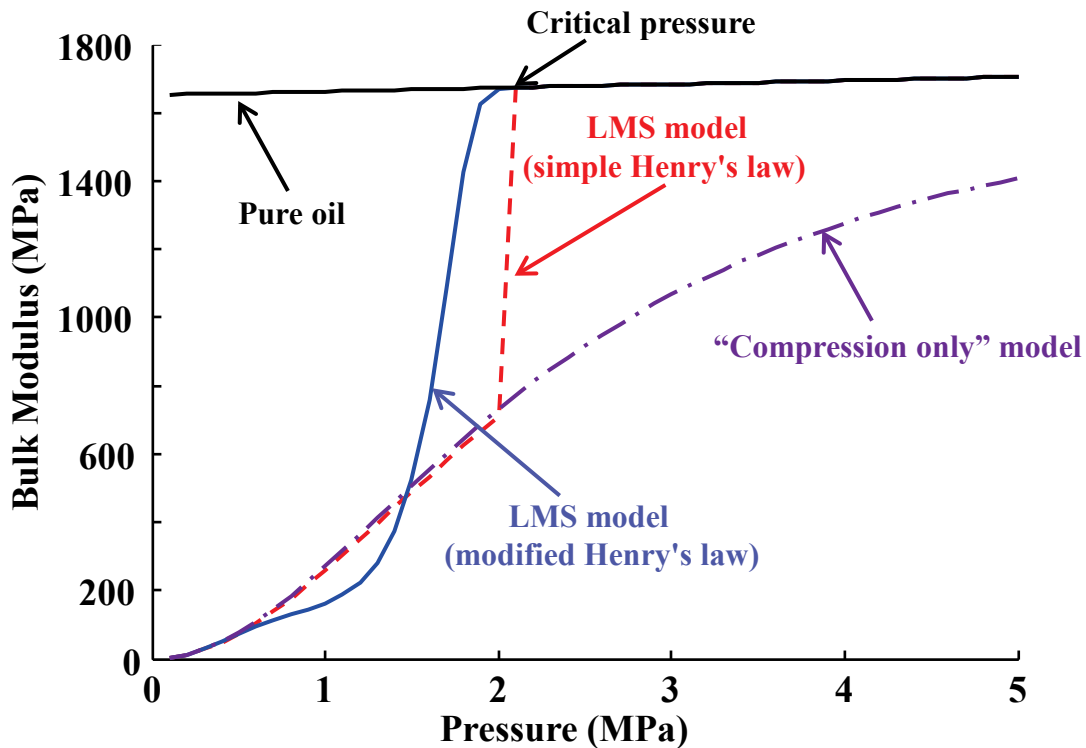


Figure 3.11 Comparison of LMS Models with the compression only model

Moreover, it is physically expected that models which consider both compression and the dissolving of air in the oil (like the LMS model) would always have bulk modulus values greater

than the compression only models. This trend of what would physically be expected was not observed in the LMS model and hence use of these modified versions can only be used with great care. The lack of really understanding the fundamentals behind the dissolving and compression of air bubbles must be addressed in more detail and is the subject of the remaining Chapters in this thesis.

CHAPTER 4: NEW EFFECTIVE BULK MODULUS MODEL FOR THE MIXTURE OF HYDRAULIC OIL AND AIR

4.1 Introduction

The effective bulk modulus of oil inside a chamber is affected by the air content, pressure, temperature, pipe rigidity and interface conditions between the oil and the air (Yu et al., 1994). Assuming the oil is inside a rigid container, the theoretical relationship to find the oil effective bulk modulus in the presence of the mixture of oil and air, has been derived by various researchers. In Chapter 3, these relationships were examined and two different models of effective bulk modulus of oil were investigated based on the air volumetric variation assumption. These two models were categorized as:

- 1) “Compression only” models: Models which only consider the volumetric compression of air, and
- 2) “Compression and dissolve” models: Models which consider both the volumetric compression of air and the volumetric reduction of air due to air dissolving into solution.

A general model of the oil effective bulk modulus for the first group of models was recommended based on the standard definition of the “volumetric fraction of air at atmospheric pressure” and using the tangent bulk modulus definition. Experimental verification of these groups of models was presented by Kajaste et al. (2005) and recently by Sunghun and Murrenhoff (2012). In Kajaste et al. (2005), the air was added as a free pocket at the top of the test cylinder and the maximum amount of air added was 1%. In Sunghun and Murrenhoff (2012), the air content was varied in a range up to 0.5%. The air was injected through a valve, but the air distribution was unknown or at least not mentioned in the paper. Both studies successfully verified the effective bulk modulus model in the range of their experimental limitations. However, the applicability of the model for higher percentages of air content (for example 5% which is common in mobile hydraulic systems (Bock et al., 2010)) and different types of distribution of air bubbles in oil needs to be studied both theoretically and experimentally.

For the second groups of models in which the dissolving effect of the entrained air in oil according to Henry’s law has been also included, a common problem was found in which the effective bulk modulus model experienced a discontinuity at some “critical” pressure. A commonly used model of this type is the LMS model (modified Henry’s law) (LMS IMAGINE, 2008). At the critical pressure point where the air is fully dissolved, a discontinuity appears. This

discontinuity is related to the first derivative in Henry's law equation. The derivative is not continuous at the critical pressure and to compensate for this, Henry's law is adjusted mathematically, to smooth out the transition through the critical pressure region. However, this modified Henry's law is not based on the sound physical concepts of what is really happening when the air is both compressed and dissolved.

In this chapter, the reason for the discontinuity is discussed and a new model is proposed in which the discontinuity problem no longer exists. Experimental verification of the new model and suggestions for model improvements will be discussed in the next chapters.

4.2 Effective bulk modulus of a mixture of oil and air

4.2.1 Development of the initial new effective bulk modulus model

In the introduction, it was mentioned that a discontinuity existed in some models at the critical pressure point. This section will demonstrate how this discontinuity arises and how it can be changed to more closely represent the physical behavior of the effective bulk modulus of the mixture of oil and air. The theoretical model representing the effective bulk modulus of the mixture of oil and air developed by LMS IMAGINE (2008), is given by

$$K_{LMS} = \frac{V_{l_0} + V_{g_0} \left(\frac{P_0}{P} \right)^{\frac{1}{n}} \frac{T}{T_0} \theta}{\frac{V_{l_0}}{K_l} + \frac{T}{T_0} \left(\frac{P_0}{P} \right)^{\frac{1}{n}} \left(\frac{\theta V_{g_0}}{nP} - V_{g_0} \frac{d\theta}{dP} \right)}. \quad (4.1)$$

Note that in the LMS model, it is assumed that the θ is the same for the isothermal and adiabatic conditions. This assumption cannot be valid for adiabatic conditions, since θ is derived in accordance with Henry's law which assumes isothermal conditions ($n = 1$).

It is noted that the term $(d\theta/dP)$ in Eq. (4.1) is not continuous at the critical pressure point (see Fig.4.1) and introduces a discontinuity in the LMS model (simple Henry's law). In order to obtain a continuous derivative function, LMS has changed the underlying mathematical model (Henry's law) near the critical pressure point by proposing a new θ which is smoother than the previous "real" θ and hence does not display a discontinuity in the term $(d\theta/dP)$. The difference between Henry's law and the modified Henry's law is demonstrated graphically in Fig. 4.1.

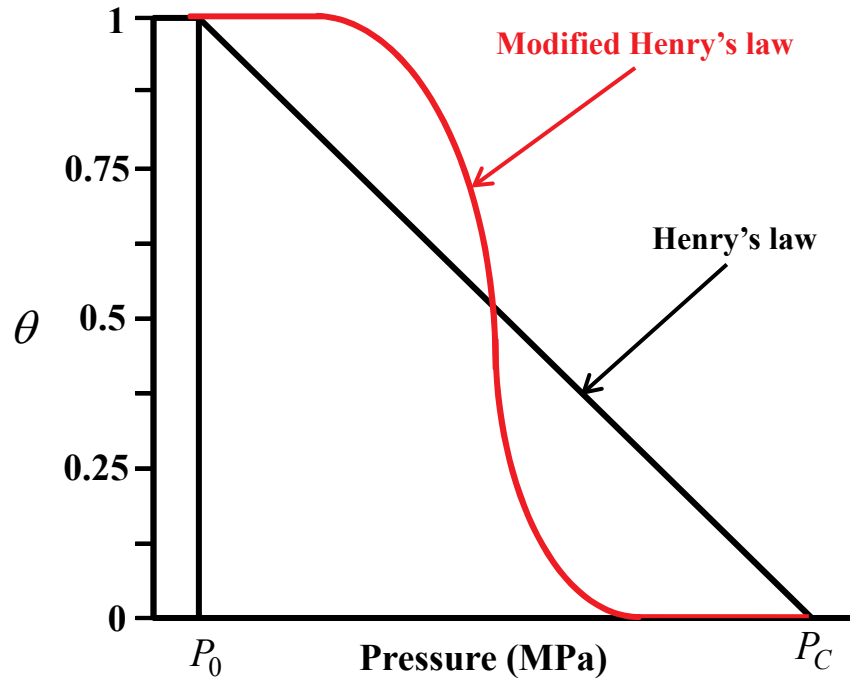


Figure 4.1 Modified Henry's law used in the LMS model

This smoothing function (modified Henry's law) is a mathematical convenience and is not based on any physical property. In the previous chapter, a theoretical comparison of the LMS models with the “compression only” model was provided where it was assumed that $X_0 = 10\%$ and $P_C = 2$ MPa. Those conditions were chosen arbitrarily just for comparison purpose. Figure 4.2 shows another comparison of the models for different assumed conditions. In the comparison of the models, it is assumed that the pure oil isothermal bulk modulus changes linearly with pressure ($K_l = 1652 + 10.4(P - P_0)$), $P_C = 5.5$ MPa and $X_0 = 3\%$. These new values are closer to practical values in hydraulic systems.

Comparison of the models shows that regardless of the critical pressure value chosen, the LMS model (simple Henry's law) is approximately the same as the “compression only” model up to the critical pressure point. This behavior contradicts the physical behavior of bulk modulus in that by increasing the density of the mixture, the bulk modulus should also increase (note that since the amount of entrained air decreases due to dissolving, the total density of the mixture of oil and air increases). This problem is compounded in the LMS model (modified Henry's law)

where at lower pressures the bulk modulus value is even below the “compression only” model. To try to understand physically what is happening was one of the motivations for this study.

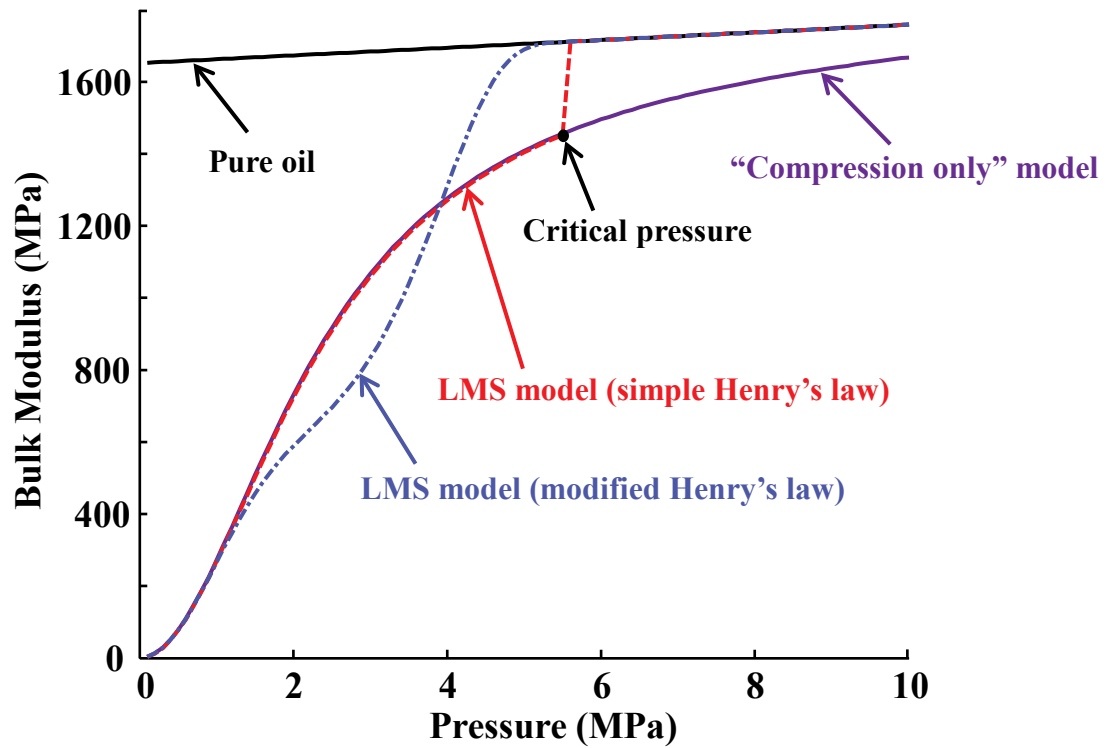


Figure 4.2 Comparison of the LMS models with the “compression only” model when $K_l = 1652 + 10.4(P - P_0)$, $P_C = 5.5$ MPa, $X_0 = 3\%$ and isothermal conditions ($n = 1$) is assumed

After investigating the LMS model, it was found that the reason for the term $(d\theta/dP)$ appearing in the LMS model was due to the way that the effective bulk modulus was derived. The LMS model was developed based on the definition of fluid bulk modulus given by

$$\frac{1}{K_{LMS}} = -\frac{1}{V_l + V_{gcd}} \left(\frac{dV_l + dV_{gcd}}{dP} \right). \quad (4.2)$$

Equation (4.2) must be examined more closely. The bulk modulus definition should only be applied to a control volume with a constant mass. The total mass consists of the mass of the oil and mass of the air (entrained and dissolved). Since the mass of the oil does not change during the compression, it is sufficient to look at only the mass of the air. During a change in pressure, two events occur simultaneously. The first event is a compression of the air (entrained and dissolved) and the second event is the dissolving of some of the entrained air into solution. Any model of bulk modulus must include both events simultaneously if the mass is to remain

constant. Recall that only entrained air affects the bulk modulus. If the mass of the entrained air changes in any model, then calculation of the bulk modulus using Eq. (4.2) is invalid. This makes modeling extremely difficult since both events occur simultaneously.

To demonstrate this, it is of interest to examine how the LMS model approaches this situation. The definition of bulk modulus if only entrained air is examined is given by

$$K_g = -V_{gc} \frac{dP}{dV_{gc}}. \quad (4.3)$$

The constraint on Eq. (4.3) is that the mass must remain constant as pressure changes. The LMS model, however, reflects the change in volume of entrained air due to both compression and dissolving ($V_{gcd} = V_{gc} \theta$), where V_{gcd} is the instantaneous volume of the entrained air as a result of the compression and loss of mass due to dissolving. V_{gc} is the instantaneous volume of entrained air when it is only compressed in accordance with the ideal gas law and θ is the mass fraction of entrained air due to dissolving. Hence the mass of the entrained air is not constant during the compression and as such the basic definition of bulk modulus is not satisfied. To demonstrate the effect that this assumption has on the bulk modulus of air, consider the following.

If the bulk modulus of air is defined in terms of the instantaneous volume of entrained air (V_{gcd}), Eq. 4.3 becomes

$$K_g = -V_{gcd} \frac{dP}{dV_{gcd}}. \quad (4.4)$$

Differentiating V_{gcd} ($V_{gcd} = V_{gc} \theta$) with respect to pressure gives

$$\frac{dV_{gcd}}{dP} = \frac{dV_{gc}}{dP} \theta + \frac{d\theta}{dP} V_{gc}. \quad (4.5)$$

Substituting Eq. (4.5) and $V_{gcd} = V_{gc} \theta$ into Eq. (4.4) gives

$$K_g = \frac{-V_{gc} \theta}{\frac{dV_{gc}}{dP} \theta + \frac{d\theta}{dP} V_{gc}}. \quad (4.6)$$

Equation (4.6) can be simplified as

$$K_g = \frac{1}{\frac{1}{V_{gc}} \frac{dV_{gc}}{dP} - \frac{d\theta}{dP} \frac{1}{\theta}}. \quad (4.7)$$

The term $-\frac{1}{V_{gc}} \frac{dV_{gc}}{dP}$ represents the inverse of bulk modulus of air and its value for isothermal process is equal to $\frac{1}{P}$. Substituting this value in Eq. (4.7) gives

$$K_g = \frac{1}{\frac{1}{P} - \frac{d\theta}{dP} \frac{1}{\theta}}. \quad (4.8)$$

It is well established that the isothermal bulk modulus of air using the form of Eq. (4.3) is

$$K_g = P. \quad (4.9)$$

However, it is quite apparent that Eq. (4.8) (based on Eq. (4.4)) will only converge to Eq. (4.9) if $\frac{d\theta}{dP}$ is zero or $\frac{1}{\theta}$ goes to infinity. Therefore, Eq. (4.8) is not representing the true bulk modulus of air as a result of using V_{gcd} in the bulk modulus definition of air (Eq. (4.4)).

Based on the above discussion, it is apparent that in Eq. (4.2), which was used by LMS to find the effective bulk modulus of the mixture of oil and air, using V_{gcd} results in the term $\frac{d\theta}{dP}$ appearing in the bulk modulus equation which produces the discontinuity.

Therefore, applying the fundamental definition of bulk modulus, the true effective bulk modulus equation for the mixture of air and oil would be

$$K_e = -(V_{gc} + V_l) \left(\frac{dP}{dV_l + dV_{gc}} \right). \quad (4.10)$$

Equation (4.10) is the true definition, because the change in the volume of entrained air is considered to be only due to compression of entrained air. In reality, however, some additional volume of entrained air is also lost due to dissolving into oil. This additional volume decrease of entrained air is not included in Eq. (4.10). Basically Eq. (4.10) is the same equation which is used in “compression only” bulk modulus model.

Now the challenge then becomes one of how the effective bulk modulus of the mixture of oil and air can be modeled when the volume of air decreases, not only because of compression,

but also because of air dissolving into the oil, knowing that the additional decrease in volume cannot be included in Eq. (4.10). To answer this question, Eq. (4.10) is written in another mathematical form as

$$\frac{1}{K_e} = -\frac{1}{V_l + V_{gc}} \left(\frac{dV_l}{dP} \frac{V_l}{V_l} + \frac{dV_{gc}}{dP} \frac{V_{gc}}{V_{gc}} \right). \quad (4.11)$$

Using oil and air bulk modulus definitions, Eq. (4.11) simplifies to

$$\frac{1}{K_e} = \frac{1}{V_l + V_{gc}} \left(\frac{V_l}{K_l} + \frac{V_{gc}}{K_g} \right). \quad (4.12)$$

Equation (4.12) is a useful equation to find the effective bulk modulus when it is desired to consider both the effect of compression and dissolving; however, some approximations are necessary which are now discussed.

Consider Fig. 4.3. For very small changes in pressure, the corresponding change in the volume of entrained air is shown. V_{g_0} shows the initial volume of entrained air at pressure P_0 (represented as point A). When the pressure increases from P_0 to P_1 , the volume of entrained air decreases according to the ideal gas law and reduces to V_{gc1} (represented as point B). As soon as pressure reaches P_1 , some of the entrained air is dissolved into the oil and the volume of entrained air decreases to V_{gcd1} (represented as point C). On the right hand side of the pressure versus volume curve, the bulk modulus curves are shown. If these changes are small enough, then the two events can indeed, be considered simultaneous.

At point B, the volume of entrained air will decrease due to the air dissolving into the oil; therefore the bulk modulus will jump from point B to point C on the bulk modulus curve. The bulk modulus at point C will still be on the “compression only” curves but on a curve which represents the “compression only” bulk modulus curve with less amount of air. Knowing the amount of entrained air at point C which is V_{gcd1} , the effective bulk modulus at point C is found by

$$\frac{1}{K_e} = \frac{1}{V_l + V_{gcd1}} \left(\frac{V_l}{K_l} + \frac{V_{gcd1}}{K_g} \right). \quad (4.14)$$

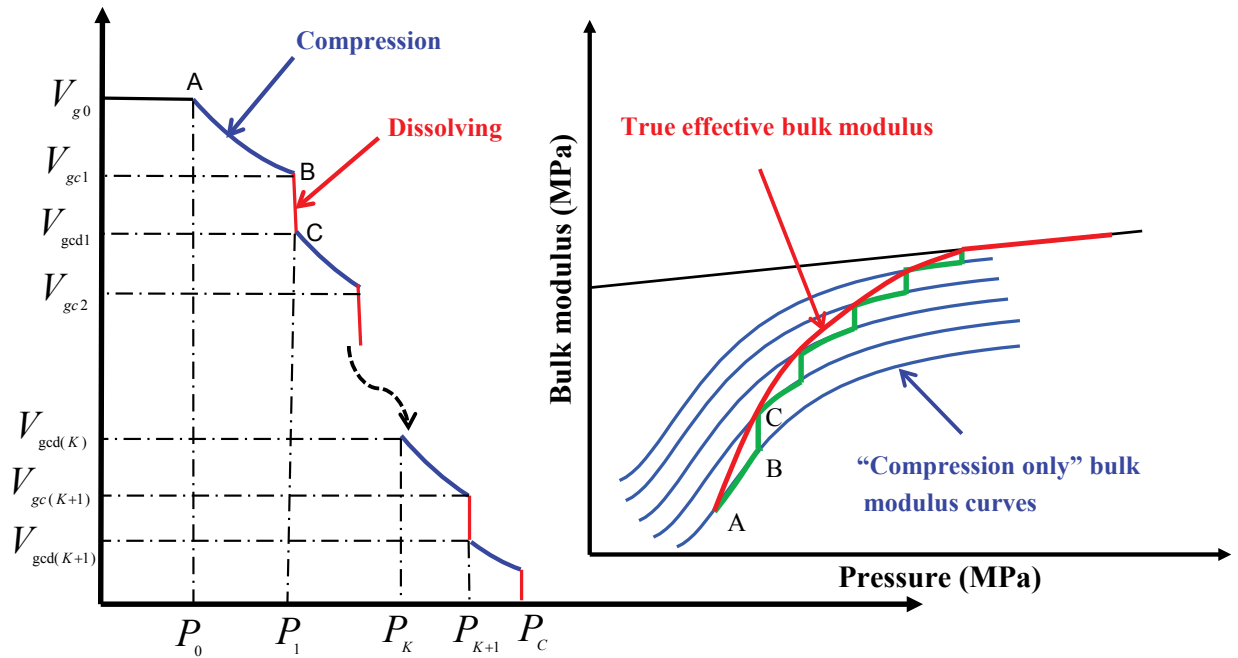


Figure 4.3 Graphical representation showing how to use “compression only” bulk modulus curves in order to find k_{eed}

If it is assumed that the pressure increase from P_0 to P_1 is slow enough that the mixture reaches to the thermodynamic equilibrium state, the true effective bulk modulus will follow the curve AC on the bulk modulus versus pressure plot. Each point on this curve represents the “compression only” bulk modulus value corresponding to the volume of entrained air at that point. If pressure increases more, theoretically there will be a point where there will be no entrained air. This point is called the **critical pressure point (P_C)**. At the critical pressure point, the effective bulk modulus becomes the pure oil bulk modulus. As it was discussed in the previous chapter, assuming equilibrium conditions, the volume of entrained air at each point was obtained following Henry’s law.

Therefore the effective bulk modulus (for isothermal process) at each point below the critical pressure point can be estimated by

$$\frac{1}{K_{ecd}} = \frac{V_{gcd}}{V} \frac{1}{K_g} + \frac{V_l}{V} \frac{1}{K_l}, \quad (4.15)$$

where

$$V_{gcd} = V_{gc} \theta = \frac{P_0 V_{g_0}}{P} \frac{T}{T_0} \theta,$$

$$\theta = \left(\frac{P_C - P}{P_C - P_0} \right),$$

$$V = V_{gc} \theta + V_l \text{ and}$$

$$K_g = P.$$

Rearranging Eq. (4.15), a theoretical model which relates the effective bulk modulus to the volumetric variations of air due to both compression and the dissolving of air in the oil, and also due to the change in volume and bulk modulus of the pure oil as a function of pressure and temperature is given by

$$\left\{ \begin{array}{l} K_{ecd} = \frac{V_l(P, T) + V_{gcd}(P, T)}{\frac{V_l(P, T)}{K_l(P, T)} + \frac{1}{P} V_{gcd}(P, T)} \quad \text{For } P < P_C \\ K_{ecd} = K_l(P, T) \quad \text{For } P \geq P_C \end{array} \right. , \quad (4.16)$$

where

$$V_{gcd}(P, T) = V_{gc}(P, T) \theta = \frac{P_0 V_{g_0}}{P} \frac{T}{T_0} \left(\frac{P_C - P}{P_C - P_0} \right),$$

$$K_l(P, T) = K_l(P_0, T) + m(P - P_0) , \text{ and}$$

$$V_l(P, T) = V_l(P_0, T) \left(1 + \frac{m}{K_l(P_0, T)} (P - P_0) \right)^{-\frac{1}{m}}.$$

This model was derived based on the assumption of an isothermal compression process and that an equilibrium condition between the air bubbles and oil was reached. Equation (4.16) can be considered to be a model of the effective bulk modulus of the mixture of the air and oil which in addition to considering both the compression and the dissolving of entrained air in the oil, assumes that the volume and bulk modulus of the pure oil changes as a function of pressure and temperature. In order to consider the effect of pressure and temperature on the pure oil volume and bulk modulus, the equations developed by Hayward (1970) which predict the isothermal and adiabatic secant bulk modulus of mineral oil can be used. Since the tangent bulk modulus value is required in the model, these predicted equations for the secant bulk modulus will be converted to the tangent bulk modulus values (Details of how to use Hayward's method to estimate the pure oil bulk modulus are given in Appendix D).

In Fig. 4.4, the proposed initial new model defined by Eq. (4.16) is compared with the LMS model (using both the simple and modified Henry's law). For comparison purpose, $P_C = 5$ MPa and $X_0 = 3\%$ were chosen. It was also assumed that oil bulk modulus changes with pressure according to $K_l = 1652 + 10.4(P - P_0)$. The plot representing the new model clearly predicts bulk modulus values larger than those predicted by the "compression only" model. Unlike the LMS models, the trend of the new model is physically more realizable and does not have the discontinuity problem already mentioned in the LMS model (simple Henry's law).

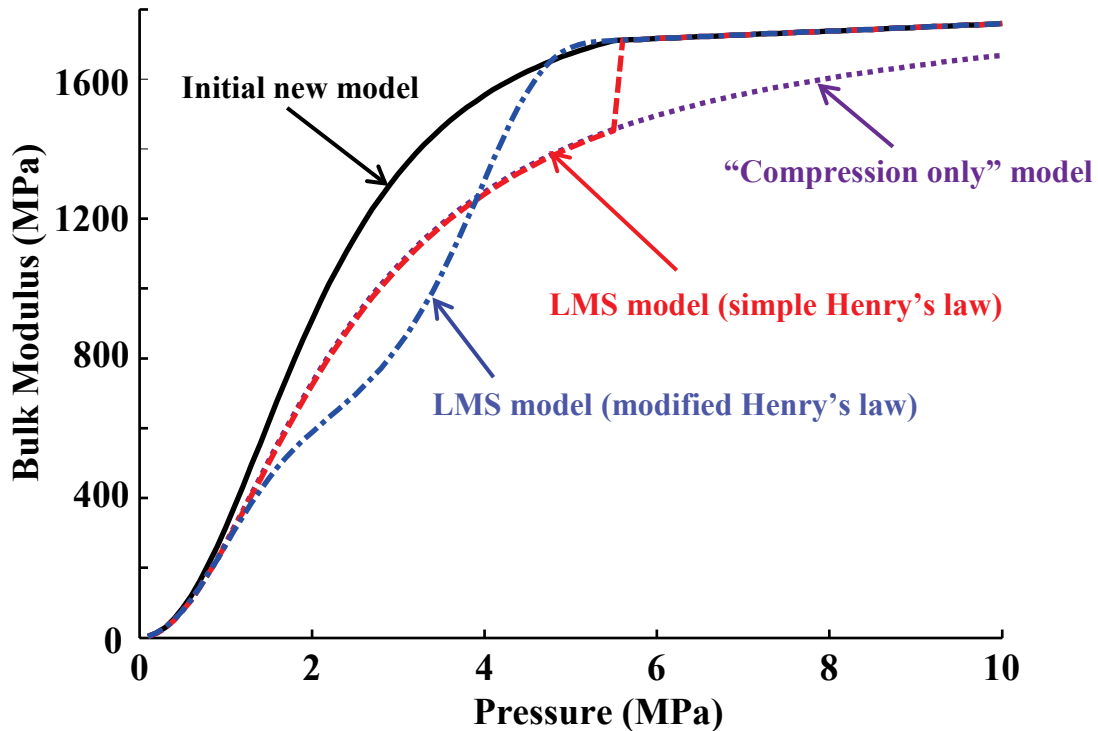


Figure 4.4 Theoretical comparison of LMS models and the initial new model with assumed conditions of $X_0 = 3\%$, $P_C = 5$ MPa and $K_l = 1652 + 10.4(P - P_0)$

4.2.2 Experimental verification of the initial new isothermal effective bulk modulus model

An initial experimental set up was built in order to investigate and compare the bulk modulus versus pressure behavior of the mixture of oil and air at a constant temperature with those predicted by the models. The experimental set up will be discussed in detail in the next Chapter. However, preliminary results indicated that the model discussed in Section 4.2.1 did not follow the experimental results very well; thus it was necessary to examine these results in greater detail. It became an objective then to use this poor correlation to improve the initial new model. This is now considered.

Figure 4.5 shows a comparison of the experimental results when $X_0 = 3.33\%$ with the initial new model, LMS models and the “compression only” model. In the region of $P > 1$ MPa, the “compression only” model underpredicts the experimental results which implies that significant dissolving is in fact occurring. It is also apparent that the LMS models also fail to predict the real behavior of the effective bulk modulus as it essentially behaves as a

“compression only” model. The reasons for the LMS model failure were already discussed when the models were compared numerically and is supported here experimentally as well.

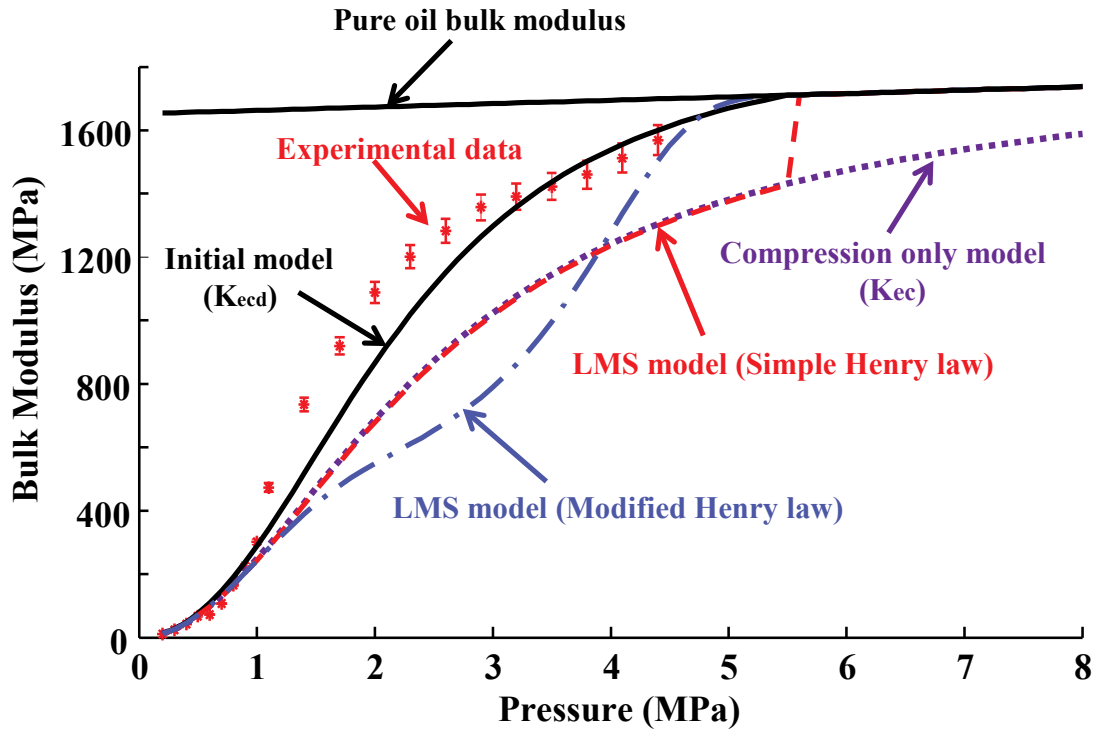


Figure 4.5 Comparison of the experimental results with the initial new model and LMS models when $X_0 = 3.33\%$, $P_C = 5.5$ MPa and $K_l = 1652 + 10.4(P - P_0)$

Figure 4.5 shows that there is also poor agreement between the measured values and the initial new model developed in Section 4.2.1 in the region of $1 \text{ MPa} < P < 3 \text{ MPa}$, which indicates that the new model needs to be revisited. It is noted that the agreement to the experimental results is superior to the other models in this range but it was not considered satisfactory for this study.

As already was explained in developing the new model, a series of “compression only” bulk modulus curves were used to show how the effective bulk modulus increases by crossing through the “compression only” bulk modulus curves. It is recalled that a new parameter called “critical pressure” was also introduced and was defined as the pressure in which all the air is dissolved into the oil and the effective bulk modulus converges to that of pure oil.

Figure 4.6 compares the experimental results with a series of “compression only” bulk modulus curves plotted for different amounts of air. The trend of the experimental results signifies that the critical pressure was not reached and the trend showed that the critical pressure

was expected to be higher than the maximum experimental pressure limit of 6 MPa. Therefore, based on the experimental results, it is expected that even at higher pressures there will be some air bubbles which have not completely dissolved into the oil.

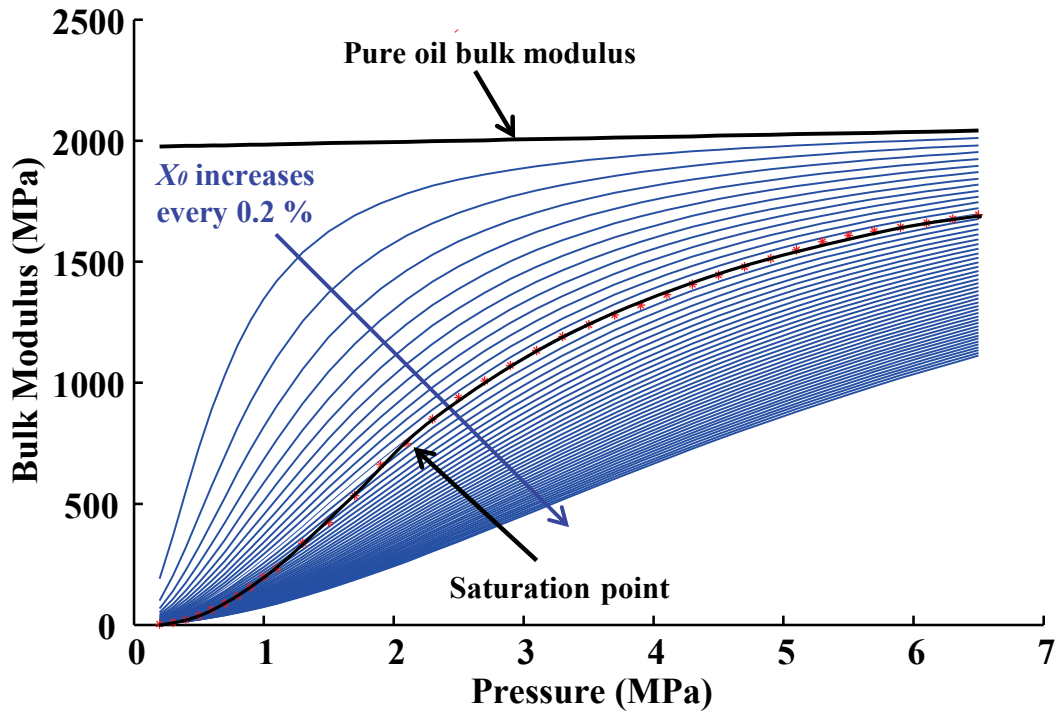


Figure 4.6 Comparison of the experimental results with a series of “compression only” bulk modulus curves for isothermal process

It can be seen from Fig. 4.6 that as pressure increases, initially the effective bulk modulus passes across the “compression only” curves due to the loss of entrained air which is dissolved into the oil. The trend of passing across the curves continues until it reaches a point labeled as the saturation point in Fig. 4.6. After this point, no significant “jumping” through the “compression only” curves is observed; indeed, the experimental results tend to follow one of the “compression only” curves. This indicates that no significant dissolving happens after this saturation point, and any remaining air can be considered that is only compressed afterwards.

As will be discussed in the next chapter, this experimental result is consistent for various amounts of initial entrained air which gives confidence to this interpretation.

The reason for this behavior may be explained by the fact that there is a practical limit to Henry’s law in which the air cannot be dissolved into the oil after it has reached a particular saturation limit. After this saturation limit occurs, any air that remains in the oil will not be

dissolved or very little will be dissolved (Wahi, 1976). Wahi reported that this practical limit was found to be within 1.3 - 1.7 MPa when nitrogen gas is dissolved in MIL-H-5606 oil. Moreover, experimental findings of Hayward (1961) showed that by compressing a column of a mixture of oil and air, initially the air bubbles are dissolving rapidly but the dissolving tends to slow down as the skin of oil around each bubble is saturated with dissolved air.

Consequently, the definition for the critical pressure where it is assumed that all the air is dissolved into the oil, needs to be re-addressed according to the saturation limit of oil. Figure 4.7 shows the new definition of the critical pressure.

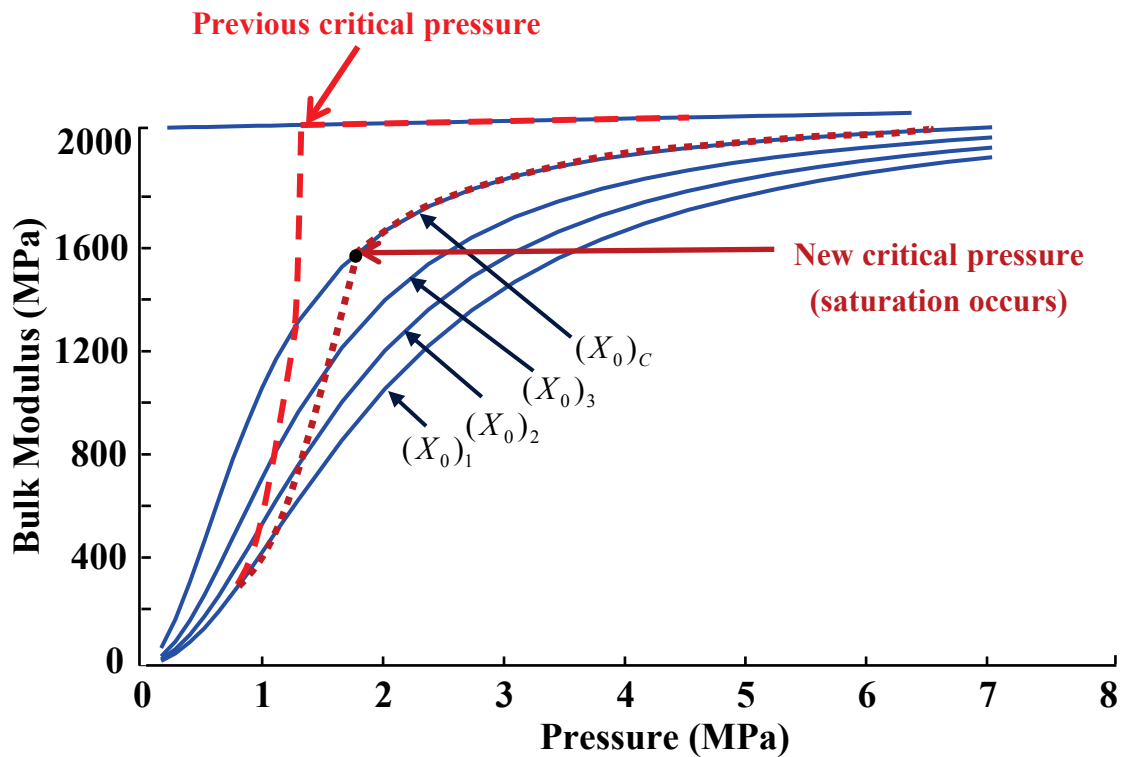


Figure 4.7 A new critical pressure definition is introduced based on the saturation limit of oil

In the new definition, after critical pressure reached, the effective bulk modulus will follow the “compression only” curve with known “ X_0 ” which here is called $(X_0)_c$. Note that $(X_0)_c$ is the same as the volumetric fraction of air at atmospheric pressure which was already defined by X_0 .

4.2.3 Final new effective bulk modulus model

According to the new definition of critical pressure, when the critical pressure is reached, the oil is saturated and no more air will be dissolved in the oil. After this critical point, the

remaining air will tend to follow a “compression only” bulk modulus curve related to the critical volumetric fraction of air $(X_0)_c$. Note that the polytropic index of air was considered to be different before and after the saturation point. n_1 is the polytropic index of air before the saturation point and n_2 is after the saturation point.

The volume of entrained air in oil when pressure is less than the critical pressure is given by

$$V_{\text{gcd}}(P, T) = \left(\frac{P_0}{P}\right)^{\frac{1}{n_1}} \frac{T}{T_0} X_0 \theta \quad P < P_C. \quad (4.17)$$

From Fig. 4.8, the volumetric fraction of air (θ) at $P < P_C$ is found by

$$\theta = \left(\frac{P_C - P}{P_C - P_0}\right) \left(1 - \frac{(X_0)_c}{X_0}\right) + \frac{(X_0)_c}{X_0}. \quad (4.18)$$

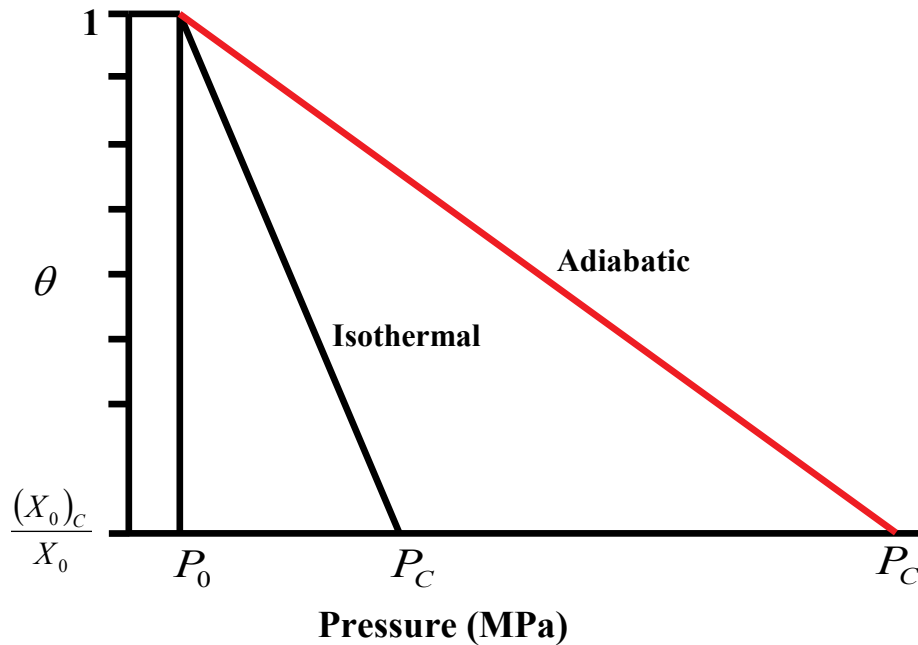


Figure 4.8 Volumetric fraction of entrained air due to dissolving which is based on the new definition for the critical pressure

Figure 4.8 shows how θ is different for isothermal and adiabatic process. In an isothermal process, when the process is assumed to be very slow, equilibrium conditions exist between the

air bubbles and the oil and Henry's law can be used to calculate the amount of air dissolved in the oil. The linear relationship shown in Fig. 4.8 between θ and pressure was derived based on the application of Henry's law. The pressure at which no more air is dissolved in the oil is P_C .

In adiabatic conditions, the mixture of oil and air is compressed quickly and equilibrium conditions between the air bubbles and oil may not be reached. In this case Henry's law cannot be directly applied. However, it can be assumed that θ follows a linear relationship with pressure where P_C is reached at much higher pressure than the isothermal process.

For pressures equal to or higher than the critical pressure, the remaining air will not be dissolved and will follow the compression rule,

$$V_{\text{gcd}}(P, T) = \left(\frac{P_0}{P}\right)^{\frac{1}{n_2}} \frac{T}{T_0} (X_0)_C \quad P \geq P_C \quad (4.19)$$

Combining Eqs. (4.17) to (4.19), a new final model which relates the effective bulk modulus to the volumetric variation of the air due to both compression and dissolving of air in the oil, and also the change in volume and bulk modulus of pure oil to the pressure and temperature is given by

$$\left\{ \begin{array}{l} K_{\text{ecd}} = \frac{V_l(P, T) + V_{\text{gcd}}(P, T)}{\frac{V_l(P, T)}{K_l(P, T)} + \frac{1}{K_{g_1}} V_{\text{gcd}}(P, T)} \quad P \leq P_C \\ \\ K_{\text{ecd}} = \frac{V_l(P, T) + \left(\frac{P_0}{P}\right)^{\frac{1}{n_2}} \frac{T}{T_0} (X_0)_C}{\frac{V_l(P, T)}{K_l(P, T)} + \frac{1}{K_{g_2}} \left(\frac{P_0}{P}\right)^{\frac{1}{n_2}} \frac{T}{T_0} (X_0)_C} \quad P > P_C \end{array} \right. , \quad (4.20)$$

where

$$K_{g_1} = n_1 P,$$

$$K_{g_2} = n_2 P,$$

$$V_{\text{gcd}}(P, T) = \left(\frac{P_0}{P}\right)^{\frac{1}{n_2}} \frac{T}{T_0} X_0 \left(\left(\frac{P_C - P}{P_C - P_0}\right) \left(1 - \frac{(X_0)_C}{X_0}\right) + \frac{(X_0)_C}{X_0} \right),$$

$$K_l(P, T) = K_l(P_0, T) + m(P - P_0), \text{ and}$$

$$V_l(P, T) = V_l(P_0, T) \left(1 + \frac{m}{K_l(P_0, T)} (P - P_0) \right)^{\frac{1}{m}}.$$

4.3 Summary and discussion

Theoretical models to find the effective bulk modulus of a mixture of oil and air were presented and the discontinuity problem associated with the LMS model was discussed and its limitations were presented. An initial new model was developed in which the effect of air dissolving into the oil according to Henry's law was considered. In this new model, the discontinuity problem no longer existed. Comparison of the initial new model with the early experimental results showed that the initial new model did not adequately represent the experimental results and needs to be revisited.

Experimental results were compared with a series of "compression only" bulk modulus curves plotted for different amounts of air. From the trend of the experimental results, a new definition for critical pressure was introduced. In this new definition, it was stated that the air cannot be dissolved into the oil after it has reached a particular saturation limit. Therefore, it was assumed that any remaining air will be only compressed after critical pressure was reached. Based on the new definition of the critical pressure, a new final model was developed for both the isothermal and adiabatic compression of the mixture of oil and air. Figure 4.10 graphically shows the difference between the final new model and the initial new model for an isothermal process.

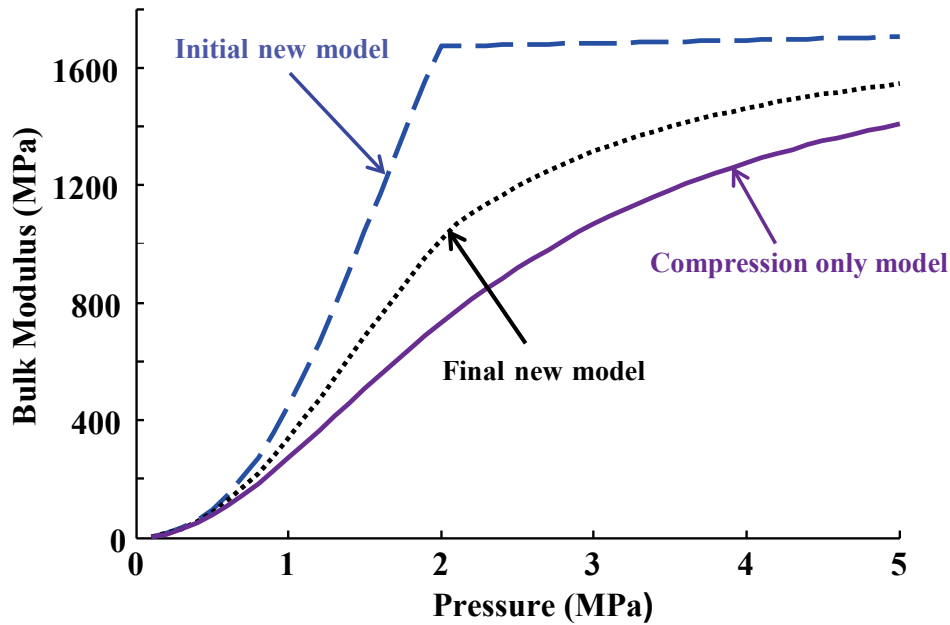


Figure 4.9 Theoretical comparison of the initial new model, final new model and compression only model when $X_{\theta} = 3\%$, $P_C = 2$ MPa and $(X_{\theta})_C = 1.5$ MPa for isothermal process

In an isothermal process, since the process is assumed to be very slow, the equilibrium conditions between the air bubbles and oil are reached and Henry's law is used to calculate the amount of dissolved air in oil. The linear relationship between θ and pressure was derived based on the application of the Henry's law. However, in an adiabatic process where the rate of compressing the mixture of oil and air is high, Henry's law cannot be directly applied. However, it can be assumed that θ follows a linear relationship with pressure where P_C is reached at much higher pressure than the isothermal process. In the next chapters, the experimental set up will be explained and the experimental verification of the new models will be considered.

CHAPTER 5: EXPERIMENTAL SETUP AND PROCEDURE

5.1 Introduction

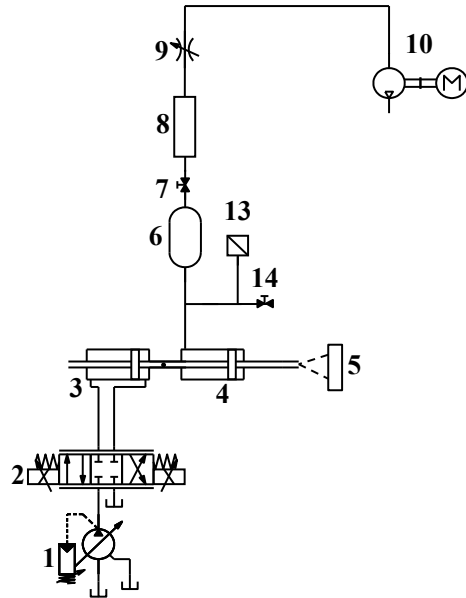
In the previous chapter, the theoretical models to find the effective bulk modulus of a mixture of oil and air were presented. An experimental system was built in order to investigate and compare the bulk modulus versus pressure behavior of a mixture of oil and air at a constant temperature with those predicted by the models. In this Chapter, the experimental set up is presented.

5.2 Experimental apparatus

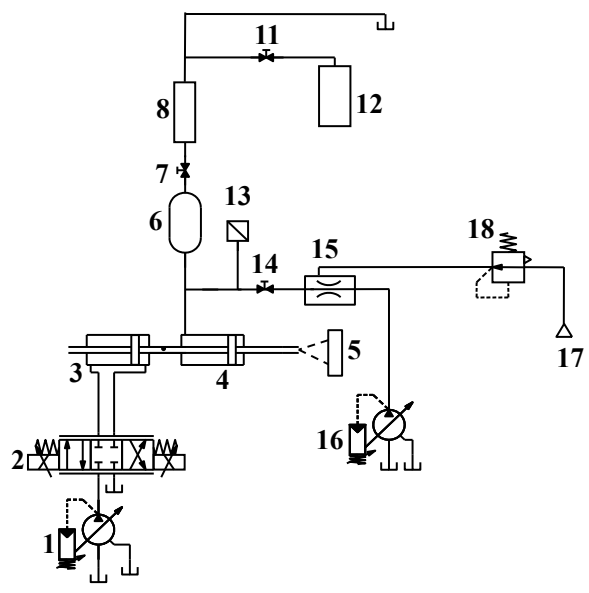
Among different methods of measuring the effective bulk modulus, the “volume change method” was chosen in this study because of its higher accuracy (Manring, 2005, Sunghun et al., 2012). In this method, the volume of a cylinder containing the fluid is changed and the bulk modulus can be determined from this change. Sunghun et al. (2012) compared the accuracy of the “volume change method” with the “mass change method” and the “sound speed method”. In the “mass change method” the volume of a cylinder containing the fluid is constant (constant control volume) and some fluid (with a controlled flow rate) is fed into the cylinder. In the “sound speed method”, the measurement of the speed of sound is used to calculate the effective bulk modulus. Sunghun et al. (2012) reported that the “volume change method” is 5 times more accurate than the “mass change method” and 25 times more accurate than the “sound speed method”. The higher accuracy of the “volume change method” is related to the accuracy of the pressure and position sensors that are used. The inferior accuracy of the “mass change method” and the “sound speed method” is due to the lower accuracy of the flow rate measurements and the sampling rate of the data acquisition system, respectively. It should be noted that these limitations in the accuracy of the “sound speed method” and “mass change method” may overcome by utilizing more accurate flow rate measurements and higher sampling rate of data acquisition system.

Schematic diagrams and a photo of the apparatus are shown in Fig. 5.1. Experiments were essentially carried out in three different phases. Figure 5.1.a shows a schematic diagram of the apparatus in the “baseline” and “lumped air” phases. With some modifications to this apparatus, the third phase of the experimental investigation, which was called the “distributed

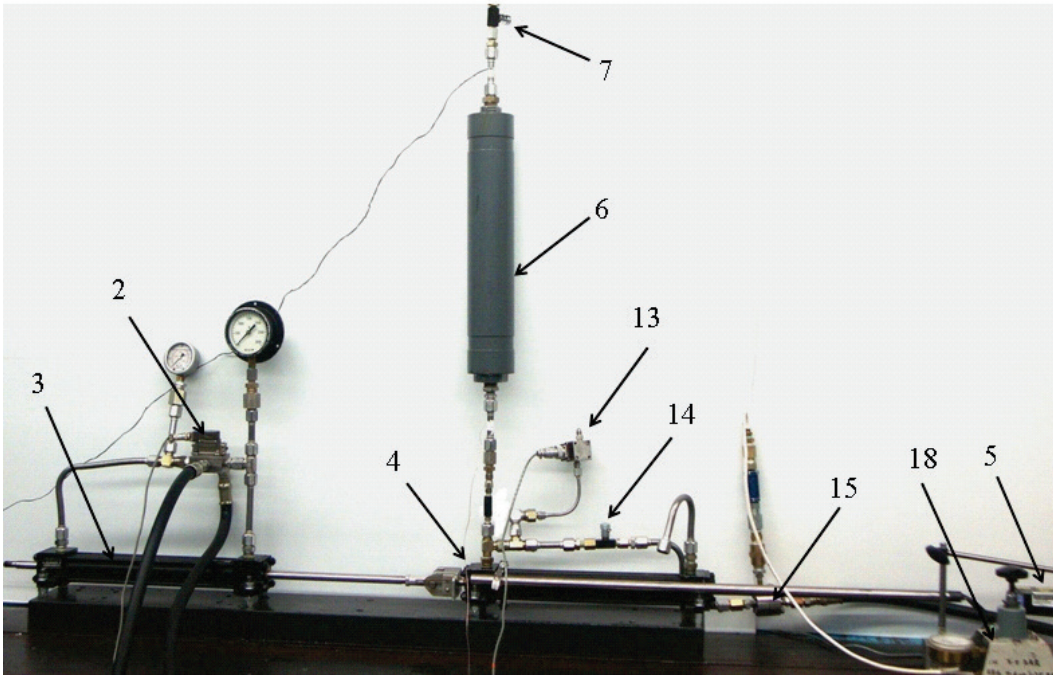
air” phase, was carried out where air was continuously injected into the system. Figure 5.1.b shows the schematic diagram of the apparatus in the third phase. An actual photo from a part of the experimental set up in the third phase is also shown in Fig. 5.1.c.



(a) Baseline and lumped air phase



(b) Distributed air phase



(c) A photo from a part of the actual experimental set up at the distributed air phase

(1) Pressure compensated variable displacement pump, (2) Pressure control servo valve, (3) Double acting double rod end hydraulic cylinder, (4) Double acting double rod end hydraulic cylinder, (5) Displacement sensor (MicroTrak II-SA), (6) Testing vessel, (7) Needle valve, (8) Transparent tube, (9) Variable throttle valve, (10) Vacuum pump, (11) Needle valve, (12) Pycnometer, (13) Pressure transducer, (14) Needle valve, (15) Venturi orifice, (16) Pressure compensated variable displacement pump, (17) Compressed air source, (18) Pneumatic pressure regulator

Figure 5.1 (a,b,c) Schematic diagrams (a) and (b) of the bulk modulus tester and a photo (c) taken from a part of the actual experimental set up

The first phase, which was called the “baseline phase”, involved the measurements of the tangent bulk modulus of the degassed test oil at different volume change rates. In this phase, steps were taken to ensure that the apparatus interior was free of any trapped air. The testing vessel was filled slowly with the oil and held vertically in order to allow air bubbles to rise out. Before installing the testing volume (6) in the circuit, the hydraulic cylinder (4) was first completely moved to the left. Then the oil was added to its chamber manually by moving it slowly to the right side. Note that the output port of the hydraulic cylinder (4) at the right end side was always connected to the atmosphere. In order to make sure that any residual air bubbles were removed from the system, a partial vacuum was also applied to the system using a vacuum pump (10). A throttle valve (9) was used to control the amount of vacuum pressure for the

degassing of the oil. Degassing was continued until no air bubbles were observed through the transparent tube (8).

After degassing the oil, the needle valve (7) was closed and the degassed oil was compressed by actuating the hydraulic cylinder (3) which was mechanically linked to the hydraulic cylinder (4). The speed of compression was controlled by the servo valve (2) through a closed loop position feedback control system. At the same time that the oil was compressed, the pressure readings of pressure transducer (13) were taken and the change in the volume of oil was measured by a displacement sensor (5). A pressure/displacement curve was recorded for each volume change rate and used for calculating the tangent bulk modulus.

The second phase of the experiments was started right after the baseline phase. In this phase, which was called the “lumped air” phase, a big air bubble was created at the top of the oil column by removing a definite amount of oil from the system through opening the needle valve (14). Since the needle valve (7) was also opened at the same time, the same amount of oil which was removed by opening the needle valve (14) was replaced by the air at the top of the oil column. After a desired amount of lumped air was obtained at the top of the oil column, both needle valves (14) and (7) were closed and the pressure/displacement curve was recorded at different volume change rates. It should be noted that the amount of air was known and controlled and hence repeatability tests were possible.

The third phase of the experimental investigation consisted of measuring the effective bulk modulus of a mixture of oil and air, where air was distributed in the oil in the form of small air bubbles. Figure 5.1.b shows the schematic diagram of the experimental set up at this phase. A photo of the actual experimental set up was also shown in Fig. 5.1.c.

A venturi orifice (15) was used to inject and mix air with the oil. It was found that the longer the time interval that air was added, the greater the amount of air that become dispersed in the oil. Unlike the previous phase, small air bubbles with different sizes were generated. Before air was injected to the system, the hydraulic cylinder (4) was first completely moved to the left side. After the air was distributed in the circuit, the hydraulic cylinder (4) was slowly moved back to the right side. Therefore, the left chamber of the hydraulic cylinder (4) was also filled with the mixture. At this time, the needle valves (14) and (7) were closed and the mixture was compressed at a specified volume change rate. The pressure/displacement curve was recorded

and used for bulk modulus calculations. As will be noted later, the amount of air at any test introduced into the system could not be controlled and thus repeatability tests were not possible.

The volume of the testing vessel, including extra volume added due to the fittings, was $2.133 \times 10^6 \text{ mm}^3$. All the measurements were taken at a temperature of $24 \pm 1 \text{ }^\circ\text{C}$.

A couple of lip type piston seals were added in the hydraulic test cylinder (4) in order to prevent leakage from the test chamber into the cylinder. Leakage tests were performed at a maximum pressure of 6.9 MPa for a duration of 3.5 minutes and no measurable amount of leakage was observed. The errors in estimating the bulk modulus caused by the deformation of the testing vessel and cylinder were estimated (see Appendix E) and removed from the final test results. The errors due to the sensors will be examined and estimated in the next section.

The volumetric fraction of air at atmospheric pressure needs to be calculated at both the second and third phases. For the second phase, this volume was controlled by the amount of oil which was removed through the system by opening the needle valve (14). For the third phase, a sample of the aerated oil was collected inside the pycnometer (12) by opening the needle valve (11). By measuring the specific weight of the collected sample with the pycnometer, the approximate volumetric fraction of air at atmospheric pressure could be found.

However, since this method was time consuming and there was also some delay in collecting the sample and initiating the experiments, another method of measuring the volumetric fraction of air at atmospheric pressure was used. This method is explained in Section 5.5.

5.3 Experimental uncertainty

The effective bulk modulus of a mixture of oil and air is calculated by measurements of pressure and displacement. Therefore it is necessary to evaluate the uncertainty related to these calculations.

Manring (2005) explained a method of deriving an expression for the maximum measurement uncertainty of the fluid bulk modulus using the “volume change method”. In order to derive this expression, he used the basic definition of the fluid bulk modulus and rearranged it in the following form

$$K = \frac{P}{\ln\left(\frac{V_0}{V}\right)}, \quad (5.1)$$

where V_0 is the fluid volume inside a cylinder at atmospheric pressure and V is the instantaneous fluid volume after compression. V_0 is given as Al_0 , where A is the area and l_0 is the cylinder length, and V is written as

$$V = V_0 - Ax = A(l_0 - x). \quad (5.2)$$

Therefore Eq. (5.1) can be written as

$$K = \frac{P}{\ln\left(\frac{l_0}{l_0 - x}\right)}. \quad (5.3)$$

Using Eq. (5.3), Manring (2005) provided an expression to obtain the maximum measurement uncertainty of the bulk modulus tester for the “volume change method”. K is a function of P , l_0 and x . Thus, the measurement uncertainty is given by

$$\varepsilon_{\max} = \pm\left(\varepsilon_P \frac{P_{\max}}{P'} + \varepsilon_l \frac{l_{\max}}{l'_0} + \varepsilon_x \frac{x_{\max}}{x'}\right), \quad (5.4)$$

where l_0 is the initial height of the fluid inside the cylinder at atmospheric pressure and x represents the decrease in the height of the fluid, when the applied force to the piston increases. The primed values of P , l_0 and x represent the measured values of these parameters, while the unprimed values of these parameters show the true values of these parameters which are unknown. The parameters ε_p , ε_l and ε_x denote the accuracy of the pressure, length and displacement sensors respectively and P_{\max} , l_{\max} and x_{\max} are the maximum measurement ranges of these sensors.

With some modifications, Eq. (5.4) can be used to estimate the maximum uncertainty of the calculated bulk modulus in the experimental set up under study. In deriving Eq. (5.4), Manring (2005) assumed that the initial volume of the fluid inside the cylinder can be obtained by measuring both l_0 and A . However, because of the complexity of the inside geometry of the testing vessel under study and the existence of extra volumes due to the fittings, another method of measuring the initial fluid volume (V_0) was used. In this method, the testing vessel, including the fittings were initially filled with water. Water was used, since it has a lower viscosity than test oil and does not stick to the inside walls of the vessel. The testing vessel was filled and held vertically in order to allow air bubbles to rise and be released from the testing vessel. The water then was poured into a graduated cylinder where measurement of the volume of fluid could be determined.

It should be noted that the measurement of l_0 was not used in this method under study and therefore Eq. (5.4) is modified to include the initial fluid volume (V_0) instead. The maximum uncertainty then becomes

$$\varepsilon_{\max} = \pm \left(\varepsilon_P \frac{P_{\max}}{P'} + \varepsilon_{V_0} \frac{V_{\max}}{V'_0} + \varepsilon_x \frac{x_{\max}}{x'} \right). \quad (5.5)$$

Detailed information regarding maximum range, baseline and measurement uncertainty of the pressure, volume and displacement sensors is given in Appendix F. From this information, the maximum uncertainty measurement of the fluid bulk modulus under study can be approximated and is represented as an error bar on appropriate plots of pressure versus fluid bulk modulus.

5.4 Calculation of the effective bulk modulus

From the discussions of previous Chapters, it was concluded that the tangent bulk modulus was the only recommended true bulk modulus that is to be used in determining the bulk modulus of a mixture of oil and air. Therefore, the tangent bulk modulus from the experimental data needs to be calculated.

In order to calculate the tangent bulk modulus at each pressure, the slope of the pressure/volume curve (dP/dV) needs to be determined at each pressure and then multiplied by the instantaneous volume at that pressure. ($K = -VdP/dV$). This pressure/volume curve can be obtained experimentally using the apparatus shown in Fig. 5.1.

From the experimental apparatus, measurements were recorded and presented as a pressure/displacement curve. By knowing the test cylinder area, this curve was converted to a pressure/volume curve which was the form that was required for determining the tangent bulk modulus. The final pressure/volume curve was obtained by applying corrections for the test vessel expansion. Information regarding how to estimate the deformation of the testing volume is given in Appendix E.

Since the recorded data of the pressure and displacement sensors were noisy, computing the derivative of pressure versus volume data using conventional finite difference methods was significantly impeded by amplified noise in the data. It has been shown that removing the noise by filtering the data, for example, may not significantly give better results (Chartrand, 2011).

A more accurate way to compute the derivative of noisy data is to fit the data with piecewise least square splines. In this method, data are divided into equal or non-equal intervals and each interval of data is represented by a separate spline. These splines are then joined together in such a way as to create a desired degree of smoothness for the fitted curve. An algorithm developed by D’Errico (2009), which uses this technique, is an excellent tool to fit an appropriate curve to the data. This algorithm is called “shape language modeling”. Figure 5.2 shows an example of how a series of piecewise least square splines fit to the pressure/volume data using this shape language modeling tool. This technique was used to fit the experimental data that were recorded during the different tests.

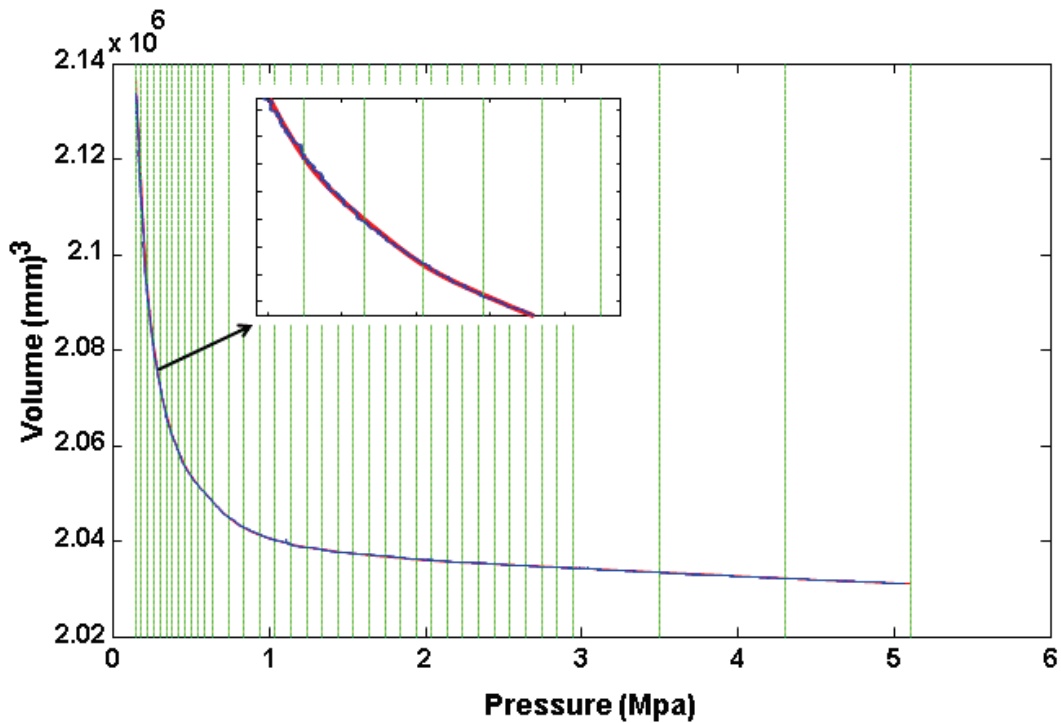


Figure 5.2 An experimentally measured pressure/volume curve is fitted with piecewise least square splines in order to facilitate the computation of dP/dV . The experimental data cannot be readily observed since the fitted curve when superimposed on the experimental data masks the data.

5.5 Experimental procedure

In this section, the experimental procedure is explained and some typical results presented. Detailed analysis of the results and comparisons with the theoretical models will be presented in the next Chapter. It is noted that a fluid temperature of $24 \pm 1^\circ\text{C}$ was maintained in all of the experiments.

Experiments were essentially carried out in three different phases. The first phase, which was called the baseline phase, involved the measurement of the tangent bulk modulus of the degassed test oil at different volume change rates. In this phase, no air was added to the oil and steps were taken to ensure that the apparatus interior was free of any trapped air.

The second phase of the experimental investigation involved the measurement of the tangent effective bulk modulus of a mixture of oil and air, where air was introduced to the system as a lumped air (free air pocket) at the top of the oil column.

The third phase of the experimental investigation consisted of measuring the tangent effective bulk modulus of a mixture of oil and air, where air was distributed in the oil in the form of small air bubbles.

For the second and third phases of the experiments, it was required to measure the amount of air at atmospheric pressure. Some methods of measuring the amount of air were introduced in Section 5.2. However, due to the limitations of those methods, another method was employed which has been also used and explained by Kajaste et al. (2005), Ruan and Burton (2006) and Sunghun et al. (2012).

In this method, a volumetric fraction of air at atmospheric pressure (X_0) was estimated from the change in the volume versus pressure curve. By drawing an asymptotic line from the maximum slope to the abscissa, X_0 was determined.

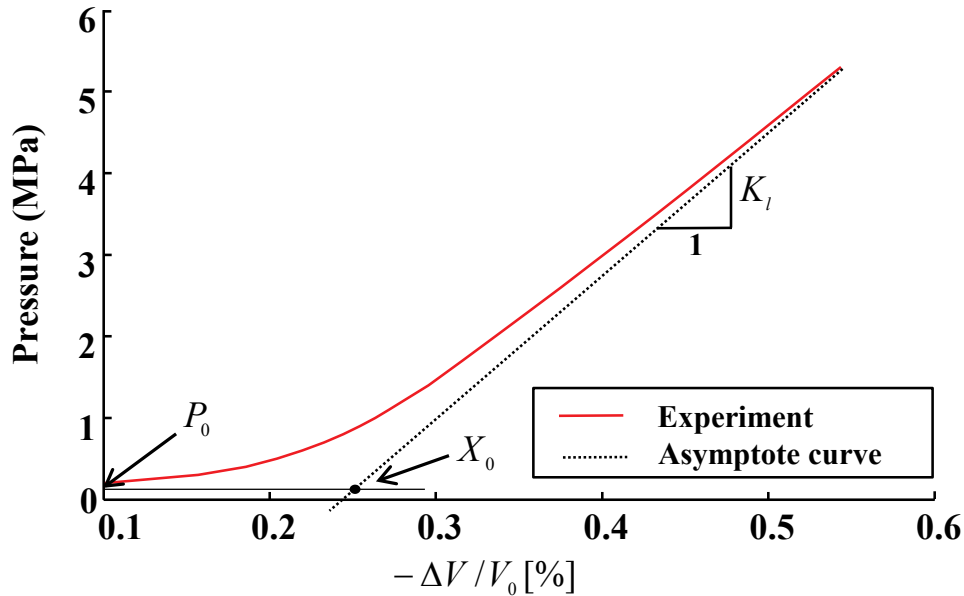


Figure 5.3 The maximum slope of a pressure versus change in the volume curve is used to obtain the volumetric fraction of air at atmospheric pressure (X_0)

5.5.1 Baseline phase

A baseline phase was carried out in order to estimate the tangent bulk modulus of the degassed test oil at different volume change rates. This phase was performed for two main reasons: to compare the results with the existing known values for the isothermal and adiabatic bulk modulus of pure oil, and to obtain the bulk modulus values for other volume change rates which lie between the isothermal and adiabatic compression curves. These baseline data will be applied in the subsequent phases to the appropriate test based on the volume change rate.

Figure 5.4 shows the rate of change in pressure as a result of applying different volume change rates at the baseline phase. As the volume change rate of the actuator changes, the rate of change in pressure would be expected to increase as shown in Fig. 5.4.

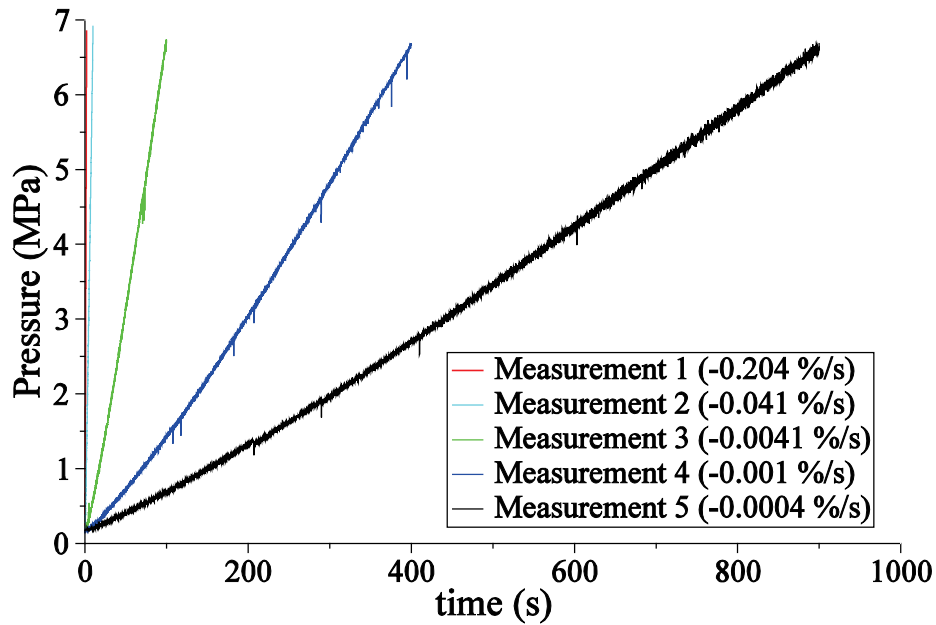


Figure 5.4 Pressure change as a result of applying different volume change rates in the baseline phase. The volume change rate is given in terms of percent of volume change per second $((\Delta V/V_0)/s)$

The corresponding bulk modulus as a function of pressure were calculated and plotted for each volume change rate. Figure 5.5 shows a *typical* result of pressure versus bulk modulus (including the uncertainty error bars) which was obtained at the baseline phase. In this example, the volume change rate was -0.0041 %/s. Note that in obtaining these bulk modulus values, the errors due to the deformation of the testing vessel and cylinder were estimated and subtracted from the final results as explained in Appendix E.

The measurement uncertainty was explained in Section 5.3 and Eq. (5.5) was provided to estimate this uncertainty. According to Eq. (5.5), the uncertainty in calculating the bulk modulus is highly dependent on the operating point and is not constant over the whole range of measurements.

At low pressures, the change in piston displacement (as pressure increases) is small and at high pressures the change in piston displacement is relatively large. As a result, the uncertainty decreases as pressure increases according to Eq. (5.5). Figure 5.6 shows how the uncertainty in measuring the bulk modulus changes with pressure. As the operating point gets closer to the

maximum measurable pressure and displacement of the sensors, the uncertainty in calculating the bulk modulus becomes as low as 3%; however, at low pressures (less than 1 MPa), the uncertainty becomes as high as 80%. This can be also observed from the error bars in Fig. 5.5. Therefore, the reliability of any measurements up to 1 MPa is in question even though the data are repeatable. As it will be shown later in Section 6.2, the greater uncertainty in the low pressure range will increase the average modeling error. This will be more discussed in Section 6.2.

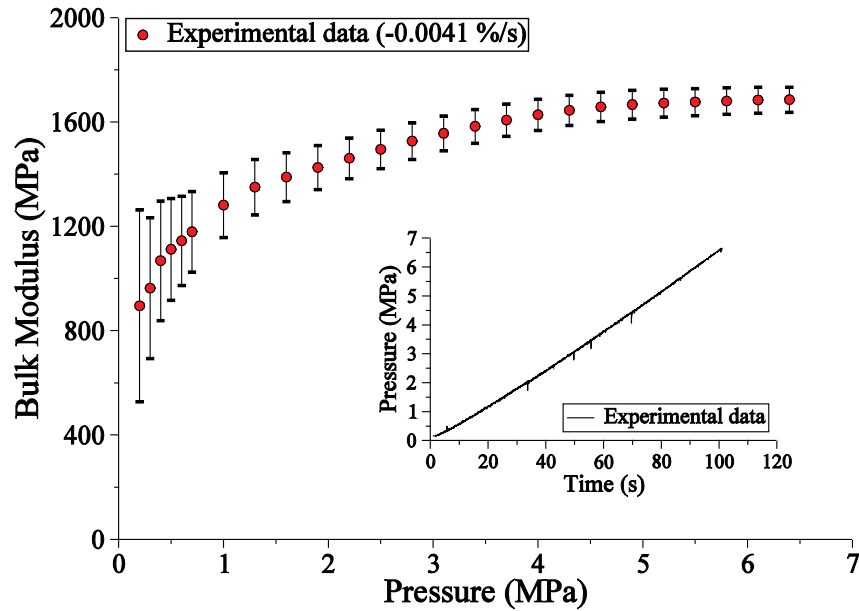


Figure 5.5 A typical example of bulk modulus measurement in the baseline phase ($-0.0041\ %/s$)

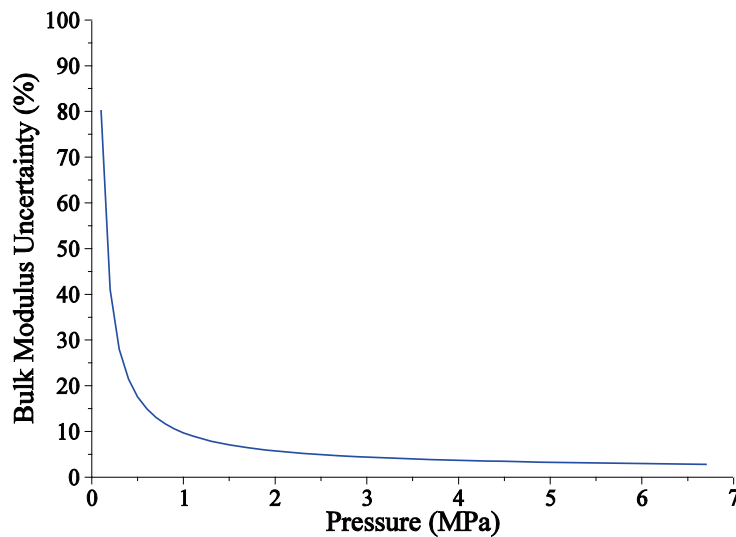


Figure 5.6 Uncertainty of bulk modulus measurements in the baseline phase

In order to make sure that the experimental results were repeatable, each measurement was repeated at least three times and it was found that the measurements were highly repeatable. For example, Fig. 5.7 shows a typical result of repeated measurements when the speed of volume change was $-0.0041\%/s$.

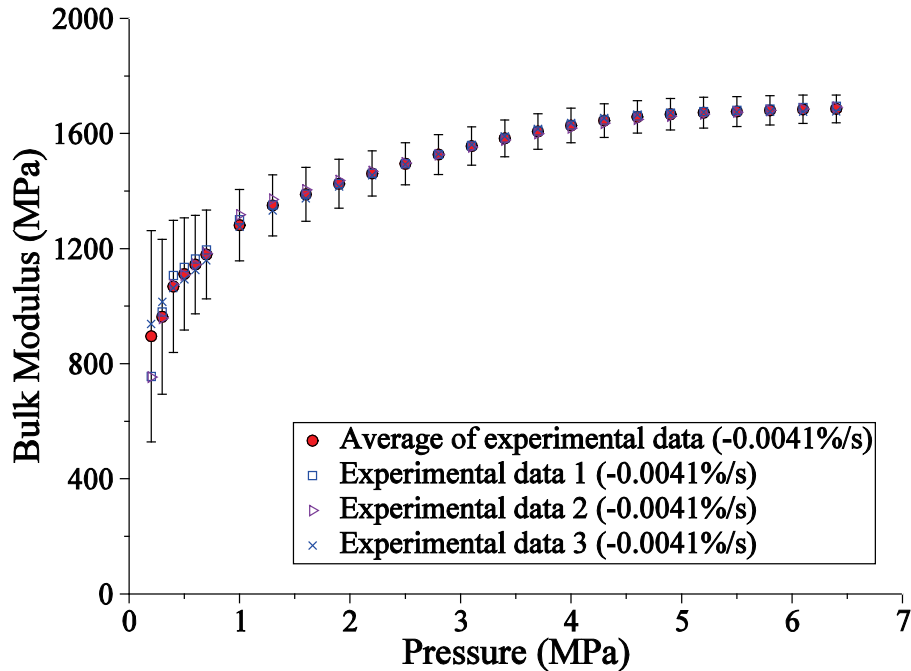


Figure 5.7 Repeatability of the results in the baseline phase when the volume change rate is $-0.0041\%/s$

5.5.2 Lumped air phase

In this phase, air was introduced in the form of “lumped air” to the top of the oil column through a procedure which was explained in the Section 5.2. The effect of different amounts of lumped air (approximately 1, 3 and 5%) on the effective bulk modulus was investigated. These values were chosen arbitrarily to compare the effects of different amounts of lumped air on the effective bulk modulus. Figure 5.8 shows that the presence of the lumped air causes the pressure/time variation of the mixture to differ considerably from the corresponding variations in the pure oil which was shown in Fig. 5.4. In the lumped air phase, the piston was required to move a further distance to reach to the maximum pressure of 6.9 MPa; therefore, a much longer compression time was needed in order to obtain the same volume change rate as the pure oil one. The $-0.0041\%/s$ was obtained for the pure oil with a compression duration of 100 s; however, in

order to obtain the same speed of $-0.0041\ \%/s$ for the mixture of 3.2% of lumped air with the oil, a compression duration of approximately 800 s was needed. This time would be much longer for the other rates.

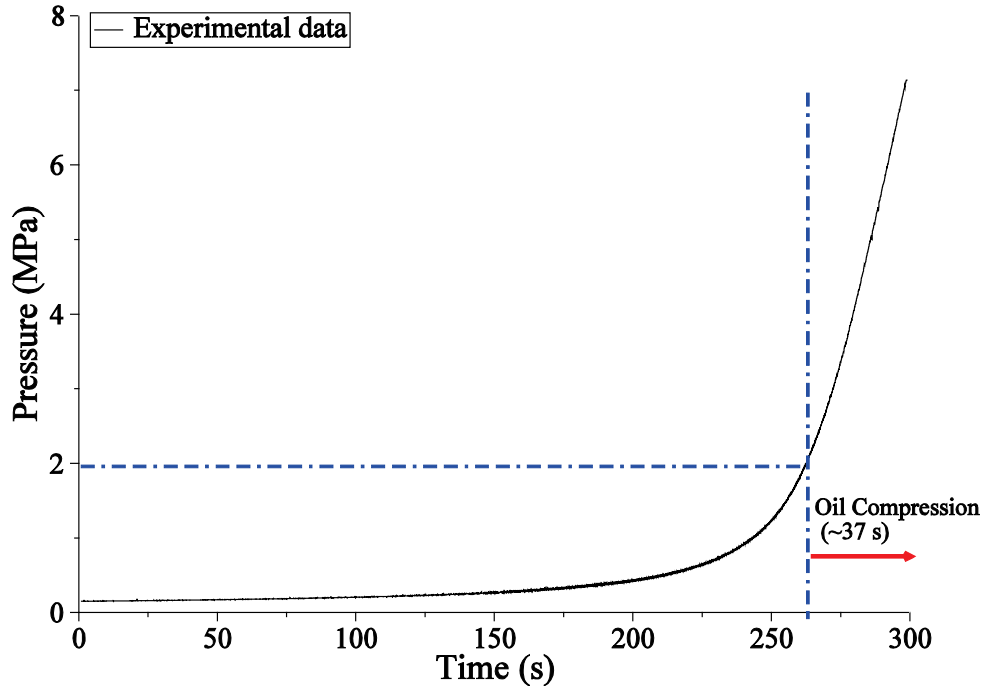


Figure 5.8 A change in the pressure when a lumped air content of 3.2% is added to the oil and the mixture is compressed with the volume change rate of $-0.0123\ \%/s$

In practice it is not necessary to make the volume change rate for the mixture of oil and air to be the same as the volume change rate of the pure oil. Instead, as illustrated in Fig. 5.8, the oil compression time can be estimated from the measured pressure/time plot. In Fig. 5.8, although the mixture of oil and air is being compressed for a duration of about 300 s, a majority of time is spent to compress the air and the oil is only compressed for a duration of 37 s approximately. The oil compression is started from the lowest point where the straight line departs from the curved line and in the example of Fig. 5.8, this happens approximately after the pressure reaches 2 MPa. As it will be discussed in the next Chapter, the bulk modulus of the pure oil is needed when theoretical models have to be compared with the experimental results. Therefore, the compression time which is found from the measured pressure/time curves is used to estimate the bulk modulus of the pure oil. The bulk modulus of the pure oil is estimated from the baseline phase based on the volume change rate.

For each amount of air added, the effective tangent bulk modulus was obtained at different volume change rate. Figure 5.9 shows a typical plot of the effective bulk modulus as a function of pressure when the amount of lumped air was 3.2%. A small graph representing the rate of increase in pressure is also inserted in Fig 5.9.

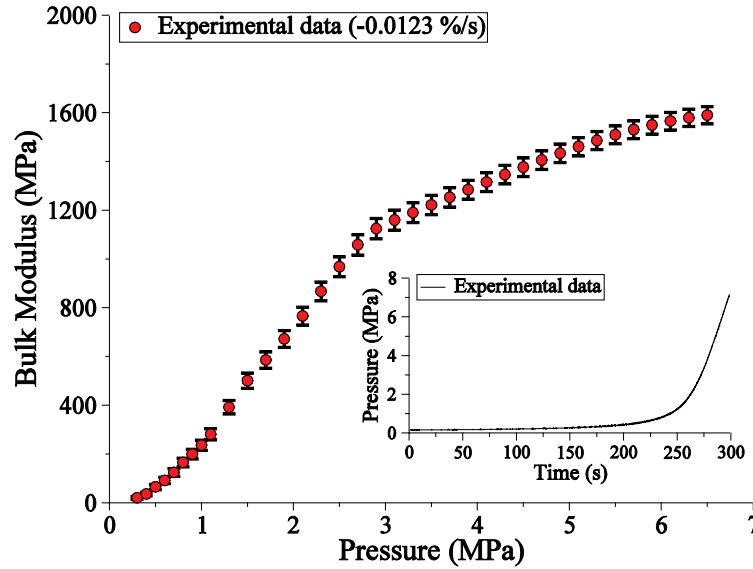


Figure 5.9 A typical example of bulk modulus measurement when the lumped air content is 3.2% and the volume change rate is $-0.0123\ %/s$

It is also interesting to compare the error bars in Fig. 5.9 with the error bars of the baseline phase in Fig. 5.5, especially up to a pressure of 1 MPa. In the baseline phase, the volume change of pure oil at low pressures was significantly smaller resulting in smaller displacements. This increased the uncertainty of the measurements according to Eq. (5.5). However, when air was added to the system, the change in volume of the mixture became larger which resulted in larger displacements of the piston and hence smaller uncertainties. Figure 5.10 shows how the uncertainty in measuring the bulk modulus changes with pressure at the lumped air phase. As the operating point gets closer to the maximum measurable pressure and displacement of the sensors, the uncertainty in calculating the bulk modulus becomes as low as 2 %; however, at low pressures (less than 1 MPa), the uncertainty becomes as high as 27%. Even though the uncertainty of 27% was calculated at the low pressures (less than 1 MPa), due to the lower bulk modulus values at this region, the resulting error bars were also very small as shown in Fig. 5.9.

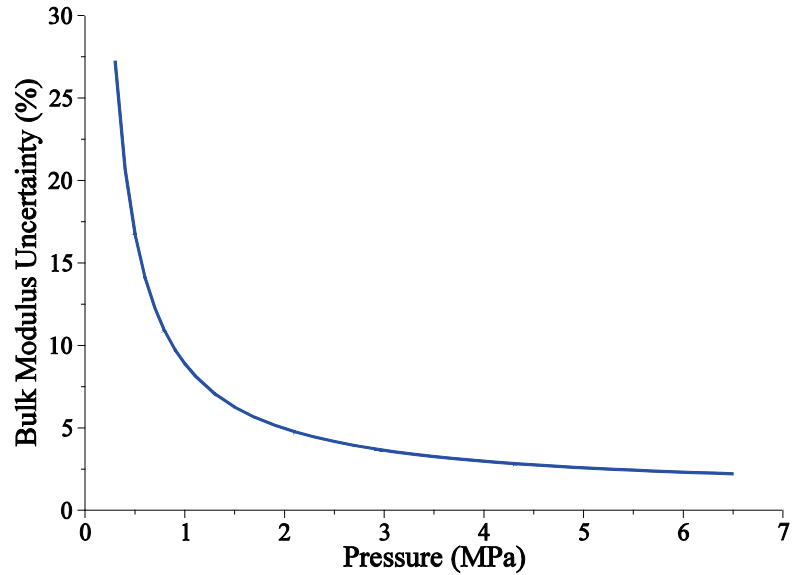


Figure 5.10 Uncertainty of bulk modulus measurements in the lumped air phase

Since the amount of air was known and controlled, repeatability tests were possible. For repeatability test, each measurement was repeated at least three times and it was found that the measurements were highly repeatable. For example, Fig. 5.11 shows a typical result of repeated measurements at the volume change rate of -0.0123% /s when the lumped air content was 3.2%.

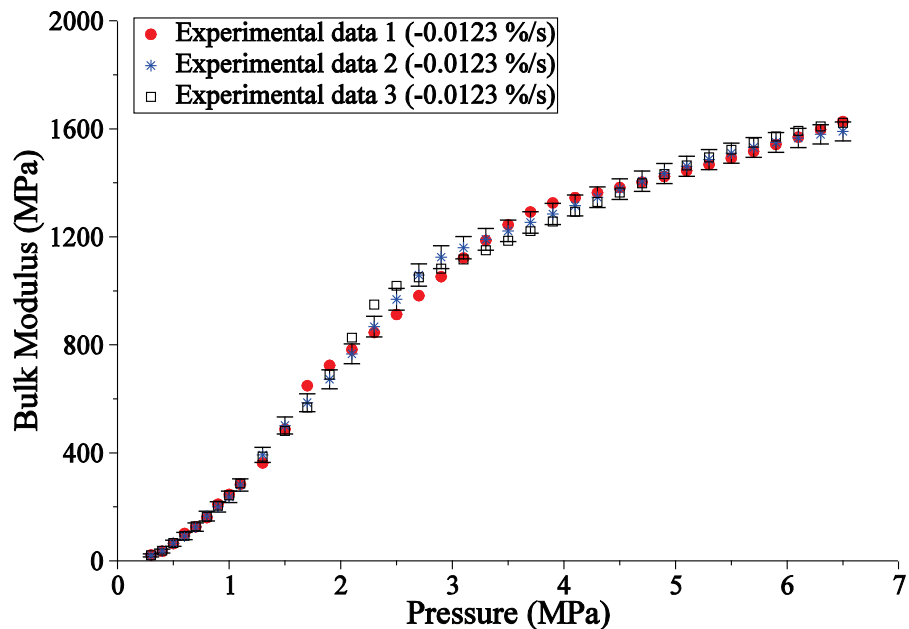


Figure 5.11 Repeatability of the results in the lumped air phase when the amount of lumped air was 3.2 % with the volume change rate of -0.0123% /s

5.5.3 Distributed air phase

In this phase, air was added continuously into the circuit through a venturi orifice for a specific amount of time. It was found that the longer the time interval that air was added, the greater the amount of air that become dispersed in the oil. Unlike the previous phase, small air bubbles with different sizes were generated.

The effect of different amounts of distributed air (approximately 2, 3.5 and 4.5%) on the effective bulk modulus was investigated. These values were chosen arbitrarily to compare the effects of different amounts of distributed air on the effective bulk modulus. For each amount of distributed air, the effective tangent bulk modulus was obtained for different volume change rates. Figure 5.12 shows a typical plot of the effective bulk modulus as a function of pressure when the amount of the distributed air was 3.48%. A small graph representing the rate of increase in pressure was also inserted in Fig 5.12. Figure 5.13 shows how the uncertainty in measuring the bulk modulus changes with pressure at the distributed air phase. The trend of change in the uncertainty with pressure is very similar to the lumped air phase one.

It must be repeated that because air content could only be ascertained after the test was completed, it was not possible to do a standard repeatability test other than to compare results that had similar air content. Figure 5.14 shows that even the amount of air and the volume change rates are slightly different at each test; however, the results are still close together.

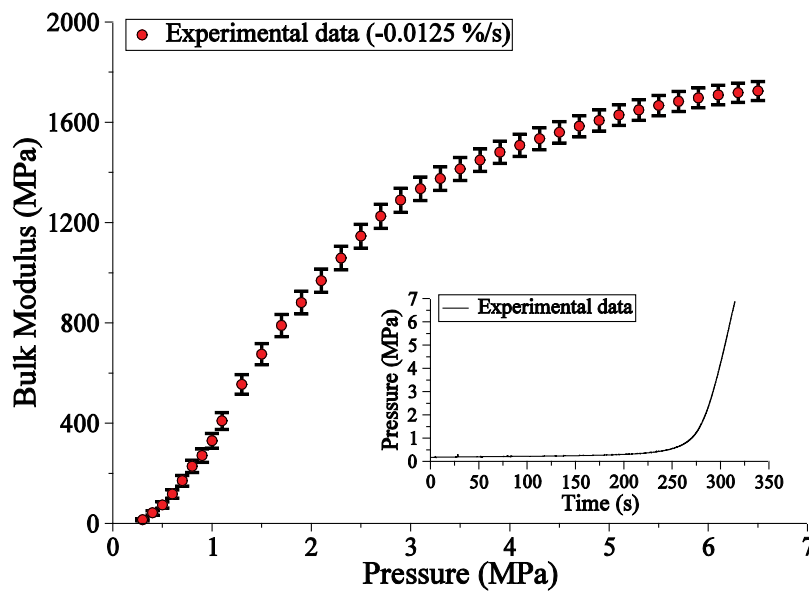


Figure 5.12 A typical example of bulk modulus measurement when the distributed air content is 3.48% and the volume change rate is $-0.0125\ %/s$

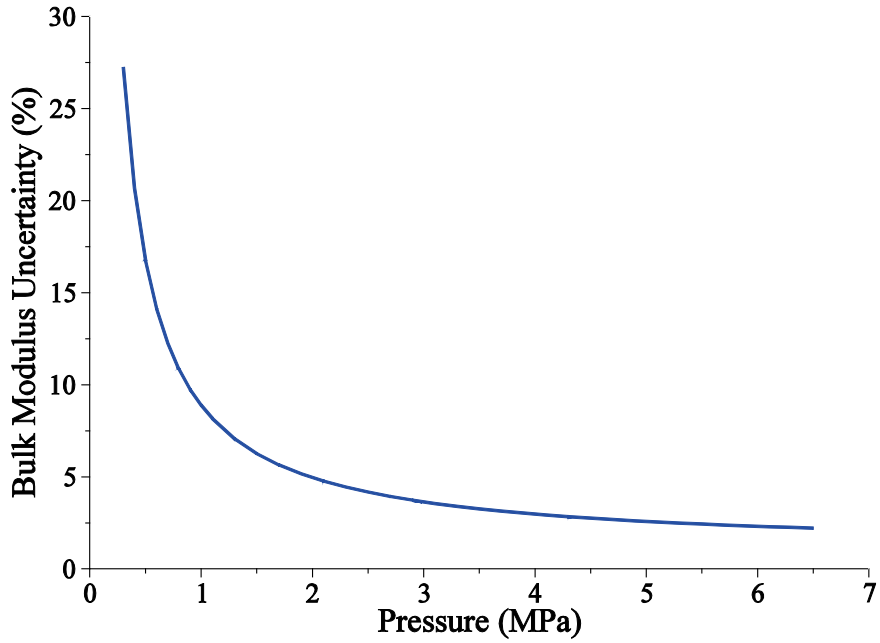


Figure 5.13 Uncertainty of bulk modulus measurements in the distributed air phase

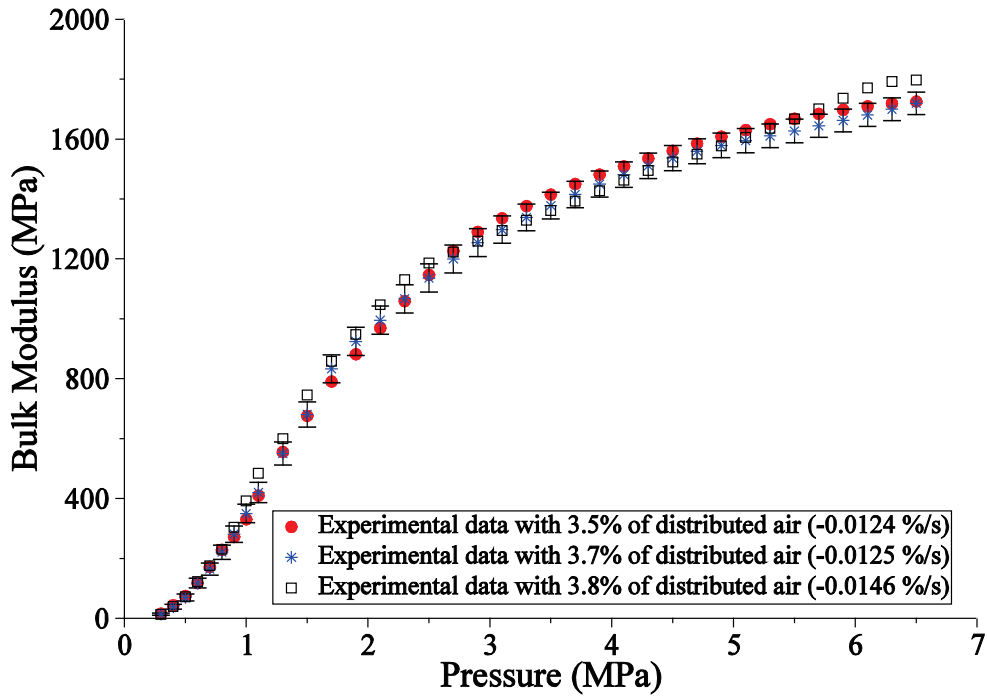


Figure 5.14 Repeatability of the results in the distributed air phase

5.6 Summary

Among different methods of measuring the fluid bulk modulus, the “volume change method” was selected for this study. This method was chosen since it had the highest accuracy compared to the other methods. Using this method, an experimental procedure was successfully incorporated to determine the tangent effective bulk modulus under different types of conditions. In addition, the experimental uncertainty of the apparatus was also estimated.

The experimental apparatus is capable of compressing the test fluid at different volume change rates. This was enabled by designing a closed loop position feedback control system. The test fluid could be used in the form of pure oil, oil and lumped air or oil and distributed air.

The experimental procedure was presented in the three phases. In the first phase, only pure oil was used as a test fluid under different volume change rates and the resulting tangent bulk modulus was obtained. This phase was called the baseline phase and the results from this phase were used in subsequent phases to determine the tangent effective bulk modulus of the oil with air added.

In the second phase, the effect of adding air as “lumped air” to the top of a column of oil was investigated at different volume change rates. Finally in the third phase air was distributed in the oil in the form of air bubbles with different sizes and distributions.

Only a typical example of experimental results at each phase was shown in this Chapter to demonstrate the procedure. In the next Chapter, more measurement results from the three phases will be presented and analyzed.

CHAPTER 6: EXPERIMENTAL RESULTS

6.1 Introduction

The objective of this Chapter is to present and discuss the results of the tests performed on the experimental system described in Chapter 5.

In the previous Chapter, three different phases of the experimental procedure were discussed. Each phase was fully explained and some typical results were presented. In this Chapter, the results of each phase will be analyzed and compared with theoretical models provided previously in Chapter 4.

6.2 Experimental results of the baseline phase

The main objective of the baseline phase was to obtain the bulk modulus of the test oil (Esso Nuto H68) in the experimental system (which may contain small amounts of air) and compare it to existing isothermal and adiabatic values found in the literature (more details are provided in Appendix D). It is difficult to obtain either pure isothermal or pure adiabatic conditions, but it can be assumed that a very rapid test would give nearly adiabatic results and a very slow test would give nearly isothermal results. For different volume change rates, the bulk modulus value would lie somewhere between values for isothermal and adiabatic conditions.

Figure 6.1 shows a typical result of pressure versus bulk modulus (at a predetermined volume change rate) for the baseline phase compared to the expected bulk modulus of pure oil. Also shown in the Figure is a pressure versus time plot of the test oil as a result of the change in volume during the test. According to the literature, the bulk modulus of any pure oil has a linear relationship with pressure (Hayward, 1971) and (Song et al., 1991). However, experimental results of Fig. 6.1 do not show a linear relationship. The bulk modulus changes nonlinearly up to a pressure of 1.5 MPa, followed by a relationship that is nearly linear. The only factor that could have contributed to this initial nonlinear behavior is the presence of small amounts of air. Despite efforts to take air out of the system, some air must have remained trapped in the container resulting in this nonlinear behaviour. The presence of these small amounts of air was also a concern of Hayward (1971), where he suggested that an initial pressure of at least 1 MPa be used when determining the bulk modulus of pure oil.

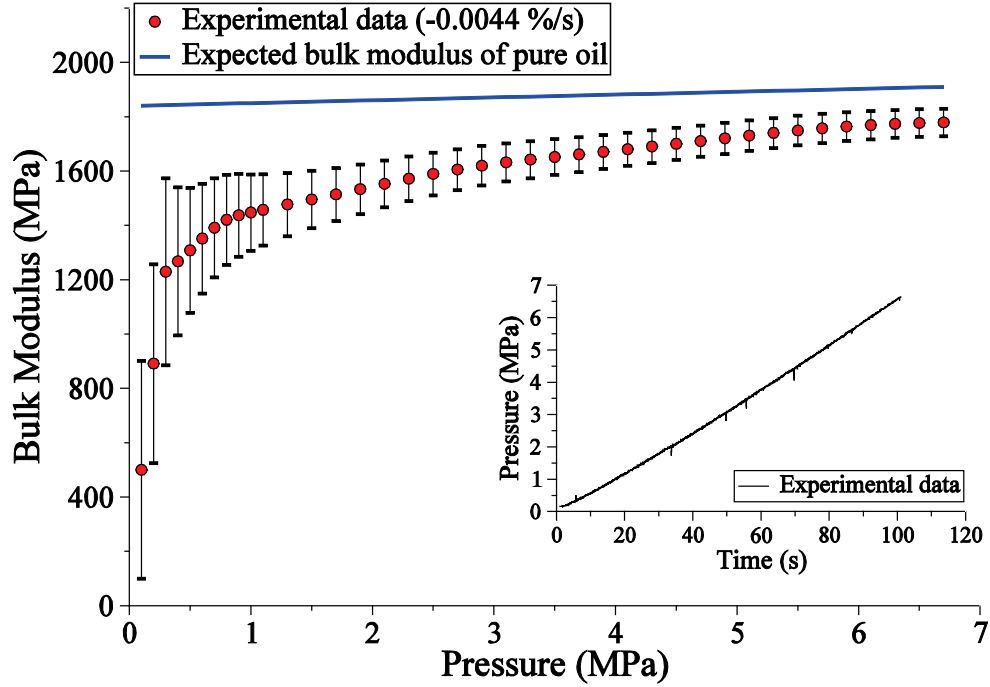


Figure 6.1 A typical example of a bulk modulus measurement in the baseline phase (-0.0044 %/s)

In order to take the effect of small amounts of air into account and to try to model this characteristic, the effective bulk modulus is defined as

$$\frac{1}{K_e} = \frac{1}{K_l(P, T)} + \beta \frac{1}{K_g}, \quad (6.1)$$

where

$$K_l(P, T) = K_l(P_0, T) + m(P - P_0),$$

$$K_g = P, \text{ and}$$

$$\beta = \frac{V_g}{V_g + V_l}.$$

Note that as explained in the previous Chapter, the effect of the deformation of the testing vessel and cylinder was estimated and subtracted off from the experimental results. Therefore, the effective bulk modulus defined in Eq. (6.1) contains only the effect of the test oil and air.

Since the initial volume of air was very small, the volumetric variation of air was not significant and thus it was assumed that the term $\frac{V_g}{V_g + V_l}$ is a constant parameter of β .

Parameter m , which shows the slope of the expected bulk modulus of pure oil, is a function of temperature. Since temperature was maintained at a constant value of $24 \pm 1^\circ\text{C}$, this parameter was expected to be constant during the experiments. The value of m is well known for mineral hydraulic oils and thus did not need to be estimated. Referring to Appendix D, $m = 10.4$ for the test oil used in the experiments. Therefore, the only parameters which were required to be estimated were $K_l(P_0, T)$ and β . In order to determine these two parameters, a least squares approach was used as follows.

A variable Z is defined as

$$Z = \begin{pmatrix} K_l(P_0, T) \\ \beta \end{pmatrix}. \quad (6.2)$$

The function $F(Z)$ is defined as the sum of squared errors between the inverse of the experimental bulk modulus and the predicted bulk modulus from Eq. (6.1)

$$F(Z) = \sum_{i=1}^N \left(\frac{1}{\hat{K}_e} - \frac{1}{K_e} \right)^2, \quad (6.3)$$

where \hat{K}_e is the effective bulk modulus measured experimentally in a hydraulic system subject to pressures P_i , $i = 1, 2, \dots, N$. The boundary condition of variable Z is determined as

$$Z_l \leq Z \leq Z_u, \quad (6.4)$$

where

$$Z_l = \begin{pmatrix} 1534 \\ 0 \end{pmatrix}, \quad \text{and} \quad Z_u = \begin{pmatrix} 1972 \\ 0.5 \end{pmatrix}.$$

The lower and upper limits of $K_l(P_0, T)$ were determined by the predicted values from appendix D. The lower limit of β was set to zero and the upper limit which represents the highest possible amount of air for the case of Figure 6.1 was set to 0.5%.

The objective of the least squares method was to determine a value of Z so that its substitution in Eq. (6.3) would minimize $F(Z)$. The least squares modeling error was determined by calculating the average error E (Yu et al., 1994),

$$E = \sqrt{\frac{1}{N} \sum_{i=1}^N \left(\frac{1}{\widehat{K}_e} - \frac{1}{K_e} \right)^2}. \quad (6.5)$$

The Matlab built in function “lsqcurvefit” was employed to find model parameters and errors with respect to the experimental data.

Once parameters $K_l(P_0, T)$ and β were determined using this least squares method, a theoretical curve based on Eq. (6.1) was determined. This is included in the figures in the next sections.

6.2.1 Isothermal tangent bulk modulus of the test oil

In order to determine the isothermal tangent bulk modulus of the test oil, the results of the slowest volume change rate were chosen. Figure 6.2 shows the experimental results of the baseline phase and the theoretical results based on the nonlinear least squares curve fit of the experimental data when the volume change rate was -0.0006 %/s. An average modeling error of $E = 76$ MPa was calculated.

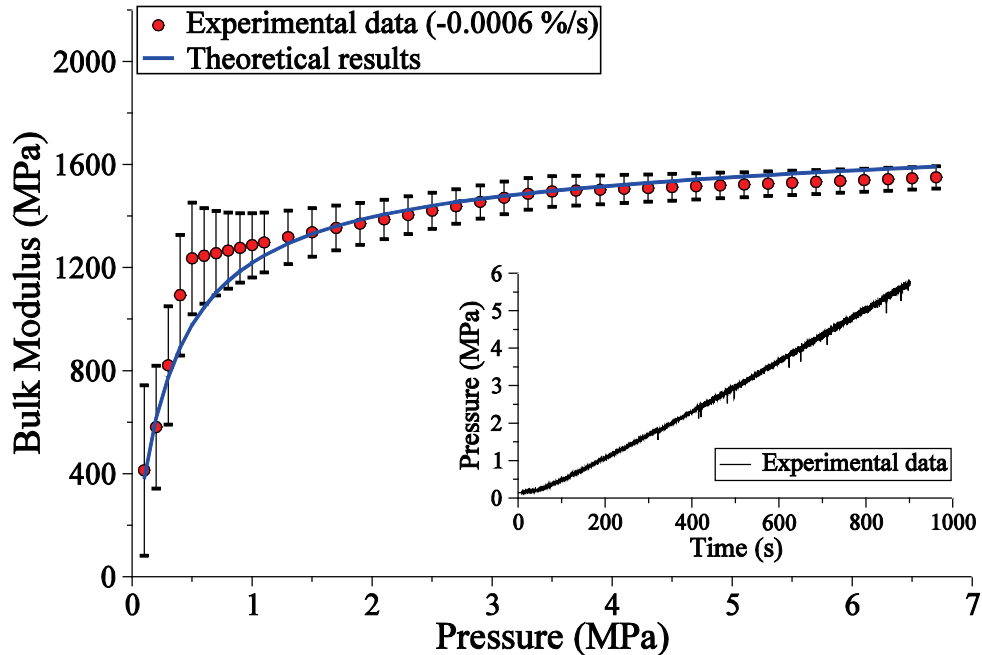


Figure 6.2 Nonlinear least squares curve fit of the experimental data in the baseline phase when the volume change rate was -0.0006 %/s.

The estimated parameters were found as

$$K_l(P_0, T) = 1603 \text{ MPa, and}$$

$$\beta = 0.0002.$$

From Appendix D, the isothermal bulk modulus value of 1615 ± 81 MPa was predicted for the test oil at atmospheric pressure and a temperature of 24°C . It was evident that the estimated value of 1603 MPa was within the predicted range which confirmed the validity of the baseline phase. The estimation of $\beta = 0.0002$ showed that a very small amount of air (0.02%) was present in the system.

6.2.2 Adiabatic tangent bulk modulus of the test oil

In order to determine the adiabatic tangent bulk modulus of the test oil, the results for the fastest volume change rate were chosen. Figure 6.3 shows the experimental results of the baseline phase and the theoretical results based on the nonlinear least squares curve fit of the experimental data when the volume change rate was $-0.216 \text{ \%}/\text{s}$. An average modeling error of $E = 158$ MPa was calculated.

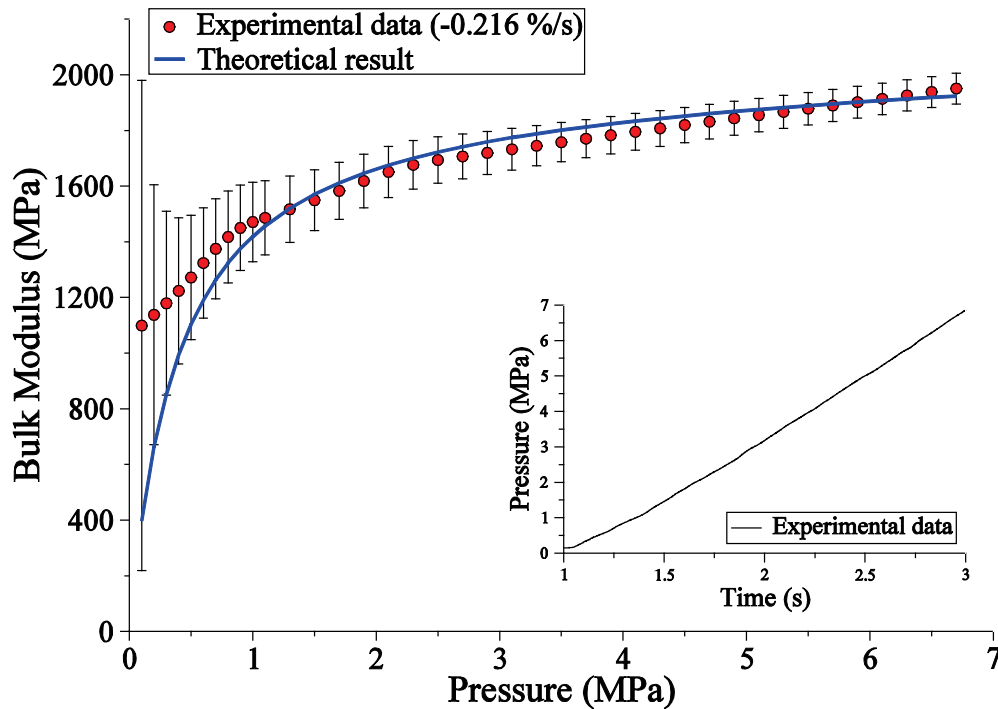


Figure 6.3 Nonlinear least squares curve fit of the experimental data in the baseline phase when the volume change rate was $-0.216 \text{ \%}/\text{s}$.

The estimated parameters were found as

$$K_t(P_0, T) = 1972 \text{ MPa, and}$$

$$\beta = 0.0002.$$

From Appendix D, an adiabatic tangent bulk modulus value of 1878 ± 94 MPa was predicted for the test oil at atmospheric pressure and a temperature of 24°C . The estimated value of 1972 MPa was within the predicted range which again confirmed the validity of the baseline phase. The same value of $\beta = 0.0002$ was estimated again which showed that regardless of the volume change rate, its value was repeatable.

6.2.3 Tangent bulk modulus of the test oil for other volume change rates

In the previous sections, the isothermal and adiabatic tangent bulk modulus values of the test oil were estimated and it was found that the estimated results were in a good agreement with known values from the literature. Obtaining bulk modulus values under purely adiabatic or purely isothermal conditions was not practical experimentally; thus it was assumed that for rapid volume change rates, the bulk modulus value was close to a value representing adiabatic conditions and for very slow compression rates it represented isothermal conditions. For other rates of volume change, the bulk modulus values were estimated using the nonlinear least squares approach. The results for three different volume change rates are shown in Fig. 6.4.

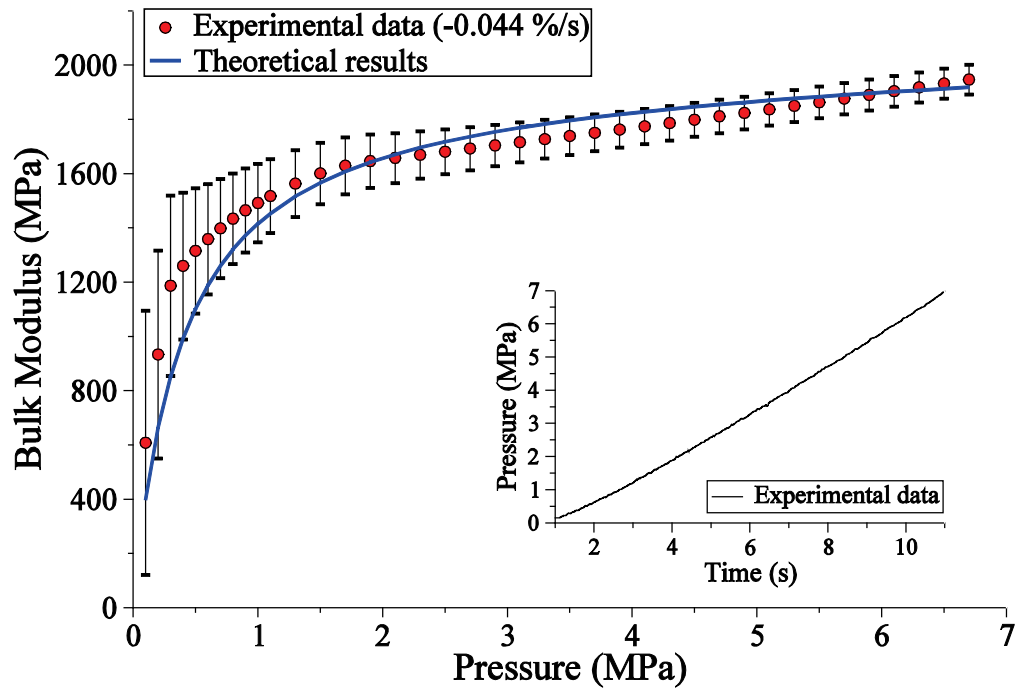


Fig 6.4.a $K_l(P_0, T) = 1966$ MPa, $\beta = 0.0002$ and $E = 109$ MPa

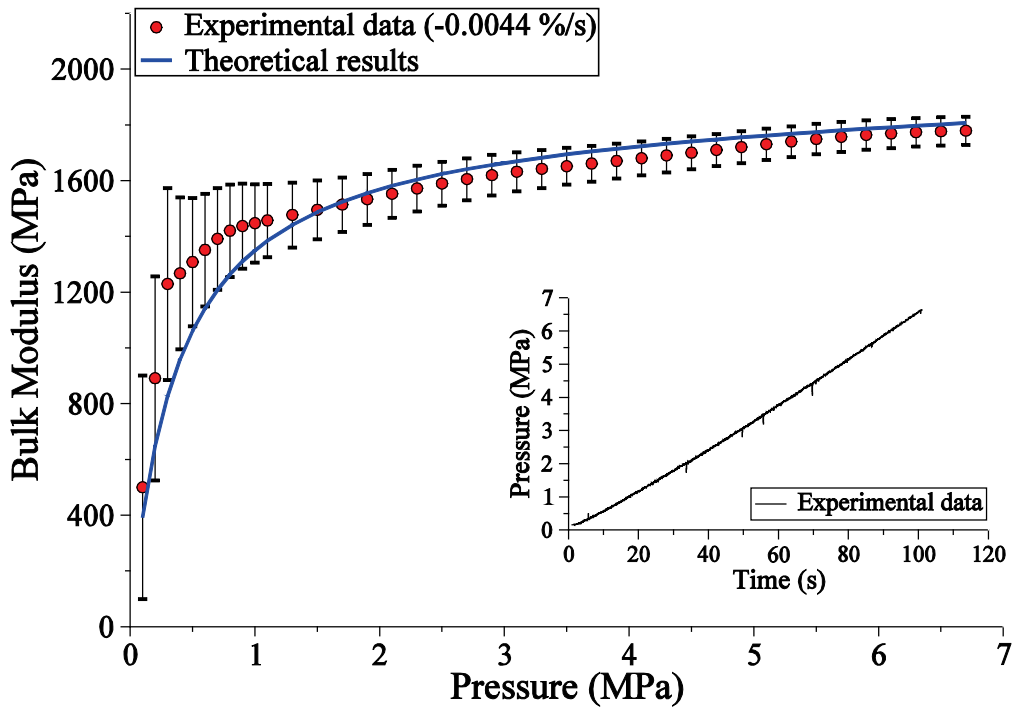


Fig 6.4.b $K_l(P_0, T) = 1841$ MPa, $\beta = 0.0002$ and $E = 119$ MPa

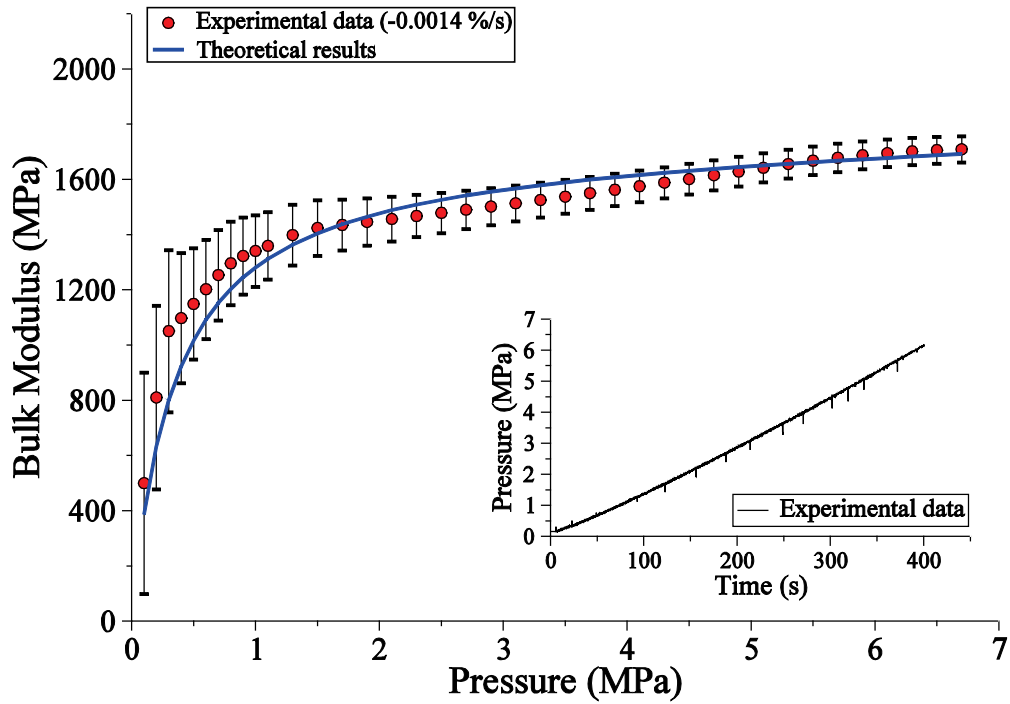


Fig 6.4.c $K_l(P_0, T) = 1713$ MPa, $\beta = 0.0002$ and $E = 77$ MPa

Figure 6.4 Nonlinear least squares curve fit of the experimental data in the baseline phase

The values of $K_l(P_0, T)$ versus oil compression time are summarized in Table 6.1. These values will be used in the next sections to determine the lower and upper limits of the test oil bulk modulus which should be used in the least squares method. As mentioned in the previous Chapter, when there is a mixture of air and oil, the pressure changes nonlinearly as the volume changes. During a typical test (for a specific volume change rate) the air compresses quickly at first and then slows down. This can be seen as the initial nonlinear part of the curve. After some time, the shape of the curve becomes linear suggesting that the air is mostly compressed and the oil is now starting to compress. This rate of compression is much faster since the pressure rises more quickly. If it is assumed that the compression in this region is mainly due to oil compression, the time it takes for the oil to compress can be used as an approximation of the oil compression time. The approximate value of the oil compression time was obtained in subsequent tests from the pressure/time curves and was related to the corresponding values of $K_l(P_0, T)$.

For the baseline phase however, the pressure/time curve was mostly linear and therefore the oil started to be compressed right from the start. For these tests, the approximate oil compression time is the total time of the test. These results are shown in Table 6.1 and these values are used to find the lower and upper limits of the test oil bulk modulus when air is added to the system.

Table 6.1 $K_l(P_0, T)$ versus the oil compression time obtained from the baseline phase

Oil compression time (s)	$K_l(P_0, T)$ (MPa)
2	1972
10	1966
100	1841
400	1713
900	1603

6.3 Experimental results of the effective bulk modulus of the lumped air phase

In this phase of the experimental procedure, air was added in the form of a “lumped air” to the top of the oil column. Since the only contact between air and oil was at the top of the oil column and the contact area was also very small, the possibility of air dissolving into the oil was minimal and assumed insignificant. Therefore, as a first choice, the “compression only” model was chosen for comparison with the experimental results of this phase. If the “compression only” model fails to accurately model the experimental data, the “compression and dissolve” model can be considered as an alternative model. The “compression only” model which was developed in Chapter 4 is given as

$$K_{ec} = \frac{V_l(P, T) + V_{gc}(P, T)}{\frac{V_l(P, T)}{K_l(P, T)} + \frac{1}{K_g} V_{gc}(P, T)}, \quad (6.6)$$

where

$$K_g = nP,$$

$$V_{gc}(P, T) = \left(\frac{P_0}{P}\right)^{\frac{1}{n}} \frac{T}{T_0} (X_0),$$

$$K_l(P, T) = K_l(P_0, T) + m(P - P_0), \text{ and}$$

$$V_l(P, T) = V_l(P_0, T) \left(1 + \frac{m}{K_l(P_0, T)} (P - P_0)\right)^{\frac{1}{m}}.$$

The same nonlinear least squares method which was explained in the baseline phase was also employed here. As was explained in the baseline phase, the parameter m is constant and is equal to 10.4. The parameter X_0 which is the volumetric fraction of air at atmospheric pressure was estimated from the change in volume versus pressure curve. This approach to finding X_0 was explained in Chapter 5. Therefore, the only two unknown parameters that needed to be estimated using the least squares method were: n and $K_l(P_0, T)$. A variable Z is defined as

$$Z = \left(\begin{array}{c} n \\ K_l(P_0, T) \end{array} \right). \quad (6.7)$$

The parameter n is the polytropic index of air which can theoretically range from 1 to 1.4, depending on the heat exchange rate between the air bubbles and the surrounding oil. For the isothermal and adiabatic compression of air, n equals to 1 and 1.4 respectively. The parameter $K_l(P_0, T)$ which is the tangent bulk modulus of oil at atmospheric pressure, takes a value within a range from 1534 to 1972 MPa, depending on the volume change rate of oil. This range can be narrowed down further by analyzing the measured pressure/time curve of each experiment and obtaining the oil compression time as was explained in the previous Chapter. The resulting oil compression time was then compared with the bulk modulus values given in Table 6.1 and a new range for $K_l(P_0, T)$ was obtained. For example, if the oil compression time of 40 s was found from the pressure/time curve of an experiment, the new range of $K_l(P_0, T)$ would be between 1841 and 1966 MPa. This method was repeated for each measurement and a new range of $K_l(P_0, T)$ was found.

The function $F(Z)$ is defined as the sum of squared errors between the inverse of the experimental bulk modulus and the predicted bulk modulus from Eq. (6.6) as

$$F(Z) = \sum_{i=1}^N \left(\frac{1}{\hat{K}_{ec}} - \frac{1}{K_{ec}} \right)^2, \quad (6.8)$$

where \hat{K}_{ec} is the effective bulk modulus measured experimentally in a hydraulic system subject to pressures $P_i, i = 1, 2, \dots, N$.

In the following sections, the experimental data and the theoretical best fit of each experiment are plotted based on the results of the least squares method. The estimated values of n and $K_i(P_0, T)$ are also given for each experiment. For comparison purposes, another two sets of theoretical results are plotted for the two extreme cases of $n = 1$ and $n = 1.4$. A plot of change in pressure with time is also shown for each experiment.

6.3.1 Experimental results with 1% of lumped air

Figure 6.5 (a, b and c) depicts the experimental and theoretical bulk modulus changes as a function of pressure for a 1% lumped air when the volume change rate was -0.659 %/s, -0.0045 %/s and -0.00118 %/s respectively.

The experimental results of Fig. 6.5.a suggest that the value of the polytropic index must be changing over the pressure range as evidenced by the move from the $n = 1.4$ curve at low pressures to the $n = 1$ curve at the higher pressures. Up to a pressure of 2 MPa, the experimental results agree well with the theoretical results for $n = 1.4$. After this pressure, the experimental results tend to follow the theoretical results for $n = 1$.

Applying the nonlinear least squares method, the average value of the polytropic index over the entire pressure range was approximated as $n = 1.068$. It was realized that even though the volume change rate was high (-0.659 %/s), the average value of n was close to the theoretical results for $n = 1$.

Figure 6.5.b shows that when the same amount of lumped air was compressed slowly (-0.0045 %/s), the experimental results fit very well with the theoretical results for $n = 1$. The same result was also obtained in Fig. 6.5.c when the volume change rate was -0.00118 %/s.

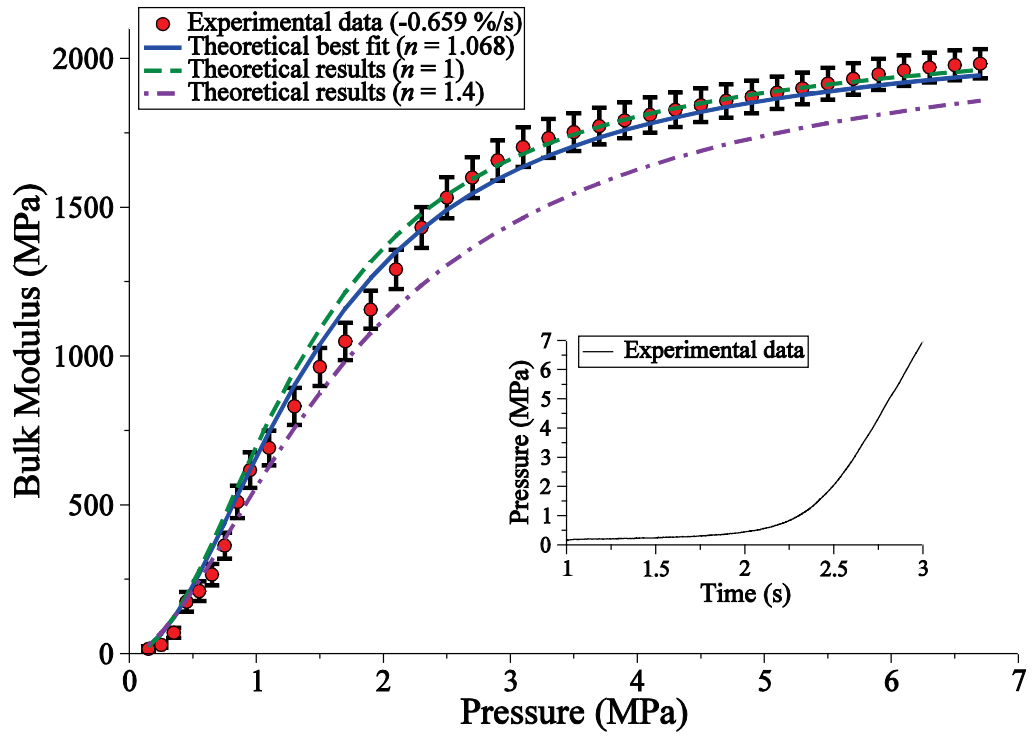


Figure 6.5.a $K_l(P_0, T) = 1972$ MPa, $n = 1.068$ and $E = 50$ MPa

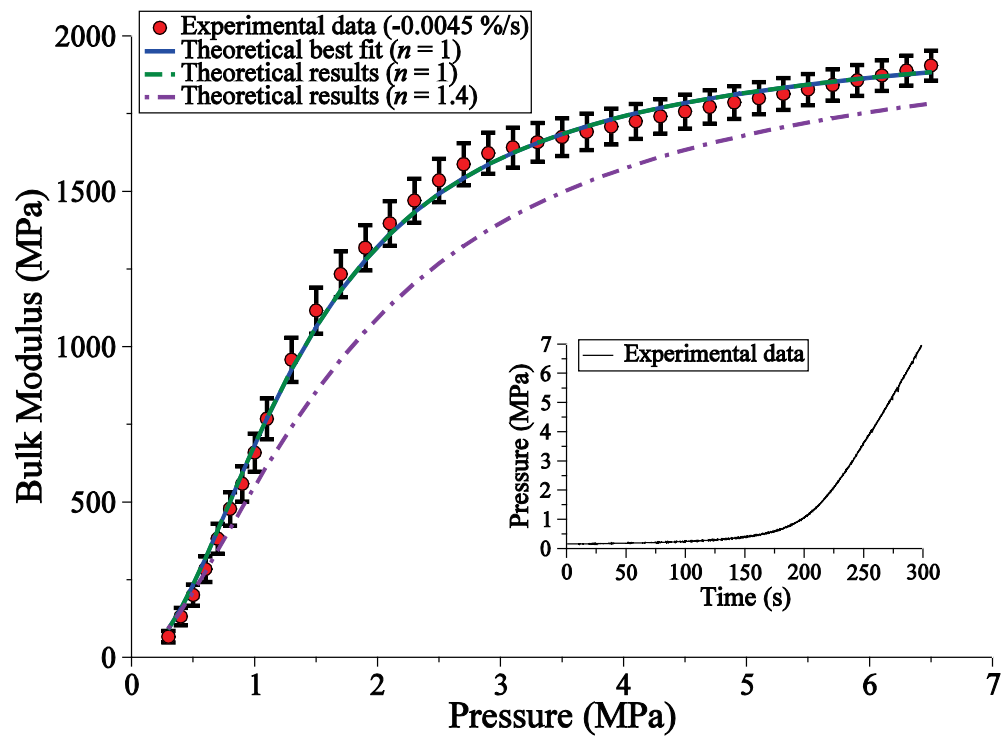


Figure 6.5.b $K_l(P_0, T) = 1898$ MPa, $n = 1$ and $E = 27$ MPa

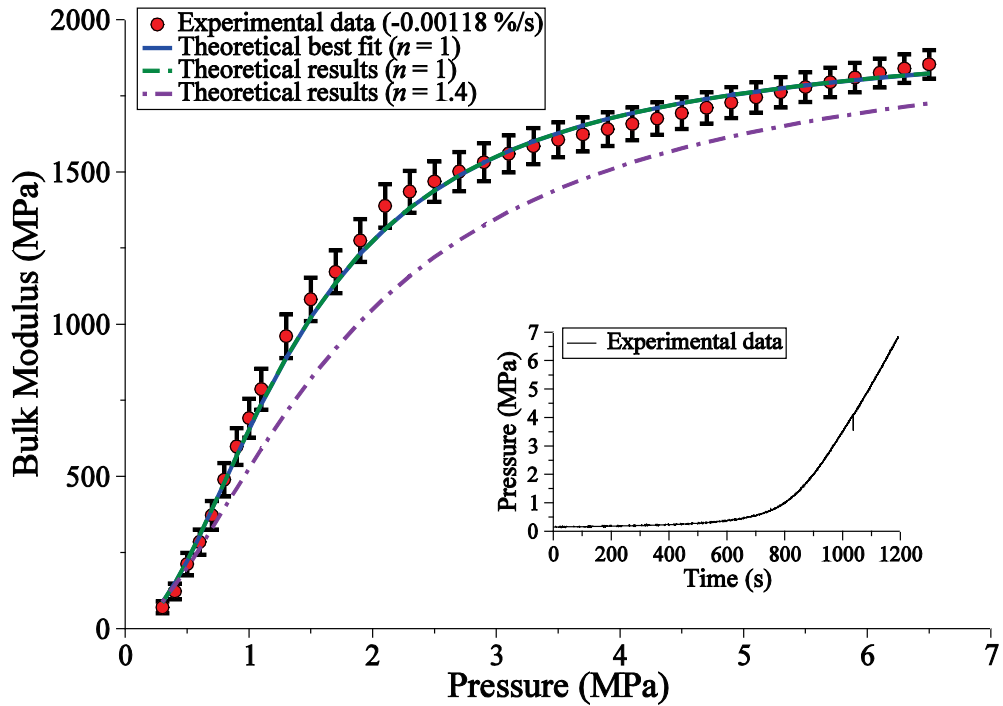


Figure 6.5.c $K_l(P_0, T) = 1838 \text{ MPa}$, $n = 1$ and $E = 31 \text{ MPa}$

Figure 6.5(a, b and c) Nonlinear least squares curve fit of the experimental data with 1% of lumped air and different volume change rates

6.3.2 Experimental results with 3% of lumped air

Figure 6.6 (a, b and c) depicts the experimental and theoretical bulk modulus changes as a function of pressure for 3% of lumped air when the volume change rate was -1.82 %/s , -0.0123 %/s and -0.00917 %/s respectively.

The experimental results of Fig. 6.6.a show that the average value of the polytropic index over the entire pressure range was approximated as $n = 1.206$. As the volume change rate was decreased, the results tended to get closer to the theoretical results for $n = 1$. In Fig. 6.6.b where the volume change rate was -0.0123 %/s , the average value of n was approximated as 1.079. Figure 6.6.c shows that decreasing the volume change rate to -0.00917 %/s , resulted in an average value of $n = 1.085$, which is still closer to the theoretical results ($n = 1$).

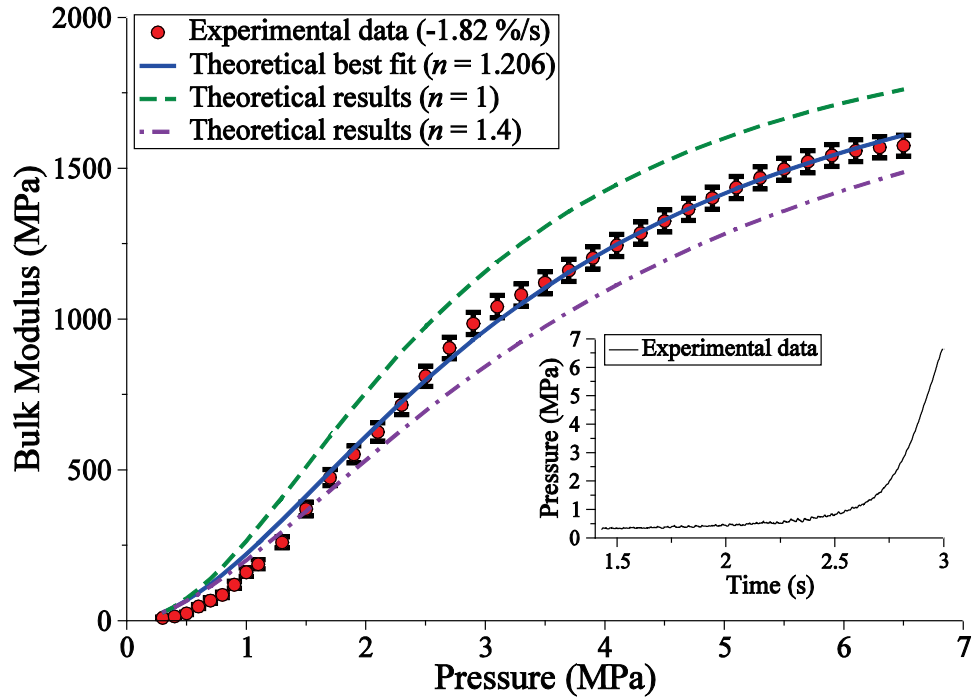


Figure 6.6.a $K_I(P_0, T) = 1972$ MPa, $n = 1.206$ and $E = 34$ MPa

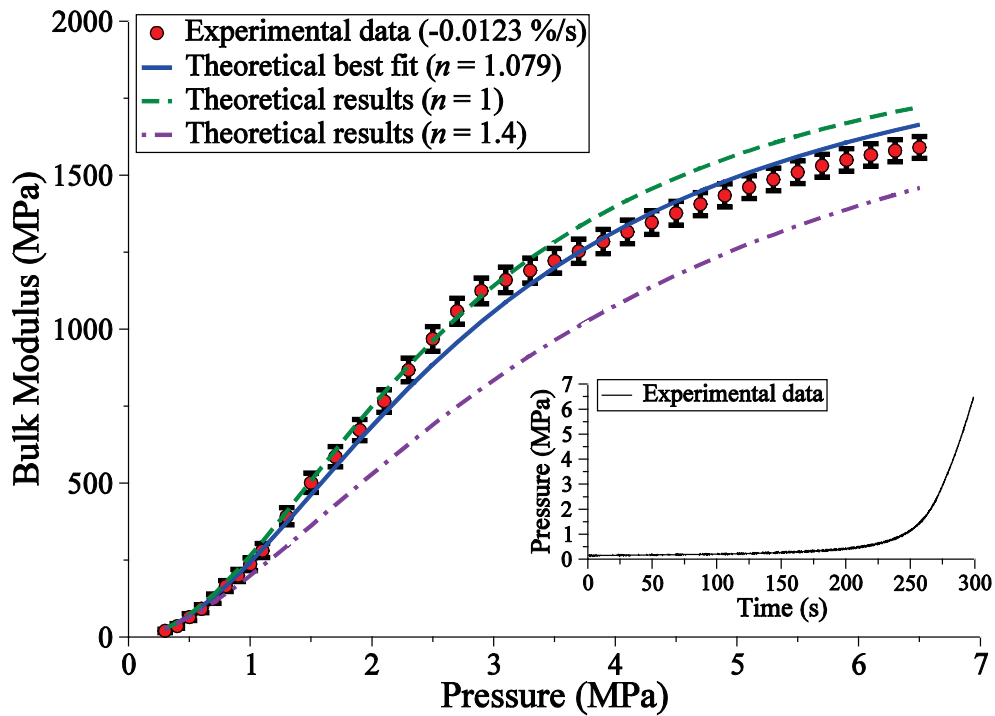


Figure 6.6.b $K_I(P_0, T) = 1920$ MPa, $n = 1.079$ and $E = 45$ MPa

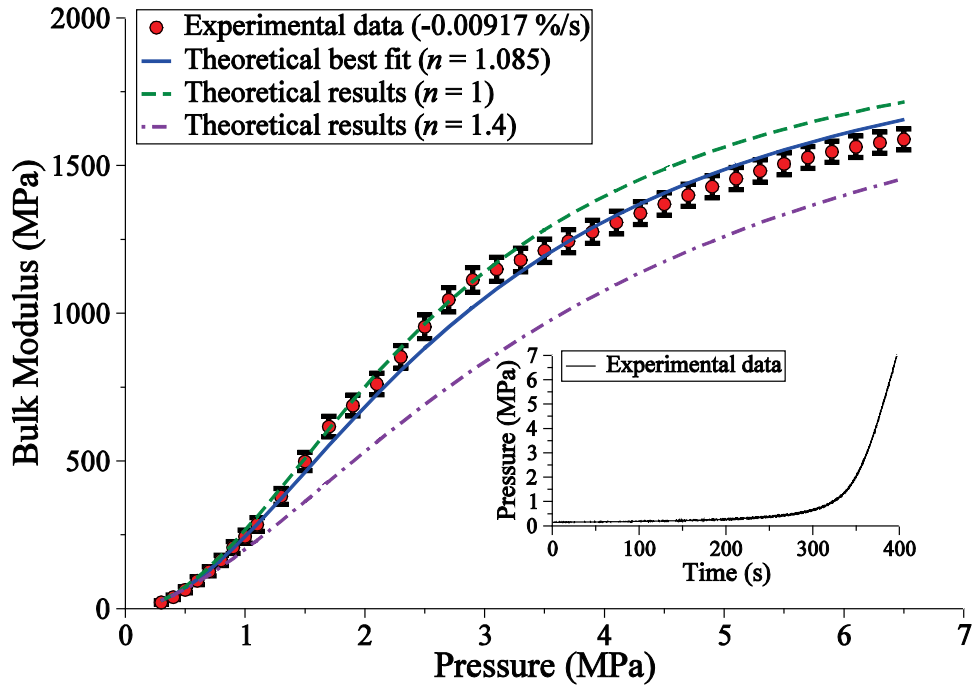


Figure 6.6.c $K_l(P_0, T) = 1910 \text{ MPa}$, $n = 1.085$ and $E = 42 \text{ MPa}$

Figure 6.6 (a, b and c) Nonlinear least squares curve fit of the experimental data with 3% of lumped air and different volume change rates

6.3.3 Experimental results with 5% of lumped air

Figure 6.7(a, b and c) depicts the experimental and theoretical bulk modulus changes as a function of pressure for 5% of lumped air when the volume change rate was -2.74 %/s , -0.0188 %/s and -0.0114 %/s respectively.

The experimental results of Fig. 6.7.a shows that the average value of the polytropic index over the entire pressure range was approximated as $n = 1.331$, which was closer to the theoretical results ($n = 1.4$).

As the volume change rate was decreased, the results tended to get closer to the theoretical results ($n = 1$). In Fig. 6.7.b where the volume change rate was -0.0188 %/s , the average value of n was approximated as $n = 1.083$. Figure 6.7.c shows that decreasing the volume change rate to -0.0114 %/s , resulted in an average value of $n = 1.059$, which was still closer to the theoretical results ($n = 1$).

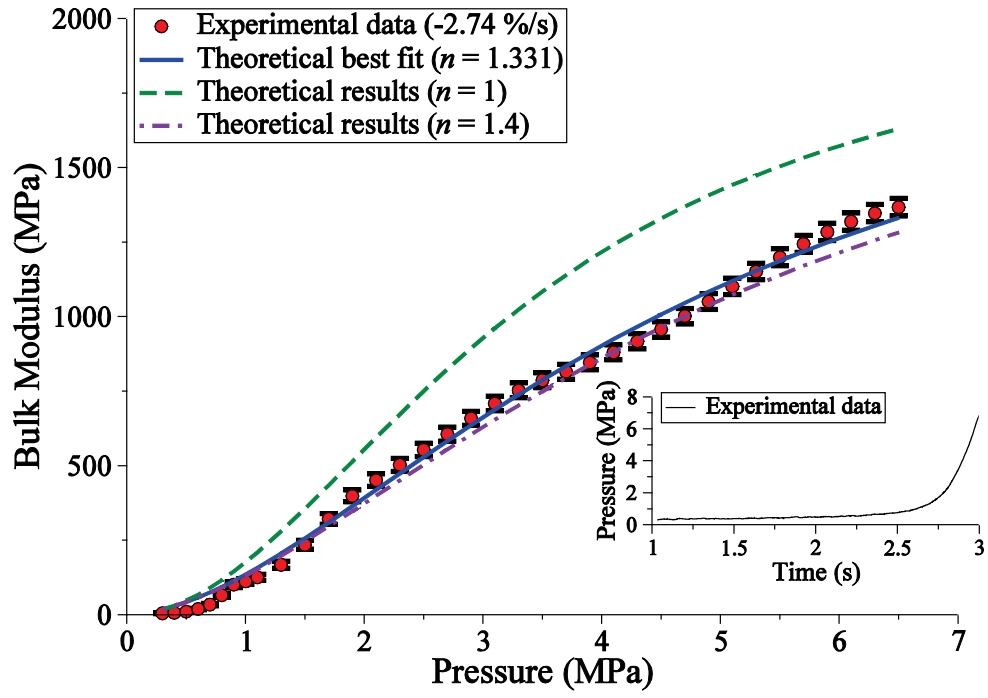


Figure 6.7.a $K_I(P_0, T) = 1972$ MPa, $n = 1.331$ and $E = 30$ MPa

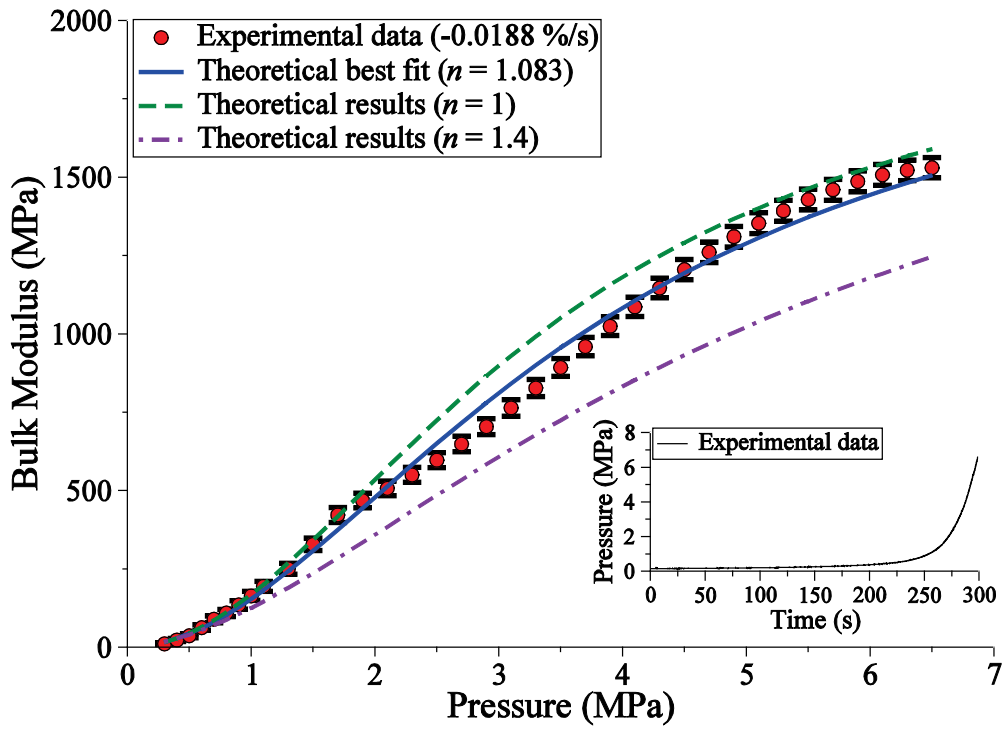


Figure 6.7.b $K_I(P_0, T) = 1930$ MPa, $n = 1.083$ and $E = 39$ MPa

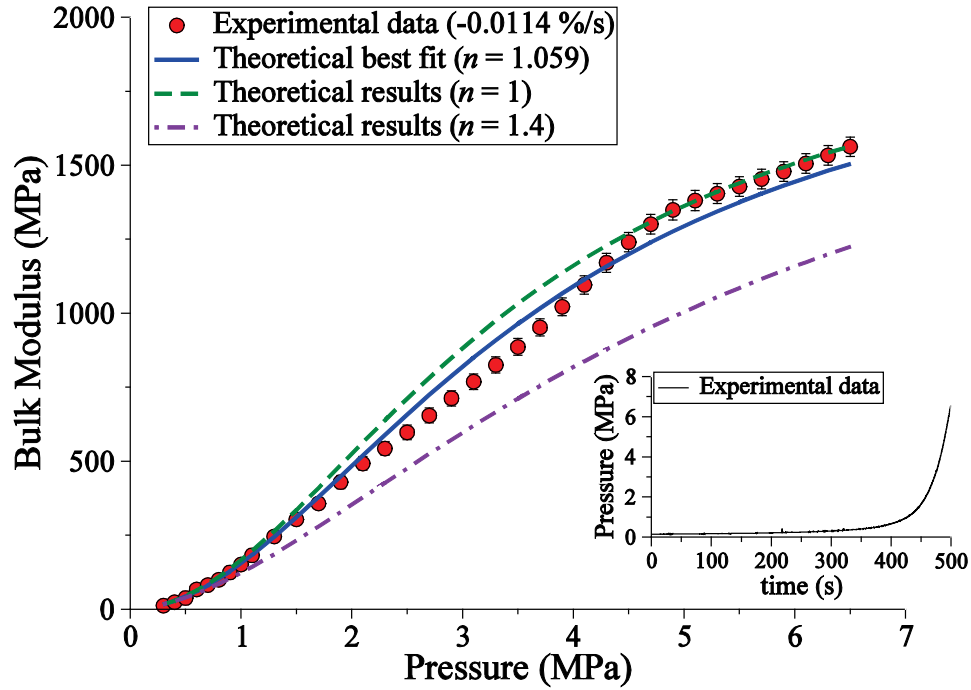


Figure 6.7.c $K_l(P_0, T) = 1900$ MPa, $n = 1.059$ and $E = 45$ MPa

Figure 6.7 (a, b and c) Nonlinear least squares curve fit of the experimental data with 5% of lumped air and different volume change rates

6.4 Experimental results of the effective bulk modulus of the distributed air phase

In this phase of the experimental procedure, air was added continuously into the circuit through a venturi orifice for a specific amount of time. As a result, small air bubbles of different sizes were generated. Unlike the lumped air phase, since each air bubble was in contact with the surrounded oil, the total contact area of the air and oil was increased. Hence, the possibility of air dissolving into the oil was also expected to increase.

Because of this increased possibility of air dissolving into the oil, the “compression and dissolve” model was chosen for comparison with the experimental results of this phase. The “compression and dissolve” model from Chapter 4 is given as

$$\left\{ \begin{array}{l}
K_{ecd} = \frac{V_l(P, T) + V_{gcd}(P, T)}{\frac{V_l(P, T)}{K_l(P, T)} + \frac{1}{K_{g_1}} V_{gcd}(P, T)} \quad \text{For } P \leq P_C \\
\\
K_{ecd} = \frac{V_l(P, T) + \left(\frac{P_0}{P}\right)^{\frac{1}{n_2}} (X_0)_C}{\frac{V_l(P, T)}{K_l(P, T)} + \frac{1}{K_{g_2}} \left(\frac{P_0}{P}\right)^{\frac{1}{n_2}} (X_0)_C} \quad \text{For } P > P_C
\end{array} \right. , \quad (6.9)$$

where

$$K_{g_1} = n_1 P,$$

$$K_{g_2} = n_2 P,$$

$$V_{gcd}(P, T) = \left(\frac{P_0}{P}\right)^{\frac{1}{n_1}} \frac{T}{T_0} X_0 \left(\left(\frac{P_C - P}{P_C - P_0}\right) \left(1 - \frac{(X_0)_C}{X_0}\right) + \frac{(X_0)_C}{X_0} \right),$$

$$K_l(P, T) = K_l(P_0, T) + m(P - P_0), \text{ and}$$

$$V_l(P, T) = V_l(P_0, T) \left(1 + \frac{m}{K_l(P_0, T)} (P - P_0)\right)^{\frac{1}{m}}.$$

The same nonlinear least squares method which was explained in the baseline phase was also employed here. As explained in the baseline phase, the parameter m is constant and is equal to 10.4. Therefore, the five unknown parameters which needed to be estimated using the least squares method were: n_1 , n_2 , $K_l(P_0, T)$, P_C and $(X_0)_C$.

The upper and lower limits of parameters n_1 , n_2 and $K_l(P_0, T)$ were determined using the same method as explained in Section 6.3. Note that n_1 and n_2 are defined as the polytropic index of air before and after the saturation point respectively. Parameter P_C was defined as the critical pressure where the oil is saturated and no more air will be dissolved into the oil. Depending on the amount of air present, parameter P_C can take on a value within a range from 0.1 MPa up to the maximum pressure of the system. Parameter $(X_0)_C$ was defined as the critical volumetric

fraction of air and it gives the amount of air which remains after the critical pressure is reached. Depending on the amount of air, $(X_0)_C$ can range from 0 to the maximum volumetric fraction of air.

Function $F(Z)$ is defined as the sum of the squares errors between the inverse of the experimental bulk modulus and the predicted bulk modulus. Using Eq. (6.6),

$$F(Z) = \sum_{i=1}^N \left(\frac{1}{\hat{K}_{ecd}} - \frac{1}{K_{ecd}} \right)^2, \quad (6.10)$$

where \hat{K}_{ecd} is the effective bulk modulus measured experimentally in the hydraulic system subject to pressures P_i , $i = 1, 2, \dots, N$.

In the following sections, the experimental data and the theoretical best fit of each experiment are plotted based on the results of the least squares method. The estimated values of n_1 , n_2 , $K_l(P_0, T)$, P_C and $(X_0)_C$ are also given for each experiment.

Another two sets of the theoretical results were plotted for the two extreme cases of $n = 1$ and $n = 1.4$. It is noted that these two sets were plotted based on the “compression only” model and presented only for comparison purposes. A plot of the change in pressure with time is also shown for each experiment.

6.4.1 Experimental results of the distributed air phase for a rapid volume change rate

Figure 6.8 (a, b and c) depicts the experimental and theoretical bulk modulus values as a function of pressure for $X_0 = 1.5\%$, 3.35% and 4.5% of distributed air when there was a rapid volume change rate. In this series of tests it was not evident where P_C occurred. For the least squares method, an upper and lower limit of P_C was needed in order to find the theoretical bulk modulus best fit curves. In this case, the upper limit of P_C was chosen to be 6.5 MPa, which corresponded to the maximum pressure range of the experiments. Because the least squares method “chose” the upper limit of P_C , it may be concluded that the real value of P_C was not reached or even beyond the maximum pressure range of the experiments.

Since $(X_0)_C$ gives the amount of air which remains after the critical pressure P_C is reached, the real values of $(X_0)_C$ may also be different than the actual values because the real

values of P_C are not known. Since the fit of the results were good, it was deemed that the theoretical values of P_C and $(X_0)_C$ are good approximations of the actual values.

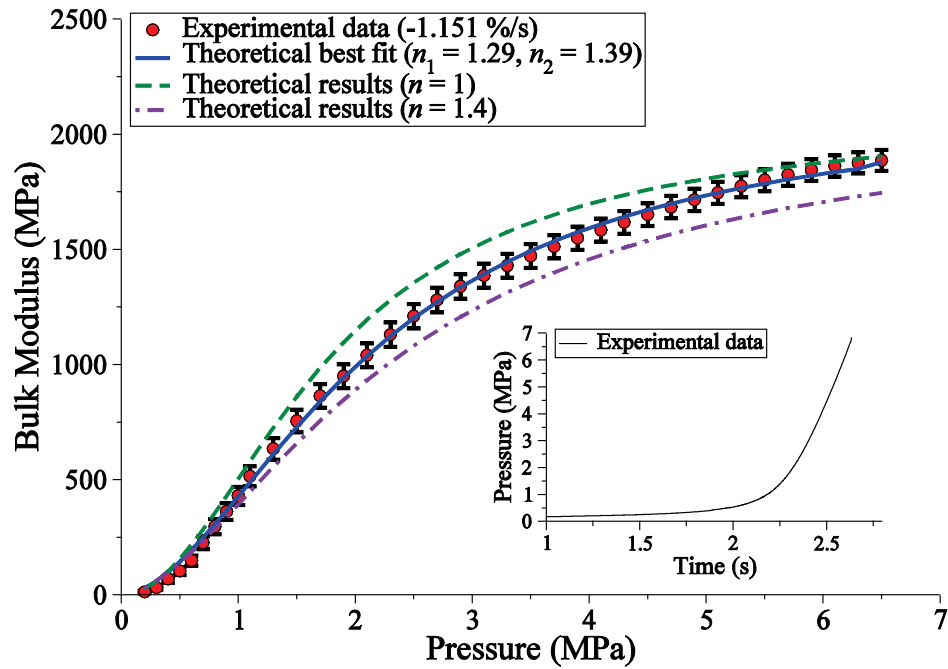


Figure 6.8.a $K_l(P_0, T) = 1972$ MPa, $X_0 = 1.5\%$, $P_C = 6.5$ MPa, $(X_0)_C = 0.97\%$ and $E = 20$ MPa

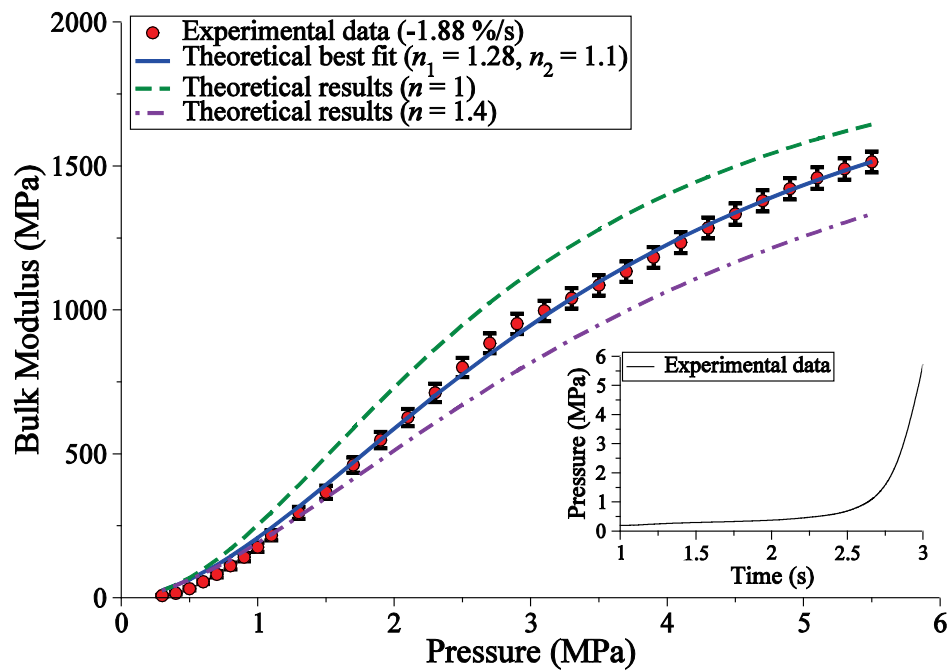


Figure 6.8.b $K_l(P_0, T) = 1970$ MPa, $X_0 = 3.35\%$, $P_C = 6.5$ MPa, $(X_0)_C = 2.49\%$ and $E = 20$ MPa

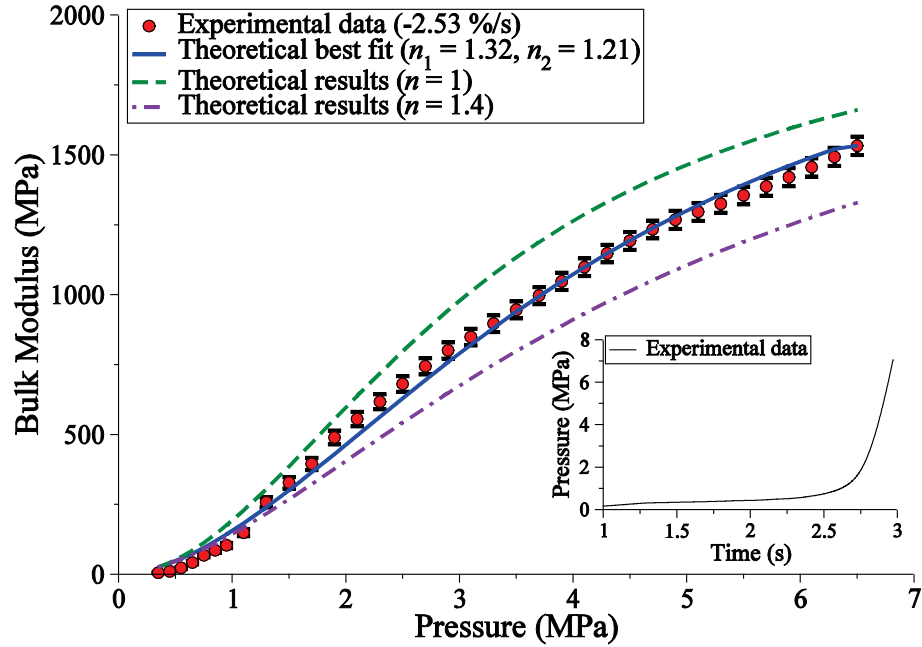


Figure 6.8.c $K_l(P_0, T) = 1970$ MPa, $X_0 = 4.5\%$, $P_C = 6.5$ MPa, $(X_0)_C = 3\%$ and $E = 31$ MPa

Figure 6.8 (a, b and c) Nonlinear least squares curve fit of the experimental data for different amounts of distributed air when the volume change rate was fast

An analysis of Fig. 6.8 (a, b and c) shows that the experimental results always lie between the two extreme cases of $n = 1$ and $n = 1.4$. This may be a result of little or no dissolving of air into the oil and can be confirmed by comparison of the experimental results with the “compression only” model in Fig. 6.9 (a,b and c). In Fig. 6.9 (a,b and c), the experimental results of $X_0 = 1.5\%$, 3.35% and 4.5% of distributed air was compared with both the “compression only” and “compression and dissolve” models. The results show that the agreement between the models and the experimental data was good. However, a comparison of the least squares modeling error (E) of the two models indicate that the “compression only” model resulted in greater values of E . For the “compression only” model the E values were 162, 139 and 129 MPa, compared with the “compression and dissolve” E values of 20, 20 and 31 MPa for $X_0 = 1.5\%$, 3.35% and 4.5% respectively. It is also noted that the polytropic index value (n) of the “compression only” model did not match with the (n_1) value of the “compression and dissolve” model. For the “compression only” model the n values were 1.16, 1.18 and 1.17 compared with the “compression and dissolve” n_1 values of 1.29, 1.28 and 1.32 for $X_0 = 1.5\%$,

3.35% and 4.5%, respectively. This suggests that the “compression only” model underestimates the amount of “ n ” due to the greater average modeling error (E). Even though the “compression only” model matched closely with the experimental results, it was less accurate than the “compression and dissolve” model. This implies that even with a rapid volume change, a small amount of air was dissolved into the oil which could be only captured by “compression and dissolve” model.

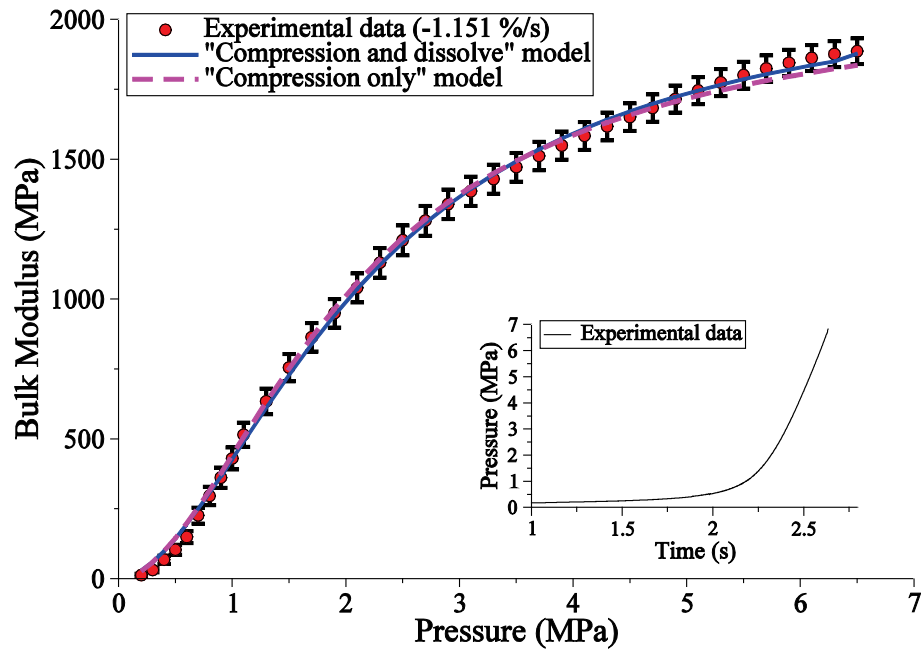


Figure 6.9.a $K_l(P_0, T) = 1972$ MPa, $X_0 = 1.5\%$, $n = 1.16$ and $E = 162$ MPa

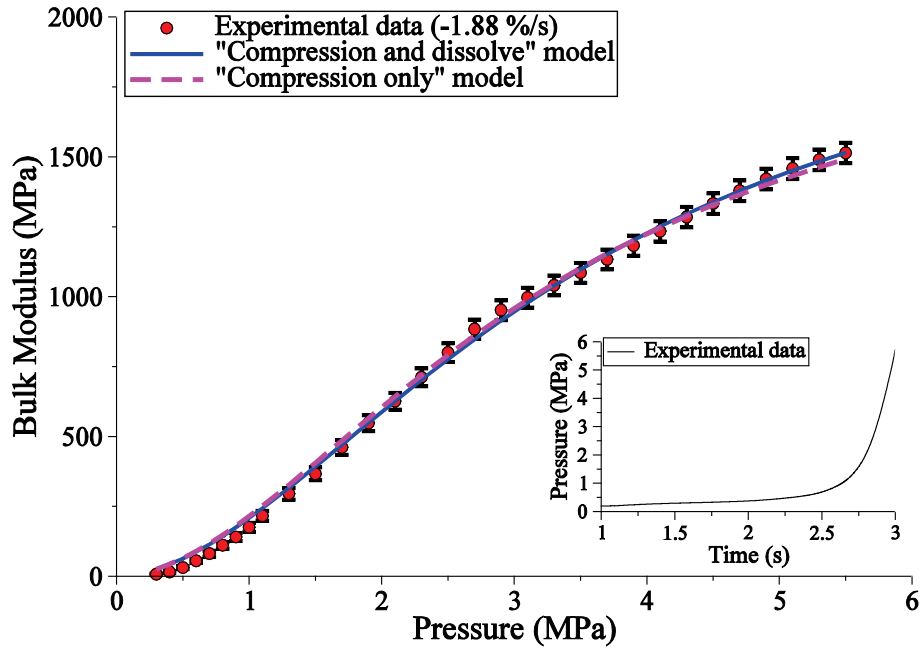


Figure 6.9.b $K_l(P_0, T) = 1970$ MPa, $X_0 = 3.35\%$, $n = 1.18$ and $E = 139$ MPa

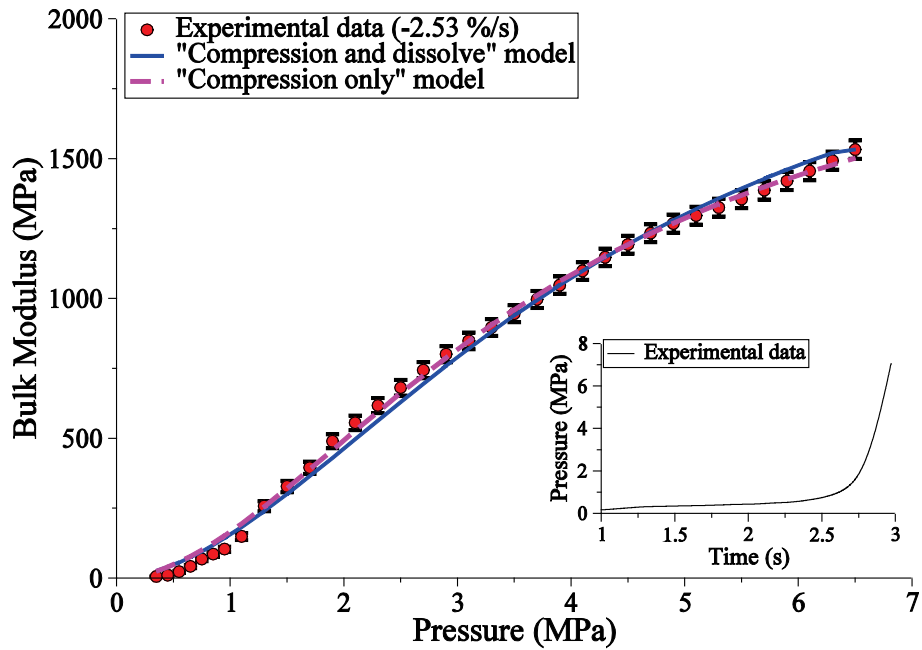


Figure 6.9.c $K_l(P_0, T) = 1970$ MPa, $X_0 = 4.5\%$, $n = 1.17$ and $E = 129$ MPa

Figure 6.9 (a, b and c) Comparison of the "compression only" and "compression and dissolve" model for different amounts of distributed air when the volume change rate was rapid (Note that the given values represent the parameters of the "compression only" model)

6.4.2 Experimental results of the distributed air phase for a slow volume change rate

Figure 6.10 (a, b) depicts the experimental and theoretical bulk modulus changes as a function of pressure for 1.8% and 1.9% of distributed air when the volume change rate was -0.00891 %/s and -0.00442 %/s respectively. The volume change rate in both cases was considered to be slow, since the total duration of the compression time was 250 and 550 s, respectively.

Figure 6.10 (a, b) show that the critical pressure value in both cases was up to the maximum pressure range of the experiments. This suggests that the real value of P_C was not reached or beyond the maximum pressure of 6.5 MPa. As a result, the real value of $(X_0)_C$ was not known, but deemed to be a good approximation because of the fit of the experimental results to the theoretical curve.

It is also evident that in both cases, after a pressure of 5 MPa was reached, the experimental results lie above the theoretical results ($n = 1$). This suggests the possibility of air dissolving into the oil which could only be captured by the “compression and dissolve” model as shown by the theoretical best fit in the figures.

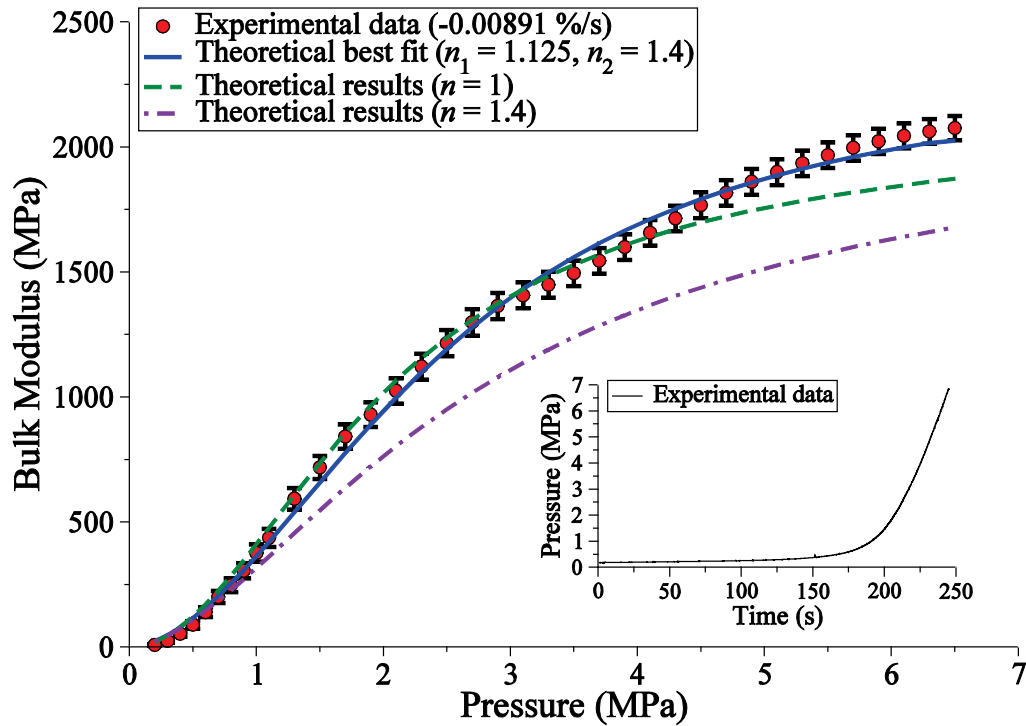


Figure 6.10.a $K_l(P_0, T) = 1935$ MPa, $X_0 = 1.8\%$, $P_C = 6.5$ MPa, $(X_0)_C = 0.1\%$ and $E = 49$ MPa

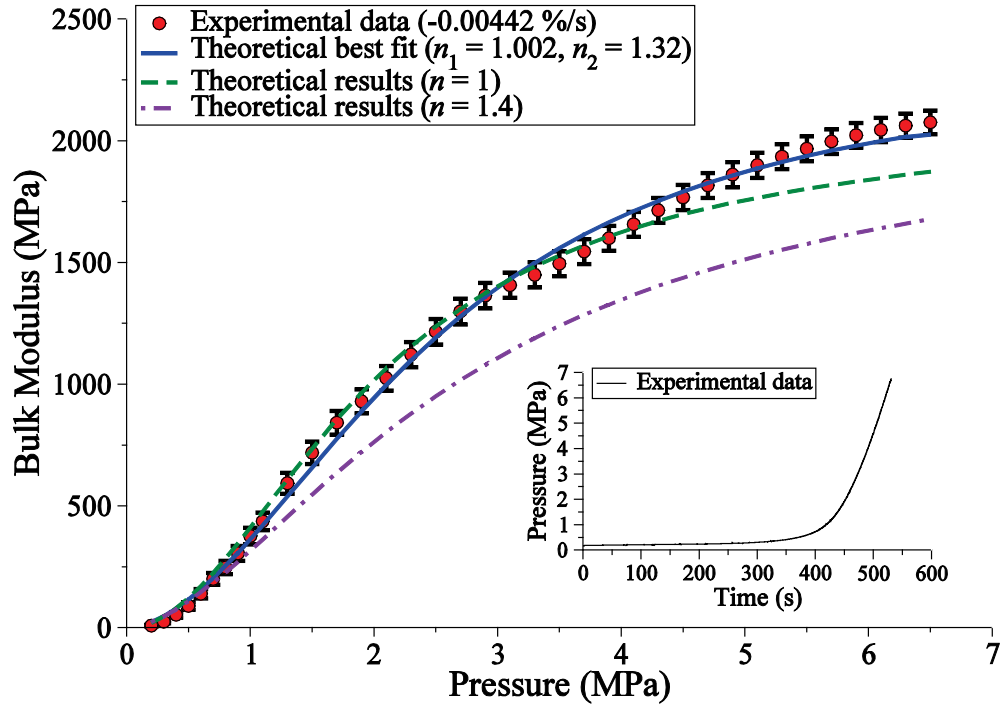


Figure 6.10.b $K_l(P_0, T) = 1900$ MPa, $X_0 = 1.9\%$, $P_C = 6.1$ MPa, $(X_0)_C = 1.09\%$ and $E = 37$ MPa

Figure 6.10 (a and b) Nonlinear least squares curve fit of the experimental data for 1.8% and 1.9 % of distributed air when the volume change rate was slow

Figure 6.11 (a , b) represents the experimental and theoretical bulk modulus changes as a function of pressure for 3.48% and 3.42% of distributed air when the volume change rate was -0.0125 %/s and -0.00618 %/s respectively. The volume change rate in both cases was considered to be slow, since the total duration of the compression time was 300 and 600 s respectively.

In both experiments, the dissolving effect of air into the oil was large enough to move all of the experimental results above the “compression only” region of the theoretical results ($n = 1$). The critical pressure of $P_C = 1.1$ MPa in Fig. 6.10.a shows that saturation occurred at a point where the remaining percentage of air, $(X_0)_C = 1.91\%$, was only being compressed after this point.

Also shown in Fig. 6.11.b was that by increasing the total compression time, the critical pressure decreased to a value of $P_C = 1$ MPa. This was expected since enough time was allowed for the air bubbles to dissolve into the oil and this lowered the saturation pressure point and also increased $(X_0)_C$ to a value of 2.22%.

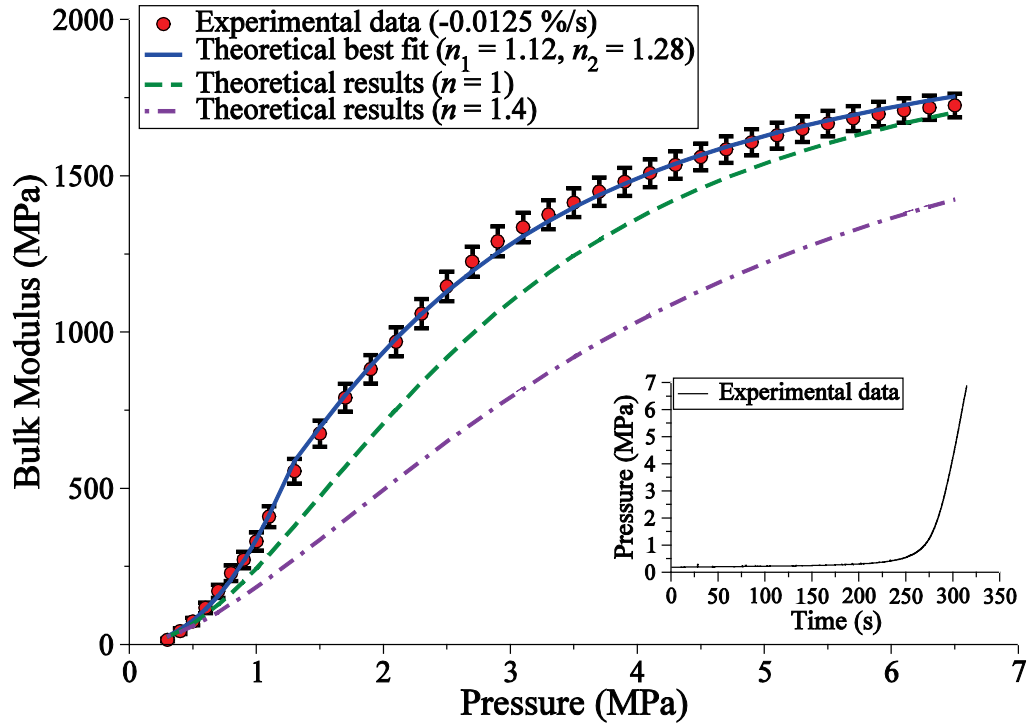


Figure 6.11.a $K_l(P_0, T) = 1925$ MPa, $X_0 = 3.48\%$, $P_C = 1.1$ MPa, $(X_0)_C = 1.91\%$ and $E = 15$ MPa

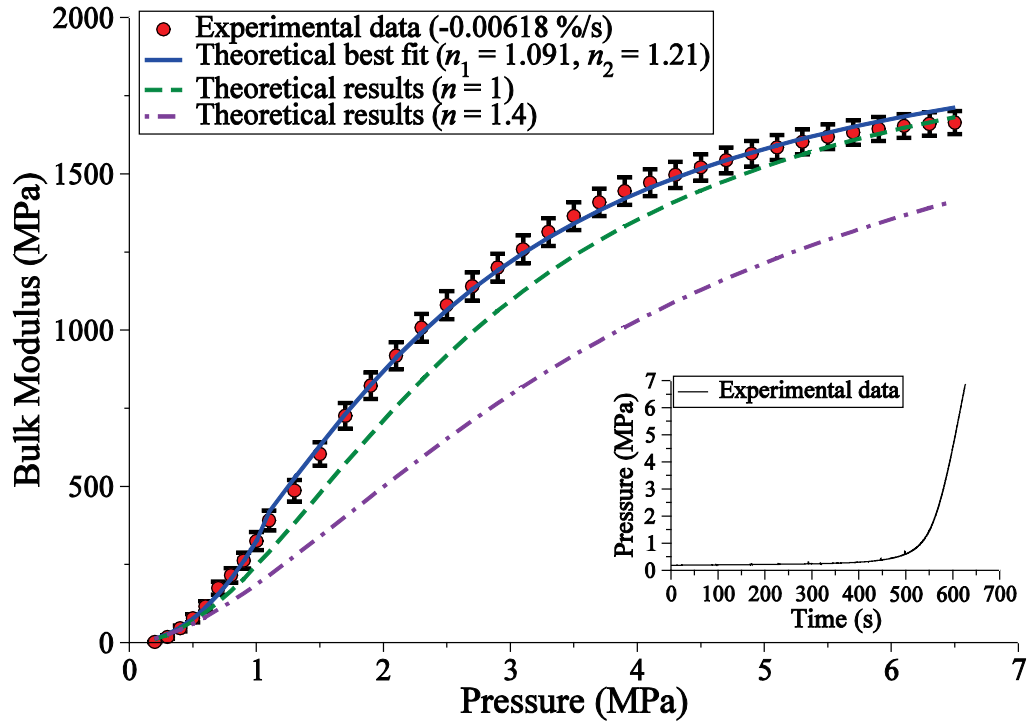


Figure 6.11.b $K_l(P_0, T) = 1890$ MPa, $X_0 = 3.42\%$, $P_C = 1$ MPa, $(X_0)_C = 2.22\%$ and $E = 18$ MPa

Figure 6.11 (a and b) Nonlinear least squares curve fit of the experimental data for 3.48% and 3.42 % of distributed air when the volume change rate was slow

Figure 6.12 (a , b) represents the experimental and theoretical bulk modulus changes as a function of pressure for 4.4% of distributed air when the volume change rate was -0.0178 %/s and -0.0115 %/s respectively. The volume change rate in both cases was considered to be slow, since the total duration of compression time was about 270 and 420 s respectively.

Again in both experiments, the dissolving effect of air into the oil moved all of the experimental results above the “compression only” theoretical results ($n = 1$). A decrease of P_C from 0.9 MPa in Fig. 6.12.a to 0.8 MPa in Fig. 6.12.b was attributed to the longer compression time. $(X_0)_C$ was the same value of approximately 2.2% in both cases.

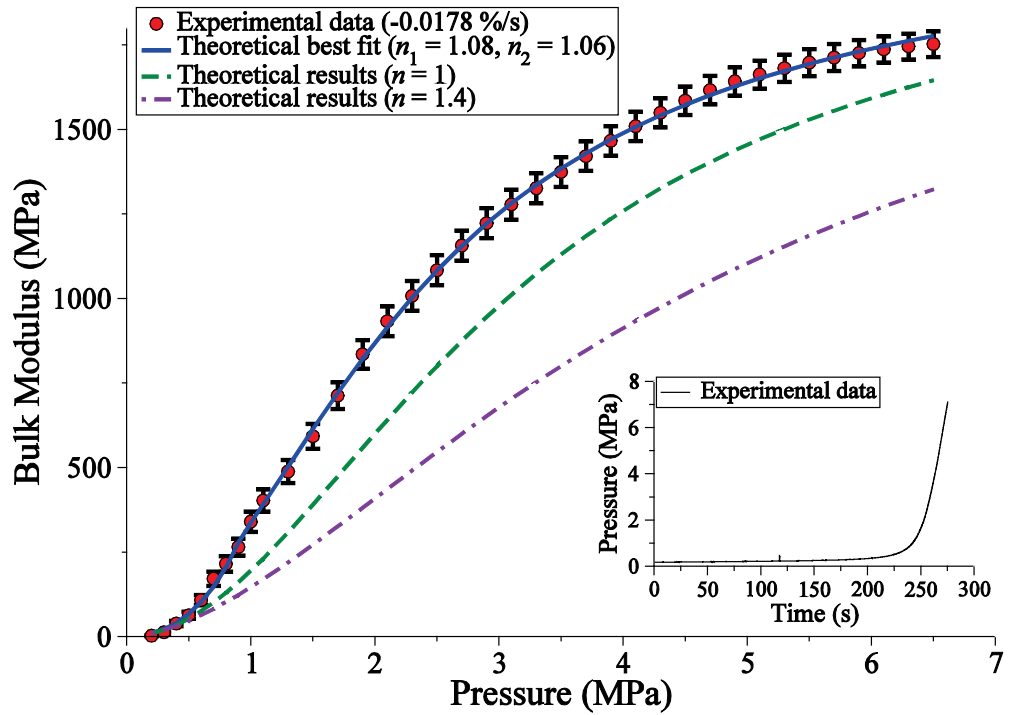


Figure 6.12.a $K_l(P_0, T) = 1940$ MPa, $X_0 = 4.4\%$, $P_C = 0.9$ MPa, $(X_0)_C = 2.18\%$ and $E = 11$ MPa

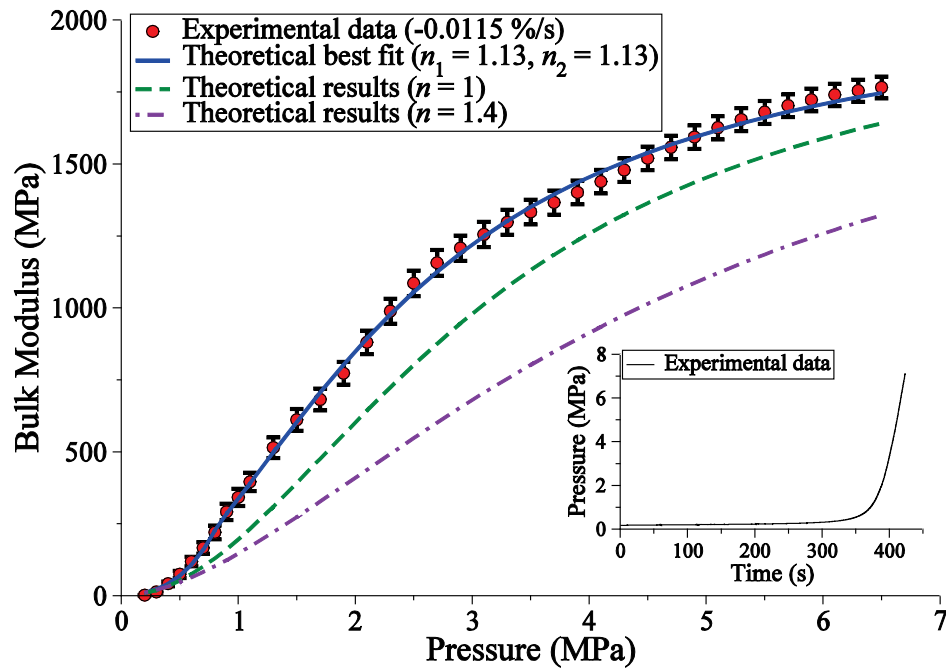


Figure 6.12.b $K_l(P_0, T) = 1932$ MPa, $X_0 = 4.4\%$, $P_C = 0.8$ MPa, $(X_0)_C = 2.12\%$ and $E = 18$ MPa

Figure 6.12 (a and b) Nonlinear least squares curve fit of the experimental data for 4.4 % of distributed air when the volume change rate was slow

6.4.3 Experimental results of the distributed air phase at an intermediate volume change rate

Figure 6.13 (a, b and c) represents the experimental and theoretical bulk modulus changes as a function of pressure for 1.9%, 3.45% and 4.4% of distributed air when the volume change rate was intermediate. The volume change rate in these cases was considered intermediate, since the total duration of the compression time was about 15 s.

Figure 6.13 (a, b and c) show that even though the compression time was relatively rapid, some dissolving of air into the oil occurred during compression. In Fig. 6.13.a, for the amount of distributed air less than 2%, the critical pressure value of $P_C = 6.4$ MPa, which is close to the maximum pressure limit of the experiments, was estimated.

As the amount of air increased to 3.45%, the critical pressure value decreased to $P_C = 2.2$ MPa with an $(X_0)_C$ value of 2.14%, indicating that 2.14% of the distributed air will be compressed only after the critical pressure (no dissolving will take place after this point).

Increasing the amount of air to 4.4% resulted in more dissolving of air into the oil; however the results of $P_C = 2.2$ MPa and $(X_0)_C = 2.24\%$ were very close to the results with 3.45% air.

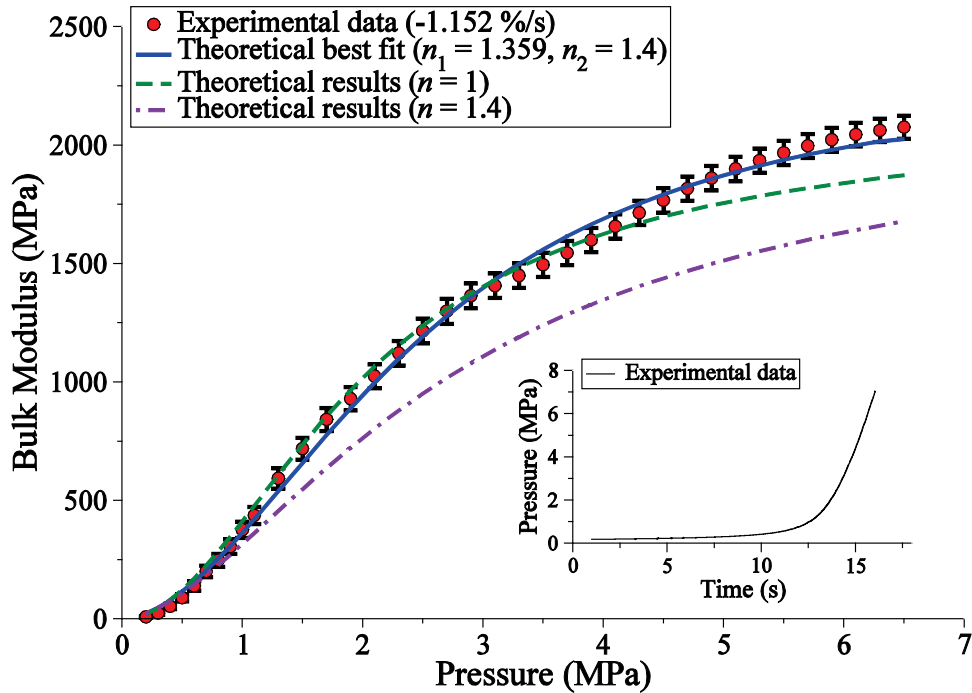


Figure 6.13.a $K_l(P_0, T) = 1972$ MPa, $X_0 = 1.9\%$, $P_C = 6.4$ MPa, $(X_0)_C = 0.1\%$ and $E = 36$ MPa

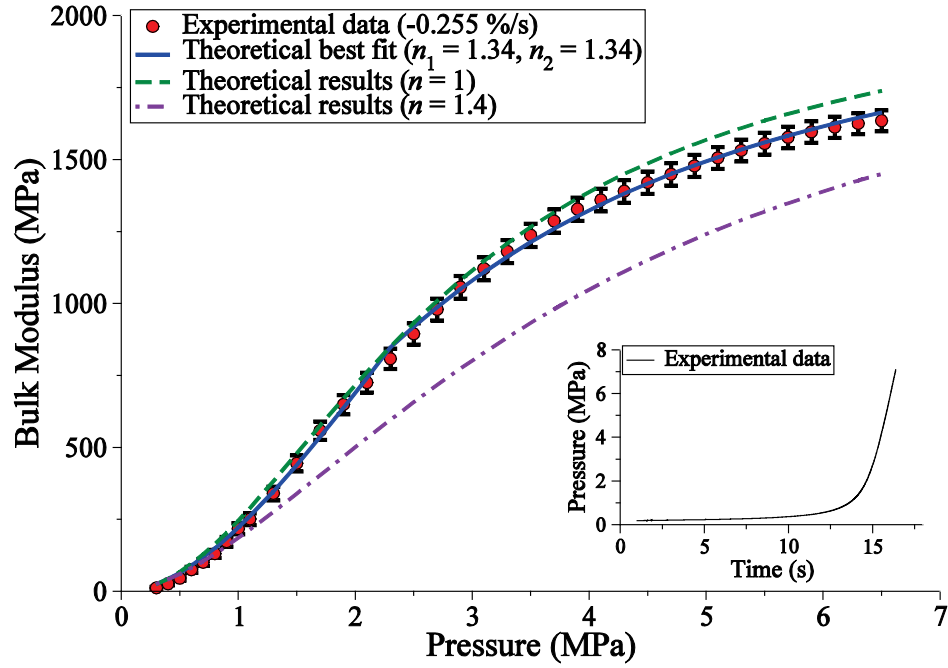


Figure 6.13.b $K_l(P_0, T) = 1970$ MPa, $X_0 = 3.45\%$, $P_C = 2.2$ MPa, $(X_0)_C = 2.14\%$ and $E = 16$ MPa

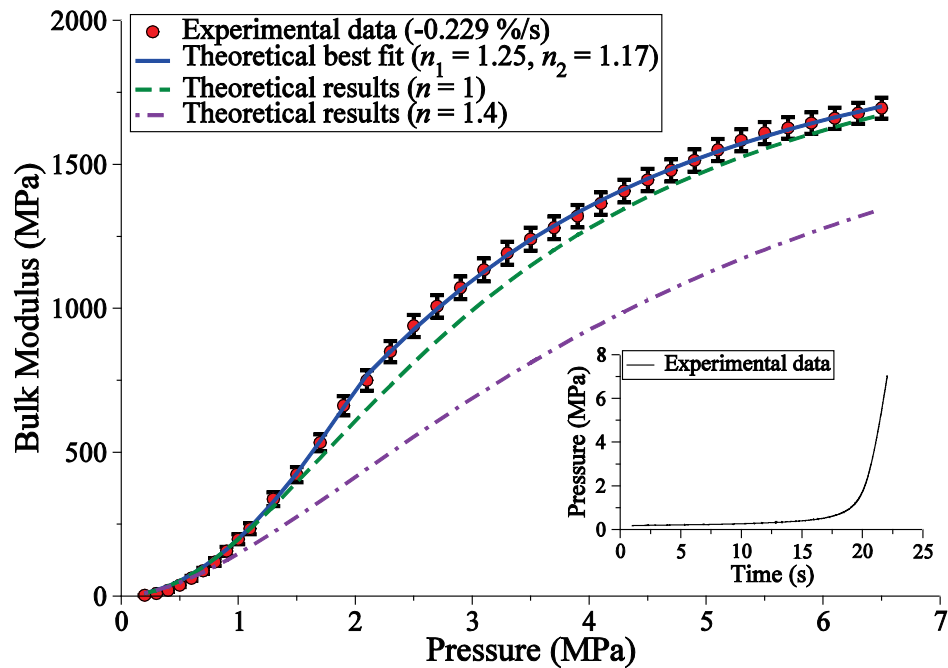


Figure 6.13.c $K_l(P_0, T) = 1972$ MPa, $X_0 = 4.4\%$, $P_C = 2.1$ MPa, $(X_0)_C = 2.24\%$ and $E = 9$ MPa

Figure 6.13 (a,b and c) Nonlinear least squares curve fit of the experimental data for 1.9%, 3.45% and 4.4 % of distributed air when the volume change rate was slow

6.5 Summary

In this chapter, all of the experimental results for the three different phases of the experimental procedure (baseline, lumped and distributed air) were presented and compared to their appropriate theoretical models. The unknown parameters in each model were determined using a nonlinear least squares method.

In the baseline phase, the isothermal and adiabatic tangent bulk modulus values of pure oil were estimated. These results were compared with existing isothermal and adiabatic values from the literature and it was found that there was good agreement between the values. This confirmed the validity of the baseline phase, as well as the experimental set up.

The bulk modulus of the pure test oil was also determined when different volume change rates were considered. The values of $K_l(P_0, T)$ versus the oil compression time were summarized in a table and used in the lumped and distributed air phases to determine the lower and upper limits of the test oil bulk modulus which was needed in the least squares method.

Experimental results of the lumped air phase were presented at three different amounts of air (1 %, 3% and 5%) at different volume change rates. It was found that regardless of the amount of air or the volume change rate, the experimental results agreed well with the “compression only” model, suggesting that an insignificant amount of air was dissolved into the oil during this phase.

There have been contradicting ideas in the literature regarding the isothermal or adiabatic nature of compression of air in the oil. Hayward (1961) reported that when a column of bubbly oil was compressed rapidly, air bubbles followed a nearly isothermal compression ($n = 1$). This result was in contradiction with the conclusions of Yu et al. (1994) who suggested that the air compression was adiabatic ($n = 1.4$). The main reason for such a divergence of opinions may be explained by the fact that the true value of the polytropic index “ n ” is influenced by many factors such as the volume change rate, the rate of heat transfer from the air to the surrounding environment and the dissolving of air into the oil.

The experimental results showed some variations in the value of “ n ” over the pressure range, indicating that the polytropic index “ n ” is not a constant and should be treated as a variable. Some deviations of the experimental results from the theoretical models (especially in the lumped air phase) have resulted more probably due to treating the polytropic index “ n ” as a

constant. The theoretical models could be improved by analyzing and modeling the heat transfer to the surroundings during the compression.

Experimental results of the distributed air phase were also presented for different amounts of air in the oil (approximately 1.5 %, 3.5% and 4.5%) at different volume change rates. The “compression and dissolve” model was chosen as a first choice for comparison with the experimental results due to the higher possibility that air would be dissolved into the oil. The experimental results were also compared with the two extreme cases of the “compression only” model ($n = 1$ and $n = 1.4$). A comparison of the experimental results with the “compression only” model gave a good insight whether any significant dissolving occurred.

Experimental results of the distributed air phase, when the volume change rate was rapid (about 2 s of total compression time) showed that the critical pressure was equal to or greater than the maximum pressure of the system. This suggested that the saturation of air into the oil may not have occurred until the maximum or higher pressure of the system. On the other hand, since the experimental results laid between the two extreme cases of $n = 1$ and $n = 1.4$, it was uncertain whether any dissolving of air into the oil occurred. Therefore, these experimental results were compared to the “compression only” model and it was concluded that a very small amount of air was dissolved which could be only captured by the “compression and dissolve” model.

Experimental results of the distributed air phase when the volume change rate was slow (about 250 or 550 s of total compression time) showed that a significant amount of air was dissolved into the oil, especially when the initial amount of air was more than 2%. The results of the slow compression tests can be divided in two groups:

- 1) When the initial amount of air was less than 2%, the critical pressure value was close to the maximum pressure range of the experiment suggesting that $(X_0)_C$ was not reached until the maximum pressure or beyond that value.
- 2) When the initial amount of air was more than 2%, the critical pressure was in the range from 0.8 to 1.1 MPa, depending on the amount of air and the volume change rate. In addition, $(X_0)_C$ was estimated to be approximately 2%. Figure 6.14 indicates that the experimental results of $X_0 = 3.42\%$ and $X_0 = 4.4\%$ tend to follow a “compression only” curve of $(X_0)_C = 2\%$ after the critical pressure of 1 MPa is reached. A slight difference at

the highest pressure was attributed to the compression of air with a slightly different value of the polytropic index (n).

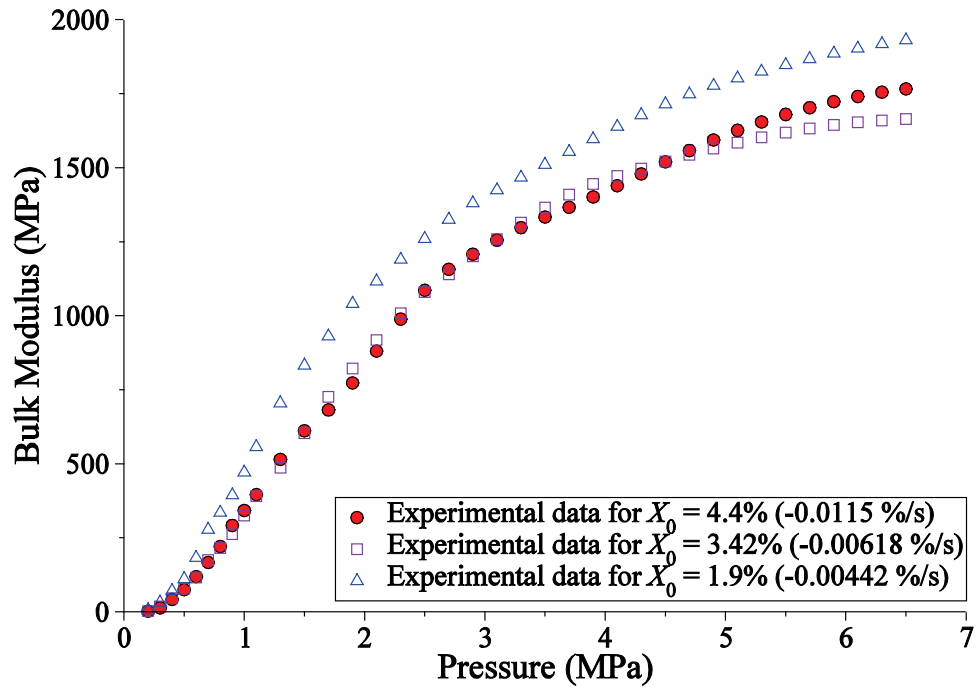


Figure 6.14. Comparison of the experimental data for different amounts of distributed air and slow volume change rate

CHAPTER 7: SUMMARY, CONCLUSIONS AND RECOMMENDATIONS

7.1 Summary

In order to summarize the achievements of the research and to present conclusions, it is necessary to recall the objectives mentioned in Section 1.2 of this thesis. The objectives were:

(1) To present a comprehensive review of the more recent literature on fluid bulk modulus that includes the common definitions used for fluid bulk modulus and a summary of methods of measurement to obtain it;

(2) To investigate and review different models of the effective bulk modulus of a mixture of hydraulic oil and air;

(3) To develop a new model based on sound physical concepts of the effective bulk modulus which arose from the review of the previous models and their limitations; and

(4) To design and fabricate an experimental set up and procedure in order to verify the new proposed model under different conditions and volume change rates.

In the following section, the research accomplishments of the objectives are listed as follows:

- Objective 1: To present a comprehensive review of the more recent literature on fluid bulk modulus that includes the common definitions used for fluid bulk modulus and a summary of methods of measurement to obtain it.

An extensive review of the fundamental concepts, definitions and experimental techniques for the measurement of fluid bulk modulus was presented in Chapter 2. Some confusion in the definition of bulk modulus was found and noted, particularly in the use of initial and final values of volume and density. Different methods of measuring the fluid bulk modulus and their limitations were also cond.

In Hayward (1965b), it was emphasized that the given pressure and temperature should always be specified when reporting bulk modulus values. Further, the justification for using a specific form of bulk modulus should also be given which is not always easy to determine.

A journal paper based on this particular review has been published (Gholizadeh et al., 2011).

- Objective 2: To investigate and review different models of the effective bulk modulus of a mixture of hydraulic oil and air.

A summary of the effective bulk modulus models for a mixture of hydraulic oil and air and the conditions/assumptions upon which these models were based on were provided in Chapter 3. In addition, some modifications to these models which would allow a comparison to be made for the same operating conditions were presented. In terms of dealing with the air in the fluid, the models were classified into two groups:

(a) “Compression only” models: models which only consider the volumetric compression of the air, and

(b) “Compression and dissolve” models: models which consider both the volumetric compression of the air and the volumetric reduction of air due to air dissolving into solution.

The chapter was concluded by discussing some of the results and presenting some guidelines on how best to choose the most appropriate formulation for a particular application.

A Journal paper based on this particular review has been published (Gholizadeh, et al., 2012.a).

- Objective 3: To develop a new model based on sound physical concepts of the effective bulk modulus which arose from the review of the previous models and their limitations.

Based on the review of Chapter 3, it was concluded that the current “compression and dissolve” models had a discontinuity at some critical pressure and did not match well with the experimental results. Thus, the discontinuity issue and the fact that the previous “compression and dissolve” models failed to truly represent the experimental measurements, were the two motivations behind the development of a new model based on sound physical principles.

The discontinuity problem associated with the current “compression and dissolve” models was addressed in Chapter 4. The reason for the discontinuity was discussed and a new “compression and dissolve” model was proposed by introducing some new parameters to the theoretical model.

Two papers were published to address the above mentioned issues. (Gholizadeh et al., 2012.b and Gholizadeh et al., 2012.c)

- Objective 4: to design and fabricate an experimental set up and procedure in order to verify the new proposed model under different conditions and volume change rates.

An experimental system was built in order to investigate and compare the bulk modulus versus pressure behavior of the mixture of oil and air at a constant temperature with those predicted by the models. The experimental set up was presented in Chapter 5.

The experimental apparatus was capable of compressing the test fluid at different rates which was enabled by designing a closed loop position feedback control system. The test fluid could be used in the form of pure oil, oil and lumped air or oil and distributed air.

The experimental procedure was presented in three phases. In the first phase, only pure oil was used as a test fluid under different rates of compression and the resulting bulk modulus was obtained. This phase was called the baseline phase and the results from this phase were used in subsequent phases to determine the effective bulk modulus of the fluid with air added.

In the second phase, the effect of adding air as “lumped air” to the top of a column of oil was investigated at different rates of compression. Finally in the third phase air was distributed in the oil in the form of air bubbles with different sizes and distributions.

The experimental results for the three different phases of the experimental procedure (baseline, lumped and distributed air) were presented and compared to their appropriate theoretical models in Chapter 6. The unknown parameters in each model were determined using a nonlinear least squares method.

A paper has been submitted to the 2013 ASME/Bath conference in Sarasota. This paper will also be submitted to the ASME Journal of Fluids Engineering.

7.2 Main contributions

The original contributions of this research study are:

- A comprehensive review of fluid bulk modulus, fundamental concepts, definitions and experimental techniques for the measurement of fluid bulk modulus was presented. Some misunderstandings in the definition of bulk modulus were found and noted. Different methods of measuring the fluid bulk modulus and their limitations were considered.
- Some modifications to the previous “compression only” models were made to allow a comparison of the models to be made for the same operating conditions.
- A new method of modeling the dissolving of air into the hydraulic oil was presented in which two new parameters P_C and $(X_\theta)_C$ were introduced.
- A novel model of the effective bulk modulus of a mixture of oil and air was developed based on sound physical concepts in which the dissolving of air into the oil was considered.

- In developing the new model, the reason for the discontinuity problem associated with the previous models was explained and resolved. This was a major contribution in modeling the “compression and dissolve” bulk modulus, since it pointed out the main issue in developing the previous “compression and dissolve” models where they applied the bulk modulus definition to a control volume with a variable mass.
- Previous experimental measurements of the effective bulk modulus of a mixture of oil and air found in the literature were limited to the case where the air was added as a free pocket (lumped air) at the top of the hydraulic oil and the maximum amount of air added was limited to 1%. In this work, the experimental results of lumped air were extended to include the amount of air up to 5%.
- For the first time, experimental measurements of the effective bulk modulus of distributed air in the hydraulic oil were presented under different volume change rates and compared with the theoretical models.
- The least squares method was introduced to find the unknown parameters of the models. In the previous literature, no attempt was made to independently verify the values of the unknown parameters (Yu et al., 1994). In this thesis, however, an attempt was made to verify the values of the parameters especially $K_l(P_0, T)$. The isothermal and adiabatic values of $K_l(P_0, T)$ in the baseline phase were verified with the known values from the literature. Then the values of $K_l(P_0, T)$ for other volume change rates were found. The values of $K_l(P_0, T)$ versus the oil compression time were used in the lumped and distributed air phases to determine the lower and upper limits of the test oil bulk modulus which was needed in the least squares method.
- The uncertainty in measuring the effective bulk modulus was calculated and it was shown how the uncertainty changes with operating point. This often does not appear in the literature.

7.3 Conclusions

It should be noted that the following conclusions are primarily based on results in which the pressure range is 0 to 6.9 MPa, X_0 range is from 1 to 5% and a constant temperature

of 24 °C is maintained. For these conditions and based on the results of this study, it is concluded that:

1. *It is very critical to fully understand the various definitions of fluid bulk modulus and use them correctly.* It should be noted that the secant bulk modulus definition can be only used to find the bulk modulus of pure oil. When the air is mixed with the oil, the secant bulk modulus definition will fail to truly represent the bulk modulus of the mixture and the tangent bulk modulus definition should be used.
2. *The given pressure, the rate of change in pressure and the temperature should be always specified when reporting the bulk modulus values.*
3. *The bulk modulus definition should only be applied to a control volume with a constant mass.* Therefore, in modeling the effective bulk modulus of a mixture of oil and air, the constraint is that the mass of air must remain constant as pressure changes. This fact was overlooked in the previous literature and led to the presence of a discontinuity in the previous “compression and dissolve” models.
4. *The “compression and dissolve” models would always have bulk modulus values greater than the “compression only” models due to the fact that the volume of entrained air decreases with both the compression and dissolving of the air into the oil.*
5. *The new “compression and dissolve” model developed in this thesis could relate the effective bulk modulus of a mixture of oil and air to the volumetric variation of the air due to both compression and dissolving of air in the oil, and also the change in volume and bulk modulus of pure oil to the pressure and temperature.*
6. *The air will stop dissolving into the oil after reaching the critical pressure P_C and any remaining air will be only compressed afterwards. The effective bulk modulus after P_C , will follow the “compression only” curve.*

7. *The value of P_C is highly dependent on the volume change rate. For rapid volume change rates, the value of P_C was equal to or greater than the maximum pressure of the system. However, the value of P_C decreased as the volume change rate was decreased.*
8. *P_C is not only dependent on the volume change rate, but also dependent on the volumetric fraction of air at atmospheric pressure (X_0). This is based on the experimental results of the slow volume change rate in the distributed air phase. For $X_0 < (X_0)_C$ the critical pressure value was close to the maximum pressure range of the experiment suggesting that the air was still dissolving and saturation had not occurred until the maximum pressure range. It was also observed that for $X_0 > (X_0)_C$, the effective bulk modulus followed a “compression only” curve of $(X_0)_C$ after the critical pressure P_C was reached.*
9. *Regardless of the value of X_0 , the critical pressure was always equal to or greater than the maximum pressure of the system for rapid volume changes, suggesting that the saturation of air into the oil may not have occurred until the maximum or higher pressure of the system. This was based on experimental results of the rapid volume change rate in the distributed air phase.*
10. *An insignificant amount of air was dissolved into the oil during the lumped air phase. This was based on the fact that the experimental results agreed well with the “compression only” model.*
11. *The “compression only” model is a special case of the “compression and dissolve” model where the value of P_C approaches infinity and $(X_0)_C$ approaches zero. Therefore, it is further concluded that the “compression and dissolve” model proposed in this thesis is a general model where it is applicable to different types of distribution of air bubbles in oil. However, the values of P_C and $(X_0)_C$ need to be estimated using experimental measurements.*

12. *The polytropic index “n” is not a constant and should be treated as a variable because some variations in the value of “n” over the pressure range occurred. The true value of the polytropic index “n” is influenced by many factors such as the volume change rate, the rate of heat transfer from the air to the surrounding environment and the dissolving of air into the oil.*
13. *The uncertainty in calculating the bulk modulus is highly dependent on the operating point and is not constant over the whole range of measurements.*

7.4 Recommendations for future work

There are a number of areas where further research can be performed regarding this research.

- The “compression and dissolve” model developed in this thesis could be extended to include a mathematical equation in which P_C is related to the rate of increase in pressure and size and distribution of the air bubbles.
- Even though the new modeling method was explained only for the case of air dissolving in to the oil, it can be also applied when air comes out of solution (air evolution). Since it is well known that the air dissolving and evolution times are different, it would be interesting to set up an experimental apparatus and investigate the experimental results of pressure versus bulk modulus for the case of air evolution.
- As it was already noted, the polytropic index “n” should not be considered as a constant parameter since its value depends on the rate of heat transfer from the air to the neighboring environment. The variations of “n” could be modeled by analyzing and modeling the heat transfer to the surroundings during the compression and incorporated into the “compression and dissolve” model.
- An experimental system which can cover a much wider pressure range needs to be developed. This would allow cases where P_C occurred at higher pressures and where the bulk modulus tended to a region where m was constant.
- The effect of temperature on the effective bulk modulus needs to be investigated in more detail. Temperature was held constant in this study, but many studies have

shown that bulk modulus does vary with temperature which also would have an affect on the values of n .

LIST OF REFERENCES

ANSI/B93.63M-1984. 1984. Hydraulic Fluid Power-Petroleum Fluids-Prediction of Bulk Moduli.

Anton Paar. 2011. Anton Paar Company, USA. http://www.anton-paar.com/Density-Sensor/59_USA_en?productgroup_id=117&Density-Sensor.

ASTM Standard D341. 2009. Standard Practice for Viscosity-Temperature Charts for Liquid Petroleum Products. *ASTM International*, West Conshohocken, PA, 2009, DOI: 10.1520/D0341-09, www.astm.org.

Berg , R. E. and Stork, D.G. 1982. *The Physics of Sound*. NY, U.S.A, Prentice Hall.

Blackstock, D. T. 2000. *Fundamentals of Physical Acoustics*. NY, U.S.A, John Wiley & Sons.

Bock, W., Braun, J., Puhl, N. and Heinemann, H. 2010. Air Release Properties of Hydraulic Fluids, Dynamic Air Release. *7th International Fluid Power Conference, IFK2010*, Aachen, Germany, March 22-24, 2010.

Borghi, M., Bussi, C., Milani, M. and Paltrinieri, F. 2003. A Numerical Approach to the Hydraulic Fluids Properties Prediction. *The Eighth Scandinavian International Conference on Fluid Power, SICFP'03*, Tampere, Finland, May 7-9, 2003.

Burton, R. 1971. *Indirect Measurement of Operational Bulk Modulus*. Master's thesis. University of Saskatchewan.

Chartrand, R. 2011. Numerical Differentiation of Noisy, Non-smooth Data. *ISRN Applied Mathematics*, Vol. 2011, Article ID 164564, 11 pages, 2011. doi:10.5402/2011/164564.

Cho, B. H., Lee, H. W. and Oh J. S. 2000. Estimation Technique of Air Content in Automatic Transmission Fluid by Measuring Effective Bulk Modulus, *International Journal of Automotive Technology*, Vol. 3(2), pp. 57- 61.

Chu, P. S. Y. and Cameron, A. 1963. Compressibility and Thermal Expansion of Oils. *Institute of Petroleum – Journal*, Vol. 49(473), pp. 140-145.

D'Errico, J. 2009. SLM-Shape Language Modeling. Matlab Central File Exchange Retrieved February 22, 2012. www.mathworks.com/matlabcentral/fileexchange/2443-slm-shape-language-modeling&watching=24443.

Ehlers, F. E. 1960. Method for Measuring Bulk Modulus of a Liquid Using a Helmholtz Resonator. *Journal of the Acoustical Society of America*, Vol. 32(5), pp. 538-546.

Fox, R. W., Pritchard, P. J. and McDonald, A. T. 2009. *Introduction to Fluid Mechanics* (7th ed.). NY, U.S.A., John Wiley & Sons.

Gholizadeh, H., Bitner, D., Burton, R. and Schoenau, G. 2012.b. Experimental Investigation of Measuring Fluid Bulk Modulus in Low Pressure Regions. *7th FPNI PhD Symposium on Fluid Power*, Reggio Emilia, Italy, June 27-30, 2012.

Gholizadeh, H., Bitner, D., Burton, R., Sumner, D., Schoenau, G., 2010. Investigation of Experimental Techniques for the Measurement of the Effective Bulk Modulus of Oil-Filled Pipes and Hoses. *7th International Fluid Power Conference*, IFK2010, Aachen, Germany, March 22-24, 2010.

Gholizadeh, H., Bitner, D., Burton, R. and Schoenau, G. 2012.c. Effective Bulk Modulus Model Verification for the Mixture of Air/Gas and Oil. *Bath/ASME Symposium on Power Transmission and Motion Control*, Bath, England, September 12-14, 2012.

Gholizadeh, H., Burton, R. and Schoenau, G. 2011. Fluid Bulk Modulus: A Literature Survey. *International Journal of Fluid Power*, Vol. 12(3), pp. 5-16.

Gholizadeh, H., Burton, R. and Schoenau, G. 2012.a. Fluid Bulk Modulus: Comparison of Low Pressure Models. *International Journal of Fluid Power*, Vol. 13(1), pp. 7-16.

Hayward, A. T. J. 1961. Air Bubbles in Oil - Their Effect on Viscosity and Compressibility. *Fluid Handling*, Vol. 143, pp. 349-352.

Hayward, A. T. J. 1963. Research on Lubricants and Hydraulic Fluids at National Engineering Laboratory. *Scientific Lubrication*, Vol. 15(3), pp. 112-124.

Hayward, A. T. J. 1965a. Compressibility Measurements on Hydraulic Fluids. *Hydraulic Pneumatic Power*, Vol. 11(131), pp. 642-646.

Hayward, A. T. J. 1965b. Compressibility of Hydraulic Fluids. *Institute of Petroleum – Journal*, Vol. 51(494), pp. 35-52.

Hayward, A. T. J. 1967. Compressibility Equations for Liquids: A Comparative Study. *British Journal of Applied Physics*, Vol. 18(7), pp. 965-977.

Hayward, A. T. J. 1970. How to Estimate the Bulk Modulus of Hydraulic Fluids. *Hydraulic Pneumatic Power*, Vol. 16(181) pp. 28-40.

Hayward, A. T. J. 1971. How to Measure the Isothermal Compressibility of Liquids Accurately. *Journal of Physics D (Applied Physics)*, Vol. 4(7), pp. 938-950.

Isdale, J. D., Brunton, W. C. and Spence, C. M. 1975. Bulk Modulus Measurement and Prediction. *NEL-591*, 28 pp.

ISO/15086-2. 2000. Hydraulic Fluid Power- Determination of the Fluid Borne Noise Characteristics of Components and Systems, Part 2: Measurement of Speed of Sound in a Fluid in a Pipe.

Johnston, D. N. and Edge, K. A. 1991. In Situ Measurement of the Wave Speed and Bulk Modulus in Hydraulic Lines. *Proceedings of the Institution of Mechanical Engineers, Part I: Journal of Systems and Control Engineering*, Vol. 205(13), pp. 191-197.

Kajaste, J., Kauranne, H., Ellman, A. and Pietola, M. 2005. Experimental Validation of Different Models for Bulk Modulus of Hydraulic Fluid. *The Ninth Scandinavian International Conference on Fluid Power, SICFP'05*, Linköping, Sweden, June 1-3, 2005.

Karjalainen, J., Karjalainen, R., Huhtala, K. and Vilenius, M. 2005. The Dynamics of Hydraulic Fluids-Significance, Difference and Measuring. *Bath Workshop on Power Transmission and Motion Control, PTMC 2005*, pp. 437-450, Bath, England, September 7-9, 2005.

Karjalainen, J., Karjalainen, R., Huhtala, K. and Vilenius, M. 2007. Fluid Dynamics-Comparison and Discussion on System Related Differences. *The Tenth Scandinavian International Conference on Fluid Power, SICFP'07*, Tampere, Finland, May 21-23, 2007.

Kim, G. and Wang, K. 2009. On-Line Estimation of Effective Bulk Modulus in Fluid Power Systems using Piezoelectric Transducer Impedance. *Journal of Intelligent Material Systems and Structures*, Vol. 20(17), pp. 2101-2106.

Klaus, E. E. and O'Brien, J. A. 1964. Precise Measurement and Prediction of Bulk Modulus Values for Fluids and Lubricants. *ASME Journal of Basic Engineering*, Vol. 86(D-3), 469-474.

LMS IMAGINE, S.A., 2008. HYD Advanced Fluid Properties, *LMS Imagine, S.A.*, Technical Bulletin no.117, Rev 8B.

Magorien, V. G. 1967. Effects of Air on Hydraulic Systems. *Hydraulics and Pneumatics*, Vol. 20(10), 128-131.

Magorien, V. G. 1968. How Hydraulic Fluids Generate Air. *Hydraulics and Pneumatics*, Vol. 21(6), pp. 104-108.

Magorien, V. G. 1978. Air in Fluid Systems. Its Effect, Measurement and Removal, *BHRA (Br Hydromech Res Assoc) Fluid Eng*, Vol. 12(1), pp. 1-18.

Manring, N. D. 1997. The Effective Fluid Bulk Modulus Within a Hydrostatic Transmission. *Journal of Dynamic Systems, Measurement and Control*, Vol. 119, pp. 462-465.

Manring, N. D. 2005. *Hydraulic Control Systems*. New York, Wiley.

Manz, D. and Cheng, W.K. 2007. On-Line Measurements of Engine Oil Aeration by X-Ray Absorption. *Transactions of the ASME. Journal of Engineering for Gas Turbines and Power*, Vol. 129(1), pp. 287-293.

Merritt, H. E. 1967. *Hydraulic Control Systems*. New York, U.S.A, Wiley.

Niezrecki, C., Schueller, J. K. and Balasubramanian, K. 2004. Piezoelectric-Based Fluid Bulk Modulus Sensor. *Journal of Intelligent Material Systems and Structures*, Vol. 15(12) pp. 893-899.

Nykanen, T. H. A., Esque, S. and Ellman, A. U. 2000. Comparison of Different Fluid Models. *Power Transmission and Motion Control, PTMC 2000*, Professional Engineering Publishing, Bath, United Kingdom, pp. 101-110.

O'Brien, J. A. 1963. *Precise Measurement of Liquid Bulk Modulus*. Master's thesis. Pennsylvania State University.

Pierce A. D. 1981. *Acoustics: An Introduction to Its Physical Principles and Applications*. New York, U.S.A, McGraw Hill.

Povey M.J.W. 1997, *Ultrasonic Techniques for Fluids Characterization*. California, U.S.A, Academic Press.

Ruan, J. and Burton, R. 2006. Bulk Modulus of Air Content Oil in a Hydraulic Cylinder. *Proceedings of 2006 ASME International Mechanical Engineering Congress and Exposition, IMECE2006 - Fluid Power Systems and Technology Division*, pp. 259-269, Chicago, U.S.A, November 5 - 10, 2006.

Smith, A. C. 1965. Some Notes on Data on Hydraulic Oil Properties Required by Systems Designers. *Scientific Lubrication*, Vol. 17(2), pp. 63-69.

Smith, L., Peeler, R. and Bernd, L. 1960. Hydraulic Fluid Bulk Modulus: Its Effects on System Performance and Techniques for Physical Measurement. *16th National Conference on Industrial Hydraulics*, pp. 179-197, Chicago, U.S.A, October 20-21, 1960.

Song, H. S., Klaus, E. E. and Duda, J. L. 1991. Prediction of Bulk Moduli for Mineral Oil Based Lubricants, Polymer Solutions, and Several Classes of Synthetic Fluids. *Journal of Tribology*, Vol. 113(4), pp. 675-680.

Stecki, J. S. and Davis, D. C. 1981. Hydraulic System Analysis - Prediction and Measurement of Effective Bulk Modulus. *Basic Fluid Power Research Journal*, Vol. 14(4), pp. 333-335.

Stecki, J. S., and Davis, D. C. 1986a, Fluid Transmission Lines - Distributed Parameter Models Part 1: A Review of the State of the Art. *Proceedings of the Institution of Mechanical Engineers. Part A. Power and Process Engineering*, Vol. 200(4), pp. 215-228.

Stecki, J. S., and Davis, D. C. 1986b, Fluid Transmission Lines - Distributed Parameter Models Part 2: Comparison of Models. *Proceedings of the Institution of Mechanical Engineers. Part A. Power and Process Engineering*, Vol. 200(4), pp. 229-236.

Sunghun, K. 2012. *Measurement of Effective Bulk Modulus and its Use in CFD Simulation*. Ph.D. thesis, Institute for Fluid Power Drives and Controls, RWTH Aachen, Germany.

Sunghun, K. and Murrenhoff, H. 2012. Measurement of Effective Bulk Modulus for Hydraulic Oil at Low Pressure. *ASME Journal of Fluids Engineering*, Vol. 134(2), pp. 021201-021201-10. doi:10.1115/1.4005672.

Temperley, H. N. V. and Trevena, D. H. 1978. *Liquids and their Properties: A Molecular and Macroscopic Treatise with Applications*, Chichester, England, Ellis Horwood.

Tavoularis, S., 2005. *Measurement in Fluid Mechanics*. Cambridge, UK, Cambridge University Press.

Totten, G. 2000. *Handbook of Hydraulic Fluid Technology*. NY, U.S.A, Marcel Dekker.

Tropea, C., Yarin, A. and Foss, J.F. 2007. *Springer Handbook of Experimental Fluid Mechanics*. Berlin, Germany, Springer- Verlag.

Wahi, M.K. 1976. Oil Compressibility and Polytopic Air Compression Analysis for Oleopneumatic Shock Struts, *Journal of Aircraft*. Vol. 13(7), pp. 527-530.

Watton, J. 2009. *Fundamentals of fluid power control*. NY, U.S.A, Cambridge University Press.

Watton, J., and Tadmori, M. J. 1988, Comparison of Techniques for the Analysis of Transmission Line Dynamics in Electrohydraulic Control Systems, *Applied Mathematical Modeling*. Vol. 12(5), pp. 457-466.

Watton, J. and Xue, Y. 1994. A New Direct Measurement Method for Determining Fluid Bulk Modulus in Oil Hydraulic Systems. *Proceedings of FLUCOME'94*, Toulouse, France, August 29 - September 1, 1994.

Wright, W. A. 1967. Prediction of Bulk Moduli and Pressure-Volume-Temperature Data for Petroleum Oils. *ASLE Transactions*, Vol. 10 (4), pp. 349-356.

Wylie, E. B. and Streeter, V. L. 1983. *Fluid Transients*. Ann Arbor, Michigan, USA, Feb Press.

Yu, J., Chen, Z. and Lu, Y. 1994. Variation of Oil Effective Bulk Modulus with Pressure in Hydraulic Systems. *Journal of Dynamic Systems, Measurement and Control*, Vol. 116 (1), pp. 146-150.

Yu, J., Kojima, E. 2000. Methods for Measuring the Speed of Sound in the Fluid in Fluid Transmission Pipes. *International Off-Highway & Powerplant Congress & Exposition, Society of Automotive Engineers*, Milwaukee, Wisconsin, U.S.A, September 11-13, 2000

Zemansky, M. W. 1957. *Heat and Thermodynamics*. NY, U.S.A, McGraw Hill.

APPENDIX A: TANGENT BULK MODULUS CALCULATION USING SECANT BULK MODULUS DATA

In this Appendix, the derivation of Eq. (2.9) is presented. In order to derive Eq. (2.9) which is used to derive tangent bulk modulus at any pressure using secant bulk modulus data, it is assumed that the secant bulk modulus (isothermal or adiabatic) can be expressed as a linear function of pressure as (Hayward, 1971)

$$\bar{K} = K_0 + mP_g, \quad (\text{A.1})$$

where m is the slope of the linear relationship. Secant bulk modulus definition yields

$$\bar{K} = -V_0 \left(\frac{P - P_0}{V - V_0} \right). \quad (\text{A.2})$$

Assuming that P_0 is at atmospheric pressure ($P_0 = 0$), Eq. (A.2) is re-written as

$$\bar{K} = \delta P_g, \quad (\text{A.3})$$

where δ is defined as

$$\delta = \frac{V_0}{V_0 - V}. \quad (\text{A.4})$$

Using the tangent bulk modulus definition and rearranging gives

$$K = -V \left(\frac{\partial P}{\partial V} \right) = -V \left(\frac{\partial P}{\partial \delta} \cdot \frac{\partial \delta}{\partial V} \right). \quad (\text{A.5})$$

From Eq. (A.4),

$$-V \left(\frac{\partial \delta}{\partial V} \right) = \delta(1 - \delta). \quad (\text{A.6})$$

Therefore Eq. (A.5) results in

$$K = -V \left(\frac{\partial P}{\partial V} \right) = \delta(1 - \delta) \left(\frac{\partial P}{\partial \delta} \right). \quad (\text{A.7})$$

Substituting Eq. (A.3) into Eq. (A.1) and differentiating yields

$$\frac{\partial P}{\partial \delta} = \frac{P_g}{m - \delta}. \quad (\text{A.8})$$

Combining Eq. (A.7) and Eq. (A.8) gives

$$K = \frac{P_g \delta (1 - \delta)}{m - \delta}. \quad (\text{A.9})$$

Substituting Eq. (A.3) into Eq. (A.9) and rearranging gives

$$K = \frac{\bar{K} (\bar{K} - P_g)}{\bar{K} - P_g m} = \frac{\bar{K} (\bar{K} - P_g)}{\bar{K} - P_g} \frac{d\bar{K}}{dP}. \quad (\text{A.10})$$

This then is Eq. (2.9) that is used in the main text.

APPENDIX B: RELATION BETWEEN ADIABATIC AND ISOTHERMAL BULK MODULUS

The objective of this appendix is to show that $\frac{C_P}{C_v} = \frac{K_S}{K_T}$.

The specific heat of liquid at constant pressure is defined as

$$C_P = \left(\frac{\partial h}{\partial T} \right)_P = T \left(\frac{\partial S}{\partial T} \right)_P, \quad (\text{B.1})$$

where h and S represent the enthalpy and entropy of liquid respectively. The specific heat of liquid at constant volume is defined as

$$C_v = \left(\frac{\partial u}{\partial T} \right)_v = T \left(\frac{\partial S}{\partial T} \right)_v, \quad (\text{B.2})$$

where u and v represent the internal energy and the volume per unit mass of liquid respectively. Therefore

$$\frac{C_P}{C_v} = \frac{\left(\frac{\partial S}{\partial T} \right)_P}{\left(\frac{\partial S}{\partial T} \right)_v}. \quad (\text{B.3})$$

Rearranging Eq. (B.3) gives

$$\frac{C_P}{C_v} = \frac{\left(\frac{\partial S}{\partial T} \frac{\partial v}{\partial v} \right)_P}{\left(\frac{\partial S}{\partial T} \frac{\partial P}{\partial P} \right)_v} = \frac{\left(\frac{\partial S}{\partial v} \right)_P \left(\frac{\partial v}{\partial T} \right)_P}{\left(\frac{\partial S}{\partial P} \right)_v \left(\frac{\partial P}{\partial T} \right)_v}. \quad (\text{B.4})$$

Substituting Maxwell relations into Eq. (B.4) results in

$$\frac{C_P}{C_v} = \frac{-\left(\frac{\partial P}{\partial T} \right)_S \left(\frac{\partial S}{\partial P} \right)_T}{-\left(\frac{\partial v}{\partial T} \right)_S \left(\frac{\partial S}{\partial v} \right)_T} = \frac{\left(\frac{\partial P}{\partial v} \right)_S}{\left(\frac{\partial P}{\partial v} \right)_T} = \frac{K_S}{K_T}. \quad (\text{B.5})$$

Therefore

$$\frac{C_P}{C_v} = \frac{K_S}{K_T}. \quad (\text{B.6})$$

APPENDIX C: PROPOGATION OF WAVE IN FLUID

The objective of this Appendix is to discuss the basics of propagation of sound in the fluid as well as the relationship between the bulk modulus and the velocity of sound.

When a column of fluid is disturbed, the fluid particles will move backwards and forwards around their equilibrium positions. The motion of these particles will create compression and rarefaction regions along the fluid. Since the direction of the movement of the fluid particles will be parallel to the direction of the propagation of wave, they are called longitudinal waves (Berg and Stork, 1982). The velocity of sound is defined as the speed of the movement of the compression and rarefaction regions and it should be noted that this speed is different from the velocity of oscillating particles around their equilibrium point (Pierce, 1981).

According to Zemansky (1957), the first equation which showed the relationship between the velocity of sound and bulk modulus was introduced by Newton, in which he stated that the velocity of sound is related to the isothermal bulk modulus. But later, Laplace showed that it was the isentropic bulk modulus. Zemansky (1957) demonstrates this by considering the compressions and expansions which take place in the mainstream (away from the pipe wall) of the fluid inside a pipe due to the propagation of the sound. The effects of viscous and thermal boundary layers which are respectively due to the viscosity of the fluid and thermal conduction between the fluid and the surface of the wall were not considered in his analysis. He concluded that at regular frequencies, the acoustic propagation in pure fluids is a very good approximation to being isentropic. Propagation becomes isothermal at frequencies of approximately 10^9 Hz in air and 10^{12} Hz in water (Pierce, 1981). It should also be noted that the isentropic condition may not apply to inhomogeneous fluids (Povey, 1997).

Deriving the expression for the speed of sound in any medium in terms of thermodynamic quantities can be found in almost every fluid mechanics text book, for example (Fox et al., 2009), in which by applying a conservation of mass and momentum to a differential control volume, the expression for the speed of sound in a medium found to be

$$C^2 = \frac{dP}{d\rho}. \quad (C.5)$$

Since as already mentioned, propagation of wave in liquids at normal frequencies is isentropic, the pressure would be only a function of density, that is

$$P = P(\rho). \quad (C.6)$$

This equation of state can be expressed as a Taylor series (Blackstock, 2000),

$$P = P_0 + A \frac{\rho - \rho_0}{\rho_0} + \frac{B}{2!} \left(\frac{\rho - \rho_0}{\rho_0} \right)^2 + \frac{C}{3!} \left(\frac{\rho - \rho_0}{\rho_0} \right)^3 + \dots \quad (C.7)$$

where coefficients A, B, C, \dots can be either determined experimentally or analytically (Blackstock, 2000). Differentiating equation (C.7) and using equation (C.5) yields

$$C^2 = \frac{A}{\rho_0} + \frac{B}{\rho_0} \left(\frac{\rho - \rho_0}{\rho_0} \right) + \frac{C}{2! \rho_0} \left(\frac{\rho - \rho_0}{\rho_0} \right)^2 + \dots \quad (C.8)$$

In the case that $\rho \rightarrow \rho_0$, C^2 will be a constant and will be represented here as C_0^2 . The coefficient A will be equal to $A = \rho_0 C_0^2$, which is the isentropic bulk modulus of the fluid for small deviations from equilibrium. The term “small signal” speed of sound should be used for C_0 , but is traditionally called as the speed of sound in order to shorten the term (Blackstock, 2000).

Therefore the relationship between the isentropic bulk modulus and the speed of sound for a lossless fluid with small perturbations from the equilibrium is

$$K_s = \rho_0 C_0^2, \quad (C.9)$$

where C_0^2 is the slope of pressure-density diagram at the static operating point P_0 and ρ_0 (Blackstock, 2000).

When the wave amplitude is high enough to break the small signal assumption, the velocity of sound is represented by C and the isentropic bulk modulus is obtained by

$$K_s = \rho C^2. \quad (C.10)$$

where C^2 is the slope of pressure-density diagram at P and ρ (Blackstock, 2000).

High pressure hydraulic systems can be accurately modeled based on the small signal analysis, but for the low pressure hydraulic systems, the presence of air bubbles in the oil, leads to a nonlinear density law and the small signal analysis will not be valid anymore.

All the equations and analysis mentioned here are based on the small signal analysis. Therefore in order to find the isentropic tangent bulk modulus of fluid, it is only required to find the speed of sound in the fluid and the density of the fluid at that operating condition. It should

be noted that the assumptions which are considered for both the fluid and the nature of the wave motion, defines the form of the wave equation from which the speed of sound can be determined (Blackstock, 2000).

Blackstock (2000) examined different models with varying complexity which the application of each model depends on the desired degree of accuracy. It is very important to use a model that accurately shows the real behavior of the system and at the same time is not complex.

Stecki and Davis (1986a, 1986b) reviewed many papers concerning the modeling of a rigid uniform transmission line. They studied seven different models and after comparing the theoretical frequency response of a fluid filled transmission line with the experimental data, they found that “two dimensional viscous compressible flow model” is suitable for modeling alternating flow systems with long transmission lines. However, the suggestions for the suitable application of other models have been also discussed. Theoretical results of this study showed that the system response is very sensitive to small variation in sonic velocity and it needs to be determined accurately.

Watton et al. (1988) have categorized the wave propagation models for laminar flow as:

(a) Lossless line model: this model considers fluid acceleration and compressibility effects and the terms containing the fluid viscosity effects are neglected. This model simplifies the computations but will give less accurate results.

(b) Average friction model: In this model, in addition to including fluid acceleration and compressibility effects, another term is also added to account for the effects of the friction effects. Friction factor in this model can be either obtained experimentally or by Hagen-Poiseuille formula. Assuming constant resistance coefficient makes the results to be valid only over limited frequency ranges.

(c) Distributed friction model: In this model, it is assumed that the frequency of pressure and flow rate waves along the pipe will modify the velocity profile and accordingly the line resistance. Therefore line resistance will change with the frequency of propagation. Heat transfer effects between the fluid and the pipe walls are also taken into account.

Some researchers (Johnston and Edge, 1991) have used transmission line dynamics models and provided some equations in which the velocity of sound can be estimated by employing pressure ripple measurements along the line. It is obvious that the more accurate

model is used, the more accurate estimation for the velocity of sound can be found. But at the same time the complexity of the model is also increased.

However, there is another modeling approach called lumped parameter model in which the mathematical equations describing the system behavior are greatly simplified. In this method, all the resistance, capacitance or inductance effects can be gathered in one or more lumps. A condition was established under which the lumped parameter model can be valid (Watton, 2009). Under this condition, a lumped parameter model is valid when

$$\frac{2l}{C_0} < \frac{1}{f}, \quad (\text{C.11})$$

where f is the highest frequency of system oscillation that exists, l and C_0 are the length of line and the speed of the sound in the line respectively.

It is still necessary to investigate whether distributed or lumped parameter models should be used, since the accuracy of the estimation of the bulk modulus is affected by the type of the selected model.

APPENDIX D: ISOTHERMAL AND ADIABATIC BULK MODULUS ESTIMATION OF “ESSO NUTO H68” OIL

The objective of this Appendix is to estimate the isothermal and adiabatic bulk modulus (secant and tangent) of the “Esso Nuto H68” oil using experimental relations developed by Hayward (1970).

In the relationships provided by Hayward, the isothermal and adiabatic secant bulk modulus of any normal hydraulic oil is predicted within about 5% with only knowing the kinematic viscosity of oil at atmospheric pressure and 20°C. The kinematic viscosity of “Esso Nuto H68” oil was provided by the manufacturer at two temperatures of 40°C and 100°C (Table D-1). In order to obtain the kinematic viscosity value of the oil at 20°C, the relationships given by ASTM standard (ASTM-D341-2009) is used. The formulations provided by the ASTM standard, allows determining the kinematic viscosity of any mineral oil over the temperature range of -70 to 370°C, only by knowing two kinematic viscosity-temperature points.

Table D.1 Viscosity of test fluid (Esso Nuto H68) at 40°C and 100°C provided by the manufacturer

Temperature (°C)	Viscosity (cSt)
40	68
100	8.5

Figure D.1 shows a plot of kinematic viscosity versus temperature (at atmospheric pressure) for Esso Nuto H68 oil which was obtained using the ASTM standard relationships. From this plot, the kinematic viscosity of the oil at 20°C is found to be 219 cSt.

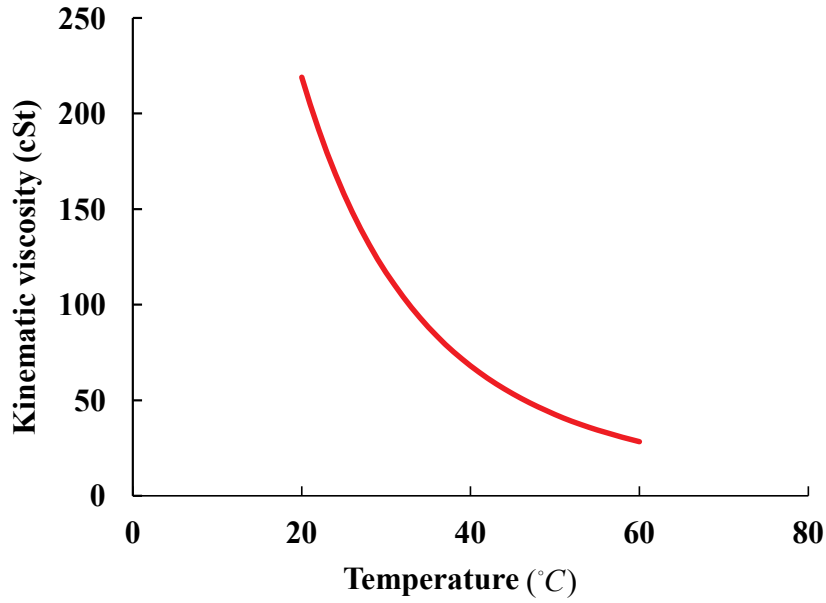


Figure D.1 Viscosity variation of Esso Nuto H68 with temperature

After obtaining the kinematic viscosity of the oil at 20°C and atmospheric pressure, the equations provided by Hayward (1970) are used to obtain the isothermal and adiabatic secant bulk modulus variation of “Esso Nuto H68” oil with pressure. These equations were determined as

$$\bar{K}_T(P, T) = \frac{K_T(P_0, T)}{10} + 5.6P_g \quad (D.1)$$

$$K_T(P_0, T) = (1.3 + 0.15 \log v(P_{atm}, 20^\circ C)) 10^{4 + \frac{20-T}{435}}$$

$$\bar{K}_S(P, T) = \frac{K_S(P_0, T)}{10} + 5.6P_g \quad (D.2)$$

$$K_S(P_0, T) = (1.57 + 0.15 \log v(P_{atm}, 20^\circ C)) 10^{4 + \frac{20-T}{417}}$$

In these equations, $v(P_{atm}, 20^\circ C)$ represents the kinematic viscosity of oil at atmospheric pressure and 20°C which for the Esso Nuto H68 oil was found to be: $v(P_{atm}, 20^\circ C) = 219$ cSt. The variation of isothermal and adiabatic secant bulk modulus of the Esso Nuto H68 oil with pressure at any temperature of interest is found using the Eqs. (D.1) and (D.2). These predicted equations

for the secant bulk modulus are converted to the tangent bulk modulus values using Eq. (D.3) given by

$$K(P, T) = \frac{\bar{K}(P, T)(\bar{K}(P, T) - P_g)}{K(P_0, T)}. \quad (D.3)$$

Figure D.2 represents a plot of the isothermal and adiabatic tangent bulk modulus of the Esso Nuto H68 oil which was plotted at a temperature of 24°C. The estimated values at a temperature of 24 °C are determined as

$$\begin{aligned} K_T(P, 24^\circ\text{C}) &= 1615 + 10.4(P - P_0) \\ K_S(P, 24^\circ\text{C}) &= 1878 + 10.4(P - P_0) \end{aligned} \quad (D.4)$$

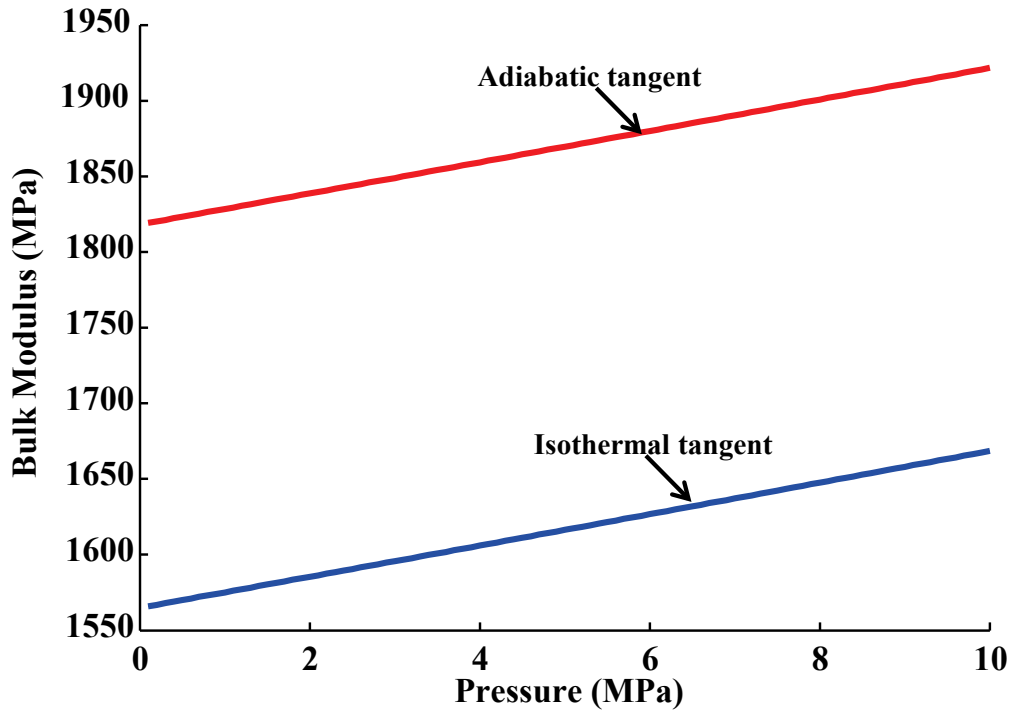


Figure D.2 Isothermal and adiabatic tangent bulk modulus variation of Esso Nuto H68 oil with pressure at a temperature of 24°C

The similar plots could be obtained for any other temperature of interest.

APPENDIX E: ESTIMATING THE DEFORMATION OF TESTING VOLUME

This appendix describes typical calculations to estimate the deformation of testing volumes in the experimental apparatus.

The testing volume in the experimental apparatus is composed of three elements: testing vessel, cylinder and pipes. These elements are all made of steel; however since they have different diameters and thicknesses, the effective bulk modulus of the three elements needs to be calculated according to Eq. E.1 (Manring, 2005),

$$\frac{1}{K_e} = \frac{V_1}{V_0} \frac{1}{K_1} + \frac{V_2}{V_0} \frac{1}{K_2} + \frac{V_3}{V_0} \frac{1}{K_3}, \quad (\text{E.1})$$

where

V_1 : volume of testing vessel at atmospheric pressure,

V_2 : volume of cylinder at atmospheric pressure,

V_3 : volume of pipes at atmospheric pressure,

V_0 : total volume at atmospheric pressure,

K_1 : bulk modulus of testing volume,

K_2 : bulk modulus of cylinder,

K_3 : bulk modulus of pipes,

K_e : effective bulk modulus of the combined containers.

Table E.1 Specifications of each element of testing volume

Dimensions	Testing vessel	Cylinder	Pipes
Outside diameter (mm)	89.0	47.9	12.8
Inside diameter (mm)	73.0	38.1	9.0
Thickness (mm)	8.0	4.9	1.9
Volume (mm ³)	1.812×10^6	2.642×10^5	5.750×10^4
Bulk Modulus (MPa)	1.860×10^4	2.117×10^4	3.071×10^4

Table E.1 shows the size (outside diameter, inside diameter, thickness and volume) and the bulk modulus associated with each of these elements. The bulk modulus of each element was calculated using Eq. E.2 (Manring, 2005),

$$\frac{1}{K} = \frac{D_o/t}{E}, \quad (\text{E.2})$$

where

D_o : outside diameter,

t : thickness,

E : modulus of elasticity.

Since all the elements are made of steel, the modulus of elasticity of steel which is equal to 2.069×10^5 MPa is used in the calculations. Using Eq. E.1 and the information provided in Table E.1, the effective bulk modulus of the testing volume was found to be $K_e = 1.909 \times 10^4$ MPa.

The change in the volume or deformation of the testing volume with pressure can be calculated by Eq. E.3 which is derived from the basic equation of bulk modulus,

$$\Delta V = V_0 \left(\left(e^{\frac{(P-P_0)}{K_e}} \right) - 1 \right). \quad (\text{E.3})$$

These equations are then used to calibrate the basic bulk modulus systems with degassed oil.

APPENDIX F: MEASUREMENT UNCERTAINTIES

This appendix illustrates the calibration and measurement uncertainties of the sensors which were used in the experimental system. Before describing each sensor, a brief review of calculating the measurement uncertainty is explained.

In order to find the total measurement uncertainty, the bias and precision uncertainties must be added appropriately using Eq. F.1 (Tavoularis, 2005),

$$U = \sqrt{b^2 + p^2}, \quad (\text{F.1})$$

where b is the bias limit and p is defined as the precision limit. Bias uncertainties are estimated by comparing the measurement readings to a known true value or standard. In many measurement processes, it is possible to have more than one bias uncertainty. In these cases, the total bias uncertainty is obtained by

$$b = \sqrt{\sum_{k=1}^K b_k^2}, \quad (\text{F.2})$$

where b_k represents each bias uncertainty. Precision uncertainties are due to random variations in the measurements and are determined by repeating the measurements and statistical evaluation of data. Assuming that the measurements follow a Gaussian distribution, the precision uncertainty can be determined by

$$p = 2\sigma_x, \quad (\text{F.3})$$

where σ_x is the standard deviation of N repeated measurements where N is considered to be more than 10 ($N > 10$) (Tavoularis, 2005).

F.1 Sensors

A number of different sensors were used in the experimental set up of the effective bulk modulus measurement in this thesis. These include pressure and displacement transducers. The pressure transducer is made by Validyne with the model DP15TL and a measurement range of 0 to 6.9 MPa. The displacement sensor is a Microtrak II stand-alone laser type sensor with model LTC-300-200-SA and a measurement range of ± 100 mm. To measure the initial volume of the

fluid inside the testing vessel, a 2000 mL graduated cylinder with an accuracy of ± 10 mL was used.

F.2 Uncertainty in measuring pressure

The pressure transducer was calibrated using a dead weight tester. The dead weight tester uses a piston of known area on which a known weight is placed to produce a standard pressure. This standard pressure is used to check the accuracy of readings from the pressure transducer. A Mansfield and Green Inc. “Twin Seal” dead weigh tester (model: 5525, serial: 163-1) with a stated accuracy of 0.1% was used. It should be noted that the same data acquisition software (Simulink) which was used to collect data during the experimental work was also used to record the calibration data. Therefore this allowed any error due to amplifier, data acquisition system and software, to be included in the calibration of the pressure transducer.

A number of different weights were added sequentially to the pan of the dead-weight tester over the expected range of the pressure transducer and the output voltage was recorded at each step (ascending data on Fig. F.1). Each output voltage is the average of 400 measurements over a period of 200 seconds. Descending data were obtained by subtracting the weights and reading the output voltage at each step. Due to the existence of hysteresis in the pressure transducer, the ascending and descending data are not reading the exact same data. The average of ascending and descending data was therefor used as the calibration data. The calibration curve for the pressure transducer is the best fit line through the average data and is shown in Fig. F.1.

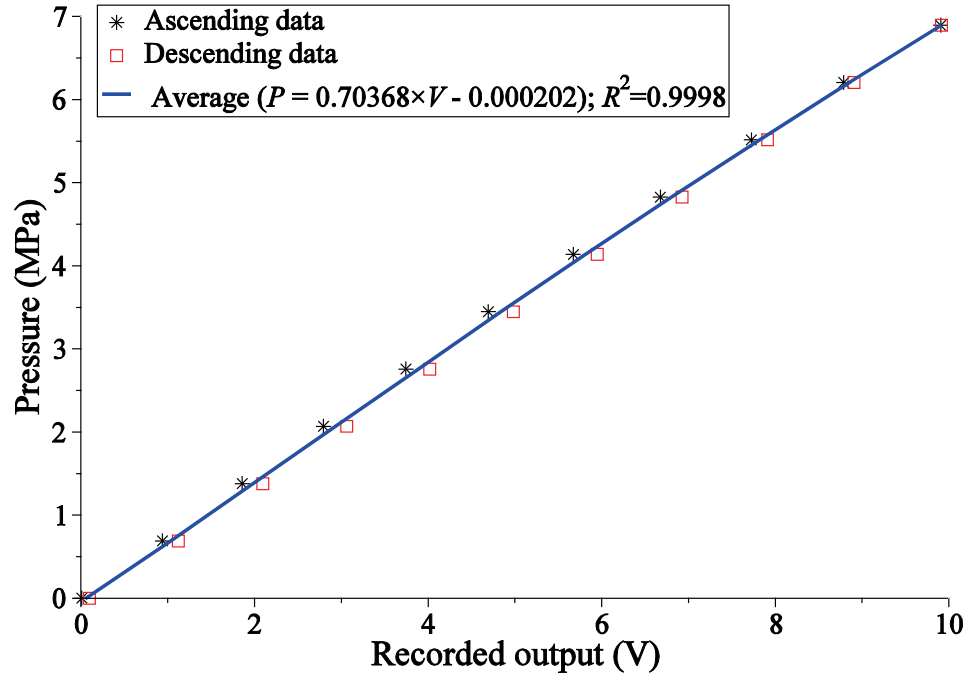


Figure F.1 Calibration curve for the pressure transducer

The curve fit is of the form

$$P = 0.704 \times V - 0.0002 . \quad (F.4)$$

There are two bias uncertainties in measuring the pressure. One is the calibration error due to the curve fit. Calibration error is defined as the difference between the measured and applied pressure. These errors were estimated at each step and the standard deviation of these errors was calculated to be 0.040 MPa. Another bias uncertainty is the value reported by the manufacturer of the dead weight tester with a stated accuracy of 0.1%. Therefore, the total bias uncertainty is calculated as

$$b = \sqrt{0.040^2 + 0.001^2} = 0.040 \text{ MPa}. \quad (F.5)$$

Since each measurement was repeated 400 times, the standard deviation of 400 measurements at each step was calculated and used in estimating the precision uncertainty. The σ_x was calculated to be 0.004 MPa. Therefore precision uncertainty is calculated as

$$p = 2\sigma_x = 2 \times 0.004 = 0.008 \text{ MPa}. \quad (F.6)$$

The total uncertainty calculation in measuring the pressure is given by

$$U = \sqrt{0.040^2 + 0.008^2} = 0.041 \text{ MPa.} \quad (\text{F.7})$$

It is usually preferred to express the uncertainty values in a dimensionless form. A dimensionless uncertainty in the measurements may be obtained by dividing the calculated uncertainty to the maximum measurement range (6.9 MPa) Therefore, the dimensionless uncertainty of the pressure measurements is $\varepsilon_p = 0.0059$.

F.3 Uncertainty in measuring displacement

The displacement sensor is a Microtrak II stand-alone laser type sensor with model LTC-300-200-SA and a measurement range of ± 100 mm. This transducer was calibrated by MTI Instruments Inc. The calibration sheet from the manufacturer states that the sensor has been calibrated by comparing to a standard with an uncertainty of ± 0.79 nm.

The sensitivity of the transducer was reported as 0.025 mm/mV with a bias uncertainty of 0.03% of full scale. Therefore the total bias uncertainty is calculated as

$$b = \sqrt{0.06^2 + (0.79 \times 10^{-9})^2} = 0.06 \text{ mm.} \quad (\text{F.8})$$

Precision uncertainty was obtained by calculating the standard deviation of multiple measurements ($N = 400$). The σ_x was calculated to be 0.1 mm. Therefore precision uncertainty is calculated as

$$p = 2\sigma_x = 2 \times 0.1 = 0.2 \text{ mm.} \quad (\text{F.9})$$

The total uncertainty calculation in measuring the displacement is given by

$$U = \sqrt{0.06^2 + 0.2^2} = 0.208 \text{ mm.} \quad (\text{F.10})$$

Therefore, for the maximum measurement range of 100 mm, the dimensionless uncertainty of the displacement measurements is $\varepsilon_x = 0.00208$.

F.4 Uncertainty in measuring volume

To measure the initial volume of the fluid inside the testing vessel, a 2000 mL graduated cylinder with a bias uncertainty (from the manufacturer) of ± 10 mL was used. Since the

measurement is only performed one time to measure the initial volume of the testing vessel, no precision uncertainty is defined for this measurement.

Therefore, for the maximum measurement range of 2000 mL, the dimensionless uncertainty of the initial volume measurements is $\varepsilon_{V_0} = 0.005$.

APPENDIX G: COPYRIGHT INFORMATION

Since the majority of the texts of Chapters 2 and 3 and some parts of Chapter 4 and 5 have been directly extracted from the author's published Journal and Conference papers, permission was asked from the copyright holders to use the materials of those papers in this thesis. The permission to use the materials of those papers is documented as follows:

- 1) Permission for the papers published in the International Journal of Fluid Power and 7th FPNI PhD Symposium on Fluid Power

On Jul 8, 2013, at 12:01 PM, "Gholizadeh, Hossein" <h.gholizadeh@usask.ca> wrote:

Dear Professor Ivantysynova:

I would really appreciate if you give me a permission for the following listed papers (which the first two are published in International Journal of Fluid Power and the last one is published in 7th FPNI PhD Symposium on Fluid Power, Reggio Emilia, Italy) to include and use most part of the papers in my Ph.D. thesis in University of Saskatchewan.

The papers are:

Gholizadeh, H., Burton, R. and Schoenau, G. 2011. Fluid Bulk Modulus: a Literature Survey. *International Journal of Fluid Power*, Vol. 12(3), pp. 5-16.

Gholizadeh, H., Burton, R. and Schoenau, G. 2012.a. Fluid Bulk Modulus: Comparison of Low Pressure Models. *International Journal of Fluid Power*, Vol. 13(1), pp. 7-16.

Gholizadeh, H., Bitner, D., Burton, R. and Schoenau, G. 2012.b. Experimental Investigation of Measuring Fluid Bulk Modulus in Low Pressure Regions. *7th FPNI PhD Symposium on Fluid Power*, Reggio Emilia, Italy.

Best Regards,
Hossein Gholizadeh

From: Monika Ivantysynova [mailto:mivantys@purdue.edu]
Sent: Monday, July 08, 2013 8:59 PM
To: Gholizadeh, Hossein
Subject: Re: Permission to use papers in my Ph.D. thesis

Dear Hossein,
sure you can use your own papers for your PhD thesis.

Best
regards

Monika

Dr. Monika Ivantysynova
MAHA Professor Fluid Power Systems
Director MAHA Fluid Power Research Center
Purdue University
School of Mechanical Engineering &
Department of Agricultural and Biological Engineering
MAHA Fluid Power Power Research Center
1500 Kepner Drive
Lafayette, IN 47905
Phone 765-447-1609
Fax 765-448-1860
mivantys@purdue.edu

2) Permission for the paper published in Bath/ASME Symposium on Power
Transmission and Motion Control

Quoting "Gholizadeh, Hossein" <h.gholizadeh@usask.ca>:

Dear Dr. Johnston:

I would really appreciate if you give me a permission for the following paper (which was published in Bath/ASME Symposium on Power Transmission and Motion Control, Bath, England) to include and use most part of the paper in my Ph.D. thesis in University of Saskatchewan. The paper is:

Gholizadeh, H., Bitner, D., Burton, R and Schoenau, G. 2012. Effective Bulk Modulus Model Verification for the Mixture of Air/Gas and Oil. *Bath/ASME Symposium on Power Transmission and Motion Control*, Bath, England.

From: ensdnj@bath.ac.uk [<mailto:ensdnj@bath.ac.uk>]

Sent: Tuesday, July 09, 2013 1:42 PM

To: Gholizadeh, Hossein

Cc: Nigel Johnston

Subject: Re: Permission to use papers in my Ph.D. thesis

Dear Hossein

That would be fine.

Best wishes

Nigel